NASA Technical Paper 1047

An Experimental and Analytical Investigation of Proprotor Whirl Flutter

Raymond G. Kvaternik and Jerome S. Kohn

DECEMBER 1977

NASA

NASA Technical Paper 1047

An Experimental and Analytical Investigation of Proprotor Whirl Flutter

Raymond G. Kvaternik
Langley Research Center
Hampton, Virginia
and
Jerome S. Kohn
Grumman Aerospace Corporation
Bethpage, New York

National Aeronautics
and Space Administration

Scientific and Technical
Information Office

1977

SUMMARY

The results of an experimental parametric investigation of whirl flutter are presented for a model consisting of a windmilling propeller-rotor, or "proprotor," having blades with offset flapping hinges mounted on a rigid pylon with flexibility in pitch and yaw. The investigation was motivated by the need to establish a large data base from which to assess the predictability of whirl flutter for a proprotor since some question has been raised as to whether flutter in the forward whirl mode could be predicted with confidence. In order to provide the necessary data base, the parametric study included variations in the pylon pitch and yaw stiffnesses, flapping hinge offset, and blade kinematic pitch-flap (δ_3) coupling over a large range of advance ratios. Fifty cases of forward whirl flutter and twenty-six cases of backward whirl flutter are documented. The measured whirl flutter characteristics, which include flutter speed, flutter frequency, direction of pylon whirl, and pylon yaw-to-pitch amplitude ratio and phase angle, are shown to be in good to excellent agreement with predictions from two different linear stability analyses which employ a two-dimensional, quasi-steady aerodynamic theory which neglects the effects of the unsteady wake, pitching moment, noncirculatory lift, and profile drag. On the basis of these results, it appears that proprotor whirl flutter, both forward and backward, can be predicted with linear stability analyses by using simple, two-dimensional, quasi-steady aerodynamics for the blade loading.

INTRODUCTION

The phenomenon known as propeller whirl flutter came under intense investigation in 1960 as a result of the loss of two Electra aircraft. Whirl flutter involves a self-sustained or divergent precessional motion or "whirl" of the propeller about its unperturbed position and can occur in a flexibly mounted propeller/nacelle installation in which the nacelle degrees of freedom allow the propeller plane to precess in response to the gyroscopic moments associated with the rotating propeller. When precession occurs, aerodynamic forces and moments which can be destabilizing on the whirl motion are generated because of cyclic angle-of-attack changes on the blade elements of the propeller. Under some conditions the precession is in the same direction as the propeller rotation (forward whirl), and under other conditions the precession is opposite (backward whirl). On conventional (nonhinged) tractor propellers, it has been found that the instability invariably occurs in the backward whirl mode.

During the period in which intense interest was being focused on whirl flutter for conventional propeller-driven aircraft, several VTOL aircraft which employed either articulated rotors or propellers having blades hinged to permit flapping were in research flight test programs. These aircraft employed the rotors or propellers for vertical flight and tilted the rotors or propellers forward approximately 90° for forward propulsion in the manner of an airplane. Because the rotors or propellers used on these aircraft perform the dual func-

tion of a lifting rotor and a propulsive propeller, the devices may be broadly referred to as propeller-rotors or "proprotors" for short. The terminology proprotor will be used in this report. Because of the flapping freedom of the blades, the whirl modes are affected, and a more complex variety of whirl flutter is possible. The concerns surrounding the Electra investigations provided the motivation to study the manner in which the whirl flutter characteristics of proprotors might be altered by the flapping freedom of the blades. Some early studies which ensued are reported in references 1 to 5.

In reference 1, the equations of motion for the whirl flutter analysis of a proprotor having offset flapping hinges were derived and employed in a stability analysis of a 0.30-meter-diameter model which was used in a companion experimental study. For the case in which the blade flapping freedom was locked out, backward whirl was obtained and was in agreement with theory. For the flapping case, forward whirl was observed but the predicted instability was in the backward mode. Only by modifying the theory to include arbitrary phase lags in the blade aerodynamics in order to approximate the unsteady effects of the wake could a forward mode of instability be predicted. Reference 2 is an analytical investigation for a specific VTOL aircraft which utilized blades with offset flapping hinges. Reference 3 presented some experimental results for a different 0.30-meter-diameter model which had provision for two hinge offsets. Backward whirl was observed when the flapping was locked out and for the larger of the two hinge offsets. Forward whirl was observed for the smaller hinge offset. In references 4 and 5 the theory of reference 1 was employed in a whirl flutter analysis of the model described in reference 3. The theory correctly predicted all the cases of backward whirl flutter but was unable to predict the forward whirl which was observed. Even by modifying the aerodynamic theory to include arbitrary phase lags to approximate the effects of the unsteady wake, forward whirl could not be predicted.

While these investigations were being conducted, whirl flutter in a backward whirl mode was encountered during a full-scale wind-tunnel test of the Bell XV-3 convertiplane. The XV-3 had two large diameter, two-bladed proprotors which were mounted on tiltable pylons attached to the tips of the wings. The XV-3 had a teetering hub. As the name implies, the hub allows flapping of the blades, but the two blades flap about the shaft as a unit, one up, the other down, in the manner of a see-saw. References 6 and 7 summarize the results of some analytical and experimental efforts aimed at explaining and correcting the whirl instability encountered on the XV-3. In particular, reference 6 indicated the possibility of both forward whirl and backward whirl for the XV-3, depending on the values of the system parameters. The possibility of both forward and backward whirl flutter was also indicated in reference 8 which examined the influence of flapping restraint on stability of a proprotor having centrally hinged blades by using a linear stability analysis and employing quasi-steady aerodynamics for the blade loading. However, no experimental results were shown to substantiate these predictions.

Some more recent work directed at examining various aspects of the dynamic behavior of proprotor systems is described in references 9 to 17. However, either because of the broad nature of the study or a lack of substantiating data, none of these studies were able to allay the skepticism which had developed regarding the ability to both predict forward whirl flutter and correlate those

predictions with experiment. With a view toward obtaining the experimental data needed for a more realistic assessment of the predictability of proprotor whirl flutter, a joint NASA/Grumman investigation of whirl flutter was conducted in the Langley transonic dynamics tunnel by employing an unpowered, 1.52-meter-diameter model of a three-blade proprotor with offset flapping hinges and kinematic pitch-flap (δ_3) coupling. The proprotor was mounted on a rigid pylon which was restrained in pitch and yaw by springs. To provide a large and varied data base, a range of pylon pitch and yaw stiffnesses, hinge offsets, and kinematic pitch-flap (δ_3) coupling angles were investigated over a wide range of windmilling advance ratios. Fifty cases of forward whirl flutter and twenty-six cases of backward whirl flutter were clearly identified. Two linear stability analyses available at the time of the experimental investigation, both employing simple two-dimensional, quasi-steady aerodynamics for the blade loading, were used in a companion whirl flutter analysis. Some preliminary results of limited scope pertaining to both the experimental and analytical aspects of this investigation were previously reported in references 18 and 19. The purpose of the present report is twofold: first, to provide a complete documentation of the experimental whirl flutter results which were given only limited treatment in references 18 and 19; second, to more fully substantiate the validity of analyses which employ simple two-dimensional, quasi-steady aerodynamics for predicting proprotor whirl flutter.

SYMBOLS

General Symbols

Physical quantities in this report are given in both the International System of Units (SI) and U.S. Customary Units. All measurements and calculations were made in U.S. Customary Units.

A_F pylon yaw-to-pitch amplitude ratio in whirl flutter mode

A_n aerodynamic integrals, $\int_{\eta_1}^{\eta_2} \frac{\eta^{n-1}}{W} d\eta$ $(n = 1, 2, 3, 4, 5)$

a section-lift-curve slope per radian

B_n aerodynamic integrals, $\int_{\eta_1}^{\eta_2} W\eta^{n-1} d\eta$ $(n = 1, 2, 3)$

c blade chord, m (ft)

D diameter of proprotor, m (ft)

e offset of flapping hinge from shaft center line, m (ft)

$f_{P,o}, f_{Y,o}$ measured uncoupled natural frequencies of pylon in pitch and yaw with proprotor nonrotating and blades locked to forward flapping stops, Hz

$[I]$	identity matrix
J_F	flutter advance ratio, $\frac{V_F}{nD}$ $\left(= \frac{\pi V_F}{\Omega R}\right)$
m	blade mass per unit length, kg/m (slug/ft)
N	number of blades
n	proprotor rotational speed, Hz
R	radius of blade (measured from center line of rotation to blade tip), m (ft)
r	local blade radius (measured from center line of rotation), m (ft)
t	time, sec
V	free-stream velocity, m/sec (ft/sec)
V_F	free-stream velocity at flutter, m/sec (ft/sec)
W	$= \sqrt{\left(\frac{V}{\Omega R}\right)^2 + \left(\frac{r}{R}\right)^2}$
δ_3	blade kinematic pitch-flap coupling angle, deg
ζ_P, ζ_Y	viscous damping of pylon relative to critical damping in pitch and yaw, respectively
ζ_β	viscous damping relative to critical damping of blade flapping motion
η	nondimensional radial coordinate, r/R
η_1, η_2	integration limits for blade aerodynamic integrals
ρ	air density, kg/m^3 (slug/ft^3)
ϕ_F	pylon yaw-to-pitch phase angle in whirl flutter mode, deg
Ω	proprotor rotational speed, rad/sec
ω_F	frequency of pylon whirl at flutter, rad/sec
ω_P, ω_Y	pylon natural frequencies in pitch and yaw, $f_{P,o}$ and $f_{Y,o}$, corrected to reflect zero coning, rad/sec
$(\dot{})$	derivative with respect to time, d/dt
$[\ ]$	square matrix

$\{\ \}$ column matrix

$[\ ]^{-1}$ matrix inverse

+ denotes forward whirl

- denotes backward whirl

Symbols for Appendix A

a_1, b_1 flapping degrees of freedom of proprotor disc in longitudinal and lateral directions, rad (see fig. A1)

C_{ϕ_y}, C_{ϕ_z} pylon viscous damping coefficients in pitch and yaw, N-m-sec/rad (lb-ft-sec/rad)

h_1, h_2 distance between proprotor hub and pylon pitch and yaw axes, respectively, m (ft)

$\bar{h}_1, \bar{h}_2$ distance between pylon center of mass and pylon pitch and yaw axes, respectively, m (ft)

I_B flapping inertia of blade, $\int_0^R r^2 m\, dr$, kg-m^2 (slug/ft^2)

$I_{p,yy}, I_{p,zz}$ mass moments of inertia of pylon in pitch and yaw about its center of mass, kg-m^2 (slug-ft^2)

I_R flapping inertia of proprotor, $\frac{N}{2} I_B$, kg-m^2 (slug-ft^2)

K_H hub flapping spring, $\frac{N}{2} k_\beta$, N-m/rad (lb-ft/rad)

K_{ϕ_y}, K_{ϕ_z} pylon stiffnesses in pitch and yaw, N-m/rad (lb-ft/rad)

k_β blade flapping spring, N-m/rad (lb-ft/rad)

M_p, M_Y mass of pylon effective in pitch and yaw, respectively, kg (slugs)

$M_R = N \int_0^R m\, dr$, kg (slugs)

$S_B = \int_0^R rm\, dr$, kg-m (slug-ft)

$S_R = NS_B$, kg-m (slug-ft)

s complex eigenvalue

β_o angle of built-in coning (precone), rad

γ Lock number, $\frac{\rho a c R^4}{I_B}$

κ $= \frac{1}{2} \gamma \Omega^2 I_R$, kg-m^2/sec^2 (slug-ft^2/sec^2)

λ inflow ratio, $V/\Omega R$

ϕ_y, ϕ_z pylon degrees of freedom in pitch and yaw (see fig. A1), rad

Symbols for Appendix B

a_1, a_2 nondimensional distance between proprotor hub and pylon pitch and yaw axes, respectively, in proprotor radii

A_ε $= A_5 - 2\varepsilon A_4 + \varepsilon^2 A_3$

C_{q_1}, C_{q_2} pylon viscous damping coefficients in pitch and yaw, N-m-sec/rad (lb-ft-sec/rad)

H inflow ratio, $V/\Omega R$

I_p, I_Y mass moments of inertia of pylon about pylon pitch and yaw axes, kg-m^2 (slug-ft^2)

I_1 $= \frac{N}{2} \int_0^R mr^2 \, dr$, kg-m^2 (slug-ft^2)

I_2 $= \frac{N}{2} \int_e^R mr(r - e) \, dr$, kg-m^2 (slug-ft^2)

I_3 $= \frac{N}{2} \int_e^R m(r - e)^2 \, dr$, kg-m^2 (slug-ft^2)

K $= \frac{\rho a c R^4 N}{4}$, kg-m^2 (slug-ft^2)

M $= N \int_0^R m \, dr + M_{HUB}$ where M_{HUB} is mass of hub, kg (slugs)

q_1, q_2, q_3, q_4 degrees of freedom (see fig. B1)

S $= \frac{N}{2}\int_e^R m(r - e)\,dr$, kg-m (slug-ft)

ε $= e/R$

λ complex eigenvalue

ν_1, ν_2 uncoupled natural frequencies of pylon/rotor combination in pitch and yaw, respectively, nondimensionalized by rotor rotational speed

ν_3 nonrotating, uncoupled flapping natural frequency of proprotor disc nondimensionalized by rotor rotational speed

τ nondimensional time, Ωt

Primes denote derivatives with respect to τ.

APPARATUS

Wind Tunnel

The experimental investigations were conducted in the Langley transonic dynamics tunnel which is a continuous flow, single return, variable pressure, slotted-throat tunnel having a test section 4.87 meters (16 feet) square with cropped corners. The control room and test section walls are provided with large windows for close viewing of the model. Although the runs were conducted in air under near atmospheric conditions at free-stream Mach numbers less than 0.30, the tunnel is capable of operation at stagnation pressures from near vacuum to slightly above atmospheric and Mach numbers up to 1.2. Either air or Freon-12 can be used as a test medium.

Model

The model (fig. 1) employed in the whirl flutter investigation was an adaptation of a 1/4.5-scale industrial model of a specific tilt-proprotor aircraft design (ref. 17) which incorporated blades with offset flapping hinges and kinematic pitch-flap (δ_3) coupling to reduce blade flapping. To obtain flutter at low tunnel speeds, the whirl flutter model employed a special-purpose reduced-stiffness pylon-to-wing-tip restraint mechanism. The resulting pylon-to-wing flexibility was such that the proprotor/pylon combination was effectively isolated from the wing and the model support structure so that the predominant freedoms were blade flapping and pylon pitching and yawing. The whirl flutter model was unpowered (that is, windmilling) and incorporated features to permit variations of selected parameters to provide a wide range of whirl flutter configurations. Parameters which were adjustable include the pylon pitch and yaw stiffnesses, hinge offset, and blade kinematic pitch-flap (δ_3) coupling.

The range of the adjustable parameters tested represents a broad spectrum of practical values. Pylon pitch and yaw frequencies, nondimensionalized by

the proprotor rotational speed, varied from 0.23 to 2.04. The ratio of pylon pitch-to-yaw stiffness varied from 0.25 to 1.85. Hinge offsets of 0.05R and 0.13R and kinematic pitch-flap (δ_3) coupling angles of +6.75°, +10.5°, +20°, and +30° were tested, although not in all possible combinations. Emphasis was placed on the configuration having a hinge offset of 0.05R and a δ_3 of +20° because these values were nearest those which might be employed in practice. Values of δ_3 less than +6.75° could not be obtained because of mechanical interference problems and model design limitations. Structural damping of the pylon, which was not adjustable, varied from $2\zeta_P = 0.005$ to $2\zeta_P = 0.032$ in pitch and from $2\zeta_Y = 0.021$ to $2\zeta_Y = 0.065$ in yaw. The inflow ratio at flutter $V_P/\Omega R$ varied from 0.34 to 1.36.

Design and construction.- The wing spar (fig. 2) consisted of a hollow aluminum beam with spanwise flanges which was attached to a steel plate at its inboard (root) end. Two wing struts extending from the tip of the wing spar to the lower edge of the steel plate provided a high level of wing vertical bending stiffness. The steel plate was attached to a support structure consisting of a tripod arrangement of tubular steel beams which was bolted to the tunnel wall and floor. A plywood panel (fig. 1) passing through the vertical plane of symmetry of the model and attached to the tripod support structure was employed both to provide a seal for the open backside of the semi-fuselage and to serve as a reflection plane. For the whirl flutter investigation, the nonstructural, segmented aerodynamic panels which provided the spanwise and chordwise distribution of wing airfoil contour were removed (fig. 2). This arrangement destroyed the wing aerodynamic lift and further decoupled the pylon motions from the wing. For convenience, however, the flaps (which were not germane to the whirl flutter investigation) were left on during testing of the configurations having a 5-percent hinge offset.

To obtain flutter at low tunnel speeds, the pylon was soft-mounted to the wing spar by means of a reduced-stiffness pylon-to-wing-tip restraint mechanism (fig. 3) which permitted independent variations in the pylon pitch and yaw stiffnesses. The natural frequencies of the wing/pylon combination (with the pylon locked to the wing tip) in the fundamental wing beamwise, chordwise, and torsional modes were 29.6 Hz, 19.7 Hz, and 39.5 Hz, respectively. With the pylon unlocked and soft-mounted to the wing, most of the combinations of pylon pitch and yaw stiffnesses resulted in frequencies of the proprotor/pylon combination which were well below 8 Hz and thus well removed from the lowest wing frequencies. It was verified, both experimentally and analytically, that even for the maximum pylon support stiffness, coupling between the proprotor/pylon system and the wing was negligible. Thus, the wing was effectively a rigid support structure for the proprotor/pylon system and the predominant freedoms were pitching and yawing of the pylon and flapping of the blades.

The pylon support mechanism (fig. 3) consisted of a boxlike housing which contained bearings allowing for freedom in pitch and yaw and two pairs of steel or aluminum bars oriented to provide restraint in pitch and yaw. The arrangement of the bearings was such that the pitch and yaw axes were noncoincident. (The yaw axis was 0.043 m (0.14 ft) ahead of the pitch axis.) All combinations of the steel and aluminum bars used to provide the pylon pitching and yawing restraints were shown to have linear load-deflection (and hence stiffness) characteristics by loading and unloading them in a bench test. The hysteresis (and

hence damping) observed during the loading and unloading was always greater for the yaw spring than for the pitch spring. The pitch and yaw stiffnesses were independently adjustable by means of a slider which could be moved along the length of either the pitch or yaw spring and locked in position; thereby the effective length (and thus stiffness) of the spring was varied. Damping in the pitch and yaw directions could not be set or varied independently but generally varied with changes in stiffness.

The blades consisted of a negatively twisted (-23°) aluminum spar having spanwise distributed beamwise, chordwise, and torsional stiffnesses and covered with a continuous (nonsegmented) balsa wood skin bonded to ribs attached to the spar of the blade. Lead weights were bonded to the spar to obtain the proper weight and balance distribution. The desired level of blade inplane stiffness was achieved by means of aluminum spar caps bonded to the upper and lower sides of the blade over the inboard third of each blade and by several layers of boron filament tape bonded to the upper and lower surfaces of the blade from the root to about the 80-percent radius. This modification resulted in a blade first elastic nonrotating inplane frequency of about 28 Hz. Since the maximum rotor rotational speed in the whirl flutter tests was 17 Hz, the minimum blade inplane frequency on a per revolution basis was 1.65. The first beamwise cantilevered elastic mode frequency of the blade was 18 Hz, and the first cantilevered torsional elastic mode frequency was 66 Hz.

A schematic illustration of the model hub and control system geometry is shown in figure 4. Each blade is attached to the hub assembly by means of a steel pin which forms the hinge about which the blade flaps. No flapping restraint is employed. The offset of the flapping hinge is varied by inserting spacers of different lengths between the inner part of the hub which is attached to the rotor shaft and the outer part which retains the flapping hinge. The blade pitch change axis is coincident with the centroidal axis of the spar which lies along the blade quarter-chord line. The pitch of the blades is varied collectively by means of a swashplate ahead of the hub which is linked to the pitch horns by pitch links.

Blade kinematic pitch-flap coupling is provided by having the pitch link attachment point on the pitch horn offset radially from the flapping hinge (the distance d_1 in fig. 4). For a leading-edge pitch horn arrangement, this geometry establishes a virtual flapping hinge so that when the blade flaps forward, the blade pitch decreases. The acute angle formed by the line defining the virtual flapping axis with the flapping hinge is the pitch-flap coupling angle δ_3. This angle is defined to be positive if the blade pitch decreases when the blade flaps forward, as in the present situation. The δ_3 angle is varied manually by moving the end of the pitch horn inboard (to reduce δ_3) or outboard (to increase δ_3).

The model for the 13-percent hinge-offset configuration (figs. 5 and 6) differed somewhat from that of the 5-percent hinge-offset configuration (figs. 1 and 3). These differences were due to the fact that the configuration having the 13-percent hinge offset could be obtained only by increasing the radius of the proprotor. This requirement necessitated the use of a new rotating swashplate and pitch link arrangement, a larger spacer, and several other minor changes in the control mechanism. To accommodate the increased blade radius,

it was necessary to remove the semi-fuselage. The wing flaps, which were left on during the testing of the 5-percent hinge-offset configuration, were also removed.

Physical properties.- The physical properties of the model proprotor and pylon for both hinge offsets are summarized in table I. The pylon inertial properties in pitch and yaw for each of the hinge offsets are different because of the noncoincidence of the pylon pitch and yaw axes. The rotating swashplate and pitch links move back and forth on the pylon as collective pitch is changed but affect the pylon inertias about the pitch and yaw axes by less than 1 percent. This variation was neglected in the analyses and is not reflected in values given in table I.

The pylon support stiffnesses in pitch and yaw, which were the parameters most varied in the test program, were determined by "plucking" the model in pitch and yaw. Prior to each run, the blades were positioned against, and secured to, the forward flapping stops at a 13.5° coning angle and the model was plucked first in pitch and then in yaw and the subsequent decaying oscillation in each degree of freedom recorded on a direct-write oscillograph. The frequencies of the resultant transient time histories were then used in combination with the known inertial properties of the model to get the pitch and yaw spring rates. The damping, as a fraction of critical, was also obtained from the traces of the decaying oscillations by using the familiar logarithmic decrement method. Typical traces of decaying oscillations obtained by plucking are shown in figure 7. The plucks were repeated after each run in order to identify any large change or structural deterioration that may have occurred during the run. In general, only negligible changes in both frequency and damping were identified by these comparisons. The measured values of frequency and damping shown in table II represent an average of the pre- and post-run values.

Instrumentation.- Blade flapping relative to the hub plane was measured on one blade by means of a soft flexure instrumented with strain gages which was clamped to the root of the blade and reached across the flapping hinge. Blade beamwise, chordwise, and torsional moments were measured on one blade by means of strain gages which were mounted on the spar of the blade at the root and at the midspan position. Data measured in the rotating system were brought out through the transmission to the fixed system by means of a slip-ring assembly. Pylon motions in pitch and yaw were measured by two accelerometers located on the forward part of the pylon and well removed from the axes of pitch and yaw. One accelerometer was oriented to sense pitch, and the other accelerometer was oriented to sense yaw. Rotor rotational speed was indicated directly on a tachometer driven by the signal from a magnetic pickup on the model. The azimuthal position of an arbitrarily selected reference blade was given by the same pickup which pulsed every 90° of rotor revolution. The pulse corresponding to a specific azimuth position of the reference blade was larger than the other three. This feature was used mainly for dynamically balancing the rotor. Electrical controls were used to vary blade collective pitch (and hence rotor rotational speed) remotely from the tunnel control room. Data were recorded on an oscillograph and on magnetic tape. A short motion picture was taken of each flutter point.

TEST PROCEDURE

For a given hinge offset and pitch-flap coupling angle, the pylon support stiffnesses and damping in pitch and yaw were first determined by plucking the pylon as described above. Whirl flutter points were then experimentally established in the following manner: A preselected windmilling rotor rotational speed was set at some low tunnel speed by remotely adjusting the collective pitch of the blades. The model was then transiently excited by plucking a lightweight cable which was attached to the pylon (fig. 3) and routed to the control room. The stability of the response was observed both visually and on an oscillograph. If the model was stable, the tunnel speed was increased by a small amount, the collective pitch retrimmed to produce the same rotor speed, and the model again excited. This procedure was repeated until a sustained, approximately constant amplitude whirl oscillation (indicating neutral stability) was observed. The tunnel conditions were then recorded as the conditions for flutter and a short motion picture of the whirl instability taken. Tunnel speed was then reduced, the rotor speed was set to a new value, and the procedure was repeated. By proceeding in this way, several whirl flutter points could be obtained for a single setting of the pylon support stiffnesses but at various values of rotational speed.

The exact point of neutral stability was established in most cases. In those cases where neutral stability was not achieved, the flutter point was established from the last few decaying (or diverging) traces by extrapolation. The cable used to excite the model was also used to restrain the model in those instances in which the pylon motions were divergent.

DESCRIPTION OF ANALYSES

Two linear stability analyses based on two different mathematical models (refs. 1 and 15) were employed in the whirl flutter analysis of the model configurations tested. Both analyses assume that the proprotor has three or more blades and is mounted on a rigid pylon which is restrained elastically in pitch and yaw by springs. The proprotor is assumed to be windmilling (unpowered) in an axial-flow condition and to consist of three or more rigid blades which are restrained elastically in flapping by springs. The blades are assumed to have constant chord and to incorporate kinematic pitch-flap (δ_3) coupling. The dynamics of the present model are taken to be expressed in terms of only four of the eight degrees of freedom considered in references 1 and 15: pitch and yaw of the pylon and two cyclic flapping modes. To an observer in the nonrotating system, the two cyclic flapping modes are patterned so that the tip path plane appears to be pitching and yawing; that is, the rotor appears to be flapping longitudinally and laterally. For a proprotor having three or more blades and operating in axial flow, the use of these tip-path-plane coordinates as degrees of freedom in lieu of the individual blade flapping coordinates as degrees of freedom is an expedient which allows for the removal of the periodicity from the equations of motion. The introduction of these coordinates amounts to a coordinate transformation and is discussed in both references 1 and 15.

A two-dimensional, quasi-steady aerodynamic theory which neglects the unsteady wake, pitching moment, noncirculatory lift, and profile drag is

employed to calculate the blade aerodynamic loading. The quasi-steady lift is taken to be completely determined by the resultant of the velocity components acting tangential and perpendicular to the blade chord at the quarter-chord of the section. The flow is assumed to be incompressible and the section-lift-curve slope to be constant over the length of the blade.

The first analysis which was used to predict the whirl flutter behavior of the model is based on that developed in reference 15 for a gimbaled proprotor. A gimbaled proprotor is characterized by blades which are rigidly attached to a hub assembly which is connected to the shaft by a gimbal (universal joint) housed within the hub. The blades of a gimbaled proprotor flap about the shaft by virtue of the gimbal mounting arrangement. Since the model tested had an offset flapping hinge, the inertial and aerodynamic restoring moment effects associated with the offset hinge were approximately accounted for in the gimbaled analysis by determining an equivalent hub spring which preserves the rotating flapping natural frequency of the hinged blade with aerodynamic forces included. The equations of motion used in the whirl flutter analysis are summarized in appendix A. The second analysis which was applied to the model is based on the derivation given in reference 1 which was developed explicitly for a proprotor having blades with offset flapping hinges. The equations of motion with four degrees of freedom appropriate to the present case are given in appendix 5 of reference 1 as a special case of the more general development. Several additions to those equations are made herein, however, in order to make them applicable to the present model. These additions include pylon inertia and damping about the pitch and yaw axes, flap-hinge damping, and a large pitch-flap coupling angle. The limits of integration for the blade aerodynamic integrals are also changed from those given in reference 1. The resultant equations are summarized in appendix B.

The steady-state coning angle of the blades during wind-on operation with the rotor in a windmilling condition was always negative (downwind) but never exceeded 1°. By use of the gimbaled proprotor analysis which accounts for blade built-in coning (precone), it was established analytically that these small coning angles have a negligible effect on the predicted whirl instability. Thus, for convenience in the adaptation of the theory of reference 1 (which did not include steady-state coning) to the present investigation, all the whirl flutter analyses were made by assuming the steady-state coning to be zero. The more general version of the gimbaled proprotor analysis which includes the wing degrees of freedom and is described in reference 15 was used to analytically verify that as a consequence of the soft pylon mounting arrangement in combination with a stiff wing support structure, the degrees of freedom of the wing had a negligible effect on the predicted whirl flutter characteristics of the model.

The structural damping about the blade flapping hinge was not measured and was taken to be zero in the analyses. This assumption was judged to be reasonable because of the low friction at the flapping hinges. Since the tunnel density varied slightly from run to run, an average value of 1.23 kg/m^3 (0.00238 $slug/ft^3$) was used in the analyses. The blade lift-curve slope was assumed to be constant and equal to 5.73 for the analytical studies. The blade aerodynamic integrals were evaluated by using a lower limit of integration which reflects the fact that because of root cutout, the lifting portion of the blade begins 8.6 cm (3.4 in.) outboard of the hinge location, and by using an upper limit

which reflects the assumption that a tip length equal to one-half of the chord develops no lift. These considerations lead to limits of integration of 0.16R and 0.94R for the 5-percent hinge-offset configurations and limits of 0.24R and 0.94R for the 13-percent hinge-offset configurations.

In the computer implementation of the analyses, the measured natural frequencies of the model in pitch and yaw, $f_{P,o}$ and $f_{Y,o}$, are read as part of the input data and corrected to reflect a zero coning condition. The resulting frequencies, in nondimensional form, are given by ω_P/Ω and ω_Y/Ω in table III. The blade kinematic pitch-flap coupling angle δ_3 varies slightly with changes in collective pitch by virtue of the varying geometry which defines this angle. These small changes are accounted for in the computer programs. The equivalent hub spring which is employed in the gimbaled propulsor analysis to account for the effects of the offset flapping hinge is a function of the blade physical properties, hinge offset, airspeed, and rotational speed. Since the flutter points identified with the model represent a large number of V,Ω combinations, the equivalent hub spring was calculated in the computer program.

RESULTS AND DISCUSSION

Comparison of Theory and Experiment

A summary of all the model configurations which exhibited a whirl flutter instability along with the pertinent data defining each flutter condition is given in table II. A companion summary plot of all the experimental flutter points identified with the model is given in figure 8 where the data are plotted as a function of the pylon yaw and pylon pitch uncoupled natural frequencies corrected to zero coning and nondimensionalized by the rotor rotational speed. The data are seen to be grouped into three distinct regions emanating from the origin: a central region associated with symmetric and nearly symmetric pylon frequencies, and two side regions associated with nonsymmetric pylon frequencies which have a boundary with the center region at pylon pitch-to-yaw frequency ratios of about 0.75 and 1.5. For configurations having pylon frequency ratios falling in these nonsymmetric regions, flutter was always in the backward whirl mode. All the cases of forward whirl flutter fall near the line of equal pitch and yaw frequencies. Ten cases of backward whirl flutter also fall in the central region. Eight of these points represent all the whirl flutter points identified with the configuration having a 13-percent hinge offset. The other two points are the two cases of backward whirl identified in run 48 for a 5-percent hinge offset.

A summary of the analytical results that correspond to the experimental results shown in table II is given in table III. The flutter phase angle ϕ_F which is obtained from the solution of the equations of appendix A is formally different from that obtained from a solution of the equations of appendix B. This difference is due to the difference in definition of the positive sense for the pylon pitch degree of freedom. (Compare figs. A1 and B1.) The phase angles from the two theories are related according to

$$\phi_F|_{\text{ref. 1}} = \phi_F|_{\text{ref. 15}} + 180^\circ$$

To provide for a direct comparison of these phase angles, the phase angles given in table III for the theory of reference 15 have been transformed to the notation of reference 1 by using the preceding relation.

A run-by-run comparison of both theories with experiment using the information provided in tables II and III is made in figure 9 for the flutter speeds and in figure 10 for the associated flutter frequencies. The flutter speeds shown are nondimensionalized by the tip speed of the rotor to give the flutter inflow ratio $V_F/\Omega R$. This ratio is related to the flutter advance ratio J_F according to $J_F = \pi V_F/\Omega R$. The flutter frequencies are nondimensionalized by the rotor rotational speed to give the frequencies on a per-revolution basis. Here, and in subsequent figures, the flutter results are given as a function of the pylon pitch uncoupled natural frequency corrected to zero coning and nondimensionalized by the rotor rotational speed. For the configurations of runs 48, 50, and 65, the analyses indicated that there were two flutter boundaries which were close to the measured flutter boundary. Both of these analytical boundaries are shown in those cases. Both theories are in good to excellent agreement with experiment for both flutter speed and flutter frequency. The direction of pylon whirl at flutter was established both visually during the test and by inspection of the pylon pitch and yaw traces on the oscillograph records. The whirl direction predicted by theory was in every case in agreement with that observed experimentally.

Flutter in the backward whirl mode occurred at low frequencies and in what might be termed a "rotor mode" since the flutter frequencies were near those of the low-frequency cyclic flapping mode with the pylon degrees of freedom locked out. Flutter in the forward whirl mode generally occurred at frequencies which were higher than those associated with flutter in the backward whirl mode and in what might be termed a "pylon mode" since the flutter frequencies were near the natural frequencies of the system in pitch and yaw with the flapping degree of freedom locked out. These aspects of the whirl dynamics of proprotor/pylon systems are discussed in references 6, 7, and 15. The flapping in a pylon mode is generally large relative to the shaft (but small relative to space) whereas the flapping is a rotor mode is generally small relative to the shaft (but large relative to space).[1] Typical mode shapes which illustrate this flapping behavior for a proprotor/pylon system with four degrees of freedom and having hinged blades are shown in references 1 and 4. Both the backward whirl and forward whirl instabilities were accompanied by divergent motions in several instances in which the flutter speed was inadvertently exceeded. There were also several instances in which both the backward and forward whirl instabilities were precipitated merely by increasing the tunnel speed, no external excitation via the lightweight plucking cable being required.

A comparison of the measured pylon yaw-to-pitch amplitude ratios and phase angles at flutter with those predicted using the theory of reference 1 is given in figures 11 and 12. Reading accuracy of the phase angle from the oscillograph records was about $\pm 10^\circ$. The phase angles in the whirl mode were not 90° (as they would be in a vacuum) but varied between about 60° and 120° because phase differences other than 90° are induced on the pylon whirl motion by the aerody-

[1]The XV-3 instability was a backward whirl associated with the low-frequency rotor flapping mode.

namic loading acting on the blades if the model pylon is not symmetric in the pitch and yaw directions. Similar comparisons, not shown, were obtained by using the theory of reference 15. Thus, in addition to correctly predicting the whirl directions, the theories of references 1 and 15 also predicted the amplitude ratios and phase angles reasonably well.

Effect of Design Parameters

Some selected composite results which show the effects of pitch-flap coupling, hinge offset, and asymmetry of the pylon support frequencies (stiffnesses) on whirl flutter stability are shown in figures 13 to 15. The effect of variation of δ_3 on stability is given in figure 13 for a configuration having nominally symmetric pylon pitch and yaw frequencies (within 5 percent of each other) and 5-percent hinge offset. The results show a strong decrease in flutter inflow ratio (and hence flutter speed for a fixed rotor rotational speed) with increasing positive δ_3. Although only positive values of δ_3 were investigated, reference 15 has shown that negative values of δ_3 are equally destabilizing on whirl flutter. Flutter is in the forward whirl mode except for the two points, denoted by solid symbols, which are in the backward whirl mode. The analytical results shown are based on the assumption of a symmetric pylon frequency configuration which is the mean of the pylon frequencies of the data points included in figure 13. Similarly, the damping used is the mean of the pitch and yaw values.

The effect of hinge offset on stability is illustrated in figure 14 for configurations having nominally symmetric pylon pitch and yaw frequencies and $\delta_3 = 20^\circ$. Increased hinge offset is seen to be strongly stabilizing. Theoretical results are again based on the use of mean values for both the pylon support frequencies and dampings.

The effect of asymmetry in the pylon support frequencies is indicated in figure 15 for the configuration having 5-percent hinge offset and $\delta_3 = 20^\circ$. Again, the symmetric data represent nominally symmetric configurations in which the pylon frequencies are within 5 percent of each other whereas the nonsymmetric data include configurations which satisfy the indicated frequency asymmetries. The flutter inflow ratio is plotted against the nondimensionalized pylon pitch natural frequency except for the cases in which $\omega_Y < \omega_P$, where the nondimensionalized yaw frequency is shown for convenience in plotting. The results confirm earlier results (refs. 9 and 15) that for highly unsymmetric configurations in the pylon support frequencies (and hence stiffnesses), whirl flutter occurs in the mode corresponding to the lower pylon frequency (stiffness) and increasing the higher frequency (stiffness) does not increase the flutter speed. Flutter is in the backward whirl mode for all the asymmetric conditions.

Analytical Damping Studies

It was stated earlier that the damping at the flapping hinge was not measured and was taken to be zero in the analyses of the model configurations which exhibited whirl flutter. Reference 16 pointed out that internal damping, that is, damping which is exhibited in the rotating system, can be destabilizing on

proprotor/pylon whirl stability. It was also stated earlier that the pylon damping in pitch and yaw was not adjustable and could not be varied independently of the pitch and yaw stiffnesses. In order to analytically identify the effect of hinge damping and pylon damping on whirl flutter stability of the present model, some analytical studies in which these parameters were varied were made on three of the model configurations. The results of these studies are given in figures 16 to 21.

The effects of hinge damping and pylon damping on whirl stability of a symmetric pylon frequency configuration in which instability occurred in the forward whirl mode are shown in figures 16 and 17, respectively. From figure 16, hinge damping is seen to reduce the inflow ratio at which the forward whirl mode becomes unstable, the reduction becoming more significant with decreasing pylon support frequency. A reduction in pylon damping (fig. 17) has a moderate destabilizing effect on stability.

The effects of hinge damping and pylon damping on whirl stability of an unsymmetric configuration in which instability occurred in a backward whirl mode are shown in figures 18 and 19, respectively. Neither hinge damping nor pylon damping is seen to have any significant effect on the backward mode of instability associated with an unsymmetric pylon frequency configuration.

The effects of hinge damping and pylon damping on whirl stability of a symmetric frequency configuration in which instability occurred in a backward whirl mode are shown in figures 20 and 21. It is seen that, again, neither hinge damping nor pylon damping has any significant effect on the backward mode of instability associated with a symmetric pylon configuration.

CONCLUSIONS

Results of an experimental parametric investigation of proprotor/pylon whirl flutter conducted in the Langley transonic dynamics tunnel are presented for a model consisting of a proprotor having blades with offset flapping hinges mounted on a rigid pylon with flexibility in pitch and yaw. The parametric study included variations in the pylon pitch and yaw stiffnesses, offset of the flapping hinge, and blade kinematic pitch-flap (δ_3) coupling over a large range of windmilling advance ratios. Fifty cases of forward whirl flutter and twenty-six cases of backward whirl flutter are documented. Measured whirl flutter characteristics, which include flutter speed, flutter frequency, direction of pylon whirl, and pylon yaw-to-pitch amplitude ratio and phase angle, are shown to be in good agreement with predictions from two different linear stability analyses which employ two-dimensional, quasi-steady aerodynamics in which the effects of the unsteady wake, pitching moment, noncirculatory lift, and blade profile drag are neglected. On the basis of the results shown, the following conclusions are indicated:

(1) Proprotor whirl flutter, both forward and backward, can be predicted with linear stability analyses which employ simple, two-dimensional, quasi-steady aerodynamics for the blade loading.

(2) Stability analyses developed for a gimbaled proprotor can be applied to proprotors having blades with offset flapping hinges provided the blade inertial and aerodynamic terms associated with the offset of the hinge are accounted for through an equivalent hub spring which preserves the rotating flapping natural frequency of the hinged blade with aerodynamic forces included.

Langley Research Center
National Aeronautics and Space Administration
Hampton, VA 23665
October 12, 1977

APPENDIX A

WHIRL FLUTTER EQUATIONS OF MOTION FOR A GIMBALED PROPROTOR

The linear equations of motion for the whirl flutter analysis of a gimbaled proprotor are given in reference 15 in the general matrix form

$$[\bar{M}]\{\ddot{\bar{q}}\} + [\Gamma]\{\dot{q}\} + [\bar{C}]\{\dot{q}\} + [\bar{K}]\{q\} = [AD]\{\dot{q}\} + [AS]\{q\} \tag{A1}$$

By ordering the four degrees of freedom shown in figure A1 in the column matrix $\{q\}$ according to

$$\{q\} = \begin{Bmatrix} a_1 \\ b_1 \\ \phi_y \\ \phi_z \end{Bmatrix} \tag{A2}$$

the square matrices appearing in equation (A1) are given by

$$[\bar{M}] = \begin{bmatrix} I_R & 0 & I_R + \frac{1}{2} S_R\beta_o h_1 & 0 \\ 0 & I_R & 0 & I_R + \frac{1}{2} S_R\beta_o h_2 \\ I_R + \frac{1}{2} S_R\beta_o h_1 & 0 & M_p\bar{h}_1^2 + I_R + M_R h_1^2 + 2S_R\beta_o h_1 + I_{P,yy} & 0 \\ 0 & I_R + \frac{1}{2} S_R\beta_o h_2 & 0 & M_Y\bar{h}_2^2 + I_{P,zz} + I_R + M_R h_2^2 + 2S_R\beta_o h_2 \end{bmatrix} \tag{A3}^2$$

---

[2]The matrix expression given in equation (A3) is a special case of the more general eight-degree-of-freedom expression for $[\bar{M}]$ given in reference 15. Six of the precone terms which appear in this expression are incorrect (low by a factor of 2). The result given by equation (A3) reflects this correction.

APPENDIX A

$$[\Gamma] = \Omega \begin{bmatrix} 0 & 2I_R & 0 & 2I_R \\ -2I_R & 0 & -2I_R & 0 \\ 0 & 2I_R & 0 & 2I_R \\ -2I_R & 0 & -2I_R & 0 \end{bmatrix} \tag{A4}$$

$$[\bar{C}] = \begin{bmatrix} C_H & & & \\ & C_H & & \\ & & C_{\phi_y} & \\ & & & C_{\phi_z} \end{bmatrix} \tag{A5}$$

$$[\bar{K}] = \begin{bmatrix} K_H & \Omega C_H & & \\ -\Omega C_H & K_H & & \\ & & K_{\phi_y} & \\ & & & K_{\phi_z} \end{bmatrix} \tag{A6}$$

$$[AD] = \kappa \begin{bmatrix} -A_5/\Omega & A_4\lambda\beta_o/\Omega & -A_5/\Omega - A_2\lambda^2 h_1\beta_o/\Omega R & -A_3\lambda h_2/\Omega R + A_4\lambda\beta_o/\Omega \\ -A_4\lambda\beta_o/\Omega & -A_5/\Omega & A_3\lambda h_1/\Omega R - A_4\lambda\beta_o/\Omega & -A_5/\Omega - A_2\lambda^2 h_2\beta_o/\Omega R \\ -A_5/\Omega & A_4\lambda\beta_o/\Omega & -A_5/\Omega - A_2\lambda^2 h_1\beta_o/\Omega R & -A_3\lambda h_2/\Omega R + A_4\lambda\beta_o/\Omega \\ & + A_3 h_1\lambda/\Omega R & -A_1\lambda^2 h_1^2/\Omega R^2 & + A_3 h_1\lambda/\Omega R \\ -A_4\lambda\beta_o/\Omega & -A_5/\Omega & A_3\lambda h_1/\Omega R - A_4\lambda\beta_o/\Omega & -A_5/\Omega - A_2\lambda^2 h_2\beta_o/\Omega R \\ - A_3 h_2\lambda/\Omega R & & - A_3 h_2\lambda/\Omega R & - A_1\lambda^2 h_2^2/\Omega R^2 \end{bmatrix} \tag{A7}$$

APPENDIX A

$$[AS] = \kappa \begin{bmatrix} -B_3 \tan \delta_3 - A_4 \lambda \beta_0 & -A_5 + \lambda \beta_0 B_2 \tan \delta_3 & A_2 \lambda^3 \beta_0 & A_3 \lambda^2 \\ +A_5 - \lambda \beta_0 B_2 \tan \delta_3 & -B_3 \tan \delta_3 - \lambda \beta_0 A_4 & -A_3 \lambda^2 & A_2 \lambda^3 \beta_0 \\ -B_3 \tan \delta_3 - \lambda \beta_0 A_4 - A_3 h_1 \lambda / R & \lambda \beta_0 B_2 \tan \delta_3 - A_5 + (\lambda / R) B_1 h_1 \tan \delta_3 & A_2 \lambda^3 \beta_0 + A_1 \lambda^3 h_1 / R & A_3 \lambda^2 \\ A_5 - \lambda \beta_0 B_2 \tan \delta_3 & -B_3 \tan \delta_3 - \lambda \beta_0 A_4 & -A_3 \lambda^2 & A_2 \lambda^3 \beta_0 \\ -(\lambda / R) B_1 h_2 \tan \delta_3 & - A_3 h_2 \lambda / R & & + A_1 \lambda^3 h_2 / R \end{bmatrix} \tag{A8}$$

To facilitate comparison of the present equations with those of reference 15, the notation of that reference is maintained as much as possible.

The viscous damping coefficients C_H, C_{ϕ_y}, and C_{ϕ_z} appearing in $[\bar{C}]$ and $[\bar{K}]$ are evaluated from the expressions

$$\left.\begin{aligned} C_H &= 2 I_R \zeta_\beta \Omega \sqrt{1 + \frac{K_{H,eq}}{I_R \Omega^2}} \\ C_{\phi_y} &= 2 \zeta_p \omega_{p,o} I_{p,o} \\ C_{\phi_z} &= 2 \zeta_\gamma \omega_{\gamma,o} I_{\gamma,o} \end{aligned}\right\} \tag{A9}$$

where ζ_β, ζ_p, and ζ_γ are the damping ratios in flap, pitch, and yaw, respectively, $\omega_{p,o} = 2\pi f_{p,o}$, $\omega_{\gamma,o} = 2\pi f_{\gamma,o}$, and $I_{p,o}$ and $I_{\gamma,o}$ are the mass moments of inertia of the model in pitch and yaw with the blades locked to the forward flapping stops. The equivalent hub spring $K_{H,eq}$ is obtained from considerations given in appendix C.

It should be noted that the hub damping coefficient C_H appears in the stiffness matrix $[\bar{K}]$ as well as in the damping matrix $[\bar{C}]$. This is a consequence of the fact that the viscous structural damping associated with the flapping motion is regarded as being in the rotating system and the equations of motion are written with respect to a fixed or nonrotating system.

Transferring the aerodynamic matrices in equation (A1) to the left-hand side and combining matrices yields the resulting equations of motion in the form:

$$[M]\{\ddot{q}\} + [C]\{\dot{q}\} + [K]\{q\} = \{0\} \tag{A10}$$

where

$$[M] = [\bar{M}]$$
$$[C] = [\Gamma] - [AD] + [\bar{C}] \tag{A11}$$
$$[K] = [\bar{K}] - [AS]$$

The matrix $[M]$ is symmetric and positive definite; $[C]$ and $[K]$ are nonsymmetric. By premultiplying equation (A10) through by $[M]^{-1}$

$$[I]\{\ddot{q}\} + [M]^{-1}[C]\{\dot{q}\} + [M]^{-1}[K]\{q\} = \{0\} \tag{A12}$$

and introducing the four generalized velocities as auxiliary variables by means of the matrix identity

$$\{\dot{q}\} - \{\dot{q}\} = \{0\} \tag{A13}$$

equations (A12) and (A13) can be combined to yield

$$\left\{\begin{array}{c}\{\dot{q}\} \\ \hline \{\ddot{q}\}\end{array}\right\} = \left[\begin{array}{c:c} 0 & [I] \\ \hline -[M]^{-1}[K] & -[M]^{-1}[C]\end{array}\right]\left\{\begin{array}{c}\{q\} \\ \hline \{\dot{q}\}\end{array}\right\} \tag{A14}$$

By defining

$$\{X\} = \left\{\begin{array}{c}\{q\} \\ \hline \{\dot{q}\}\end{array}\right\} \tag{A15}$$

equation (A14) can be written in the compact form

$$\{\dot{X}\} = [A]\{X\} \tag{A16}$$

where the definition of $[A]$ follows from equation (A14). Note that the four original second-order equations have been transformed to eight first-order equations. By assuming a solution of the form

$$\{X\} = \{X_o\}e^{st} \tag{A17}$$

equation (A16) reduces to

$$[A]\{X_o\} = s\{X_o\} \tag{A18}$$

Equation (A18) is in standard eigenvalue form and is amenable to solution by using standard eigenvalue techniques.

The solution of equation (A18) leads to eight complex eigenvalues s_p and eigenvectors $\{X_o^{(p)}\}$. Since $[A]$ is real, the eigenvalues and eigenvectors occur in four complex conjugate pairs. Only roots having positive imaginary parts need be considered since the roots having negative imaginary parts do not pro-

vide any new linearly independent solutions. The pth complex eigenvalue having a positive imaginary part has the general form

$$s_p = \alpha_p + i\beta_p \tag{A19}$$

and can be interpreted as

$$s_p = -\zeta_p\omega_p + i\omega_p\sqrt{1 - \zeta_p^2} \tag{A20}$$

where ζ_p is the damping as a fraction of critical damping and ω_p is the undamped coupled frequency. For $\omega_p \neq 0$ if $\zeta_p\omega_p > 0$, the motion is exponentially divergent. By plotting (ζ_p,ω_p) as a function of velocity in the complex plane, a concise picture of the variation of system stability with airspeed can be established.

The complex vector associated with the eigenvalue s_p can be written in the form

$$\{X_o^{(p)}\} = \begin{Bmatrix} \{x^{(p)}\} \\ \hline s_p\{x^{(p)}\} \end{Bmatrix} \tag{A21}$$

The upper four elements $\{x^{(p)}\}$ in each modal vector of eight elements define the mode shape. Since these elements are complex, phase differences exist between the component harmonic motions in a given mode. The relative amplitude and phasing between the pylon pitching and yawing motions in a given mode can be ascertained by converting the complex elements of the mode to polar form and then normalizing on one of them.

APPENDIX A

Degrees of freedom

a_1 Longitudinal flapping of proprotor disc
b_1 Lateral flapping of proprotor disc
ϕ_y Pylon pitch rotation
ϕ_z Pylon yaw rotation

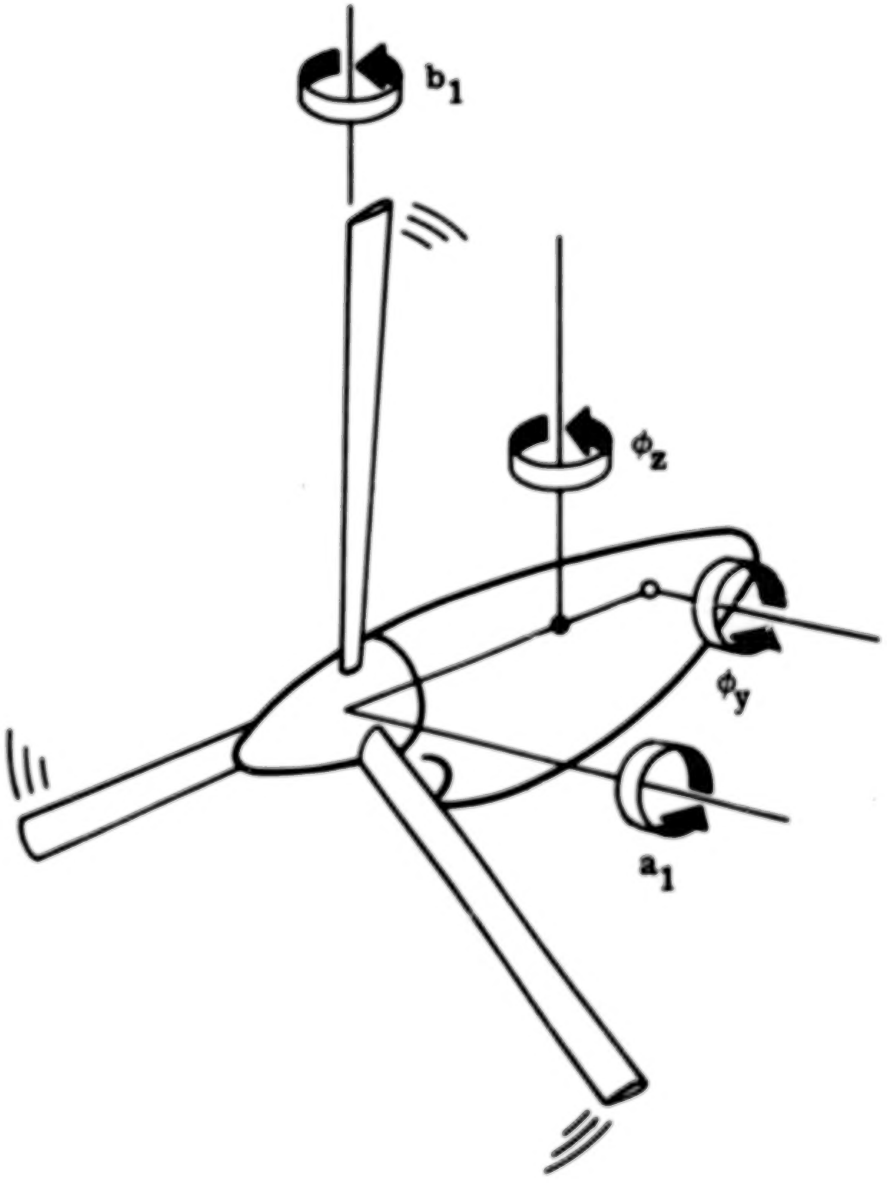

Figure A1.- Four-degree-of-freedom mathematical model for gimbaled proprotor (positive directions shown).

APPENDIX B

WHIRL FLUTTER EQUATIONS OF MOTION FOR PROPROTORS WITH HINGED BLADES

The linear equations of motion for the whirl flutter analysis of proprotors with hinged blades are given in reference 1 in the matrix form

$$[A]\{\ddot{q}\} + \Omega\left[[B] + [D]\right]\{\dot{q}\} + \left[\Omega^2\left[[C] + [E]\right] + [S]\right]\{q\} = \{0\} \tag{B1}$$

By arranging the four degrees of freedom indicated in figure B1 in sequential order in the matrix $\{q\}$, the square matrices appearing in equation (B1) (from appendix 5 of ref. 1) are given by

$$[A] = \begin{bmatrix} I_1 + a_1^2R^2M + I_P & 0 & I_2 & 0 \\ 0 & I_1 + a_2^2R^2M + I_Y & 0 & I_2 \\ I_2 & 0 & I_3 & 0 \\ 0 & I_2 & 0 & I_3 \end{bmatrix} \tag{B2}$$

$$[B] = K\begin{bmatrix} a_1^2H^2A_1 + A_5 & HA_3(a_1 - a_2) & A_5 - \epsilon A_4 & a_1H(A_3 - \epsilon A_2) \\ HA_3(a_1 - a_2) & a_2^2H^2A_1 + A_5 & -a_2H(A_3 - \epsilon A_2) & A_5 - \epsilon A_4 \\ A_5 - \epsilon A_4 & -a_2H(A_3 - \epsilon A_2) & A_\epsilon & 0 \\ a_1H(A_3 - \epsilon A_2) & A_5 - \epsilon A_4 & 0 & A_\epsilon \end{bmatrix} \tag{B3}$$

$$[D] = \begin{bmatrix} C_{q_1}/\Omega & -2I_1 & 0 & -2I_2 \\ 2I_1 & C_{q_2}/\Omega & 2I_2 & 0 \\ 0 & -2I_2 & C_R/\Omega & -2I_3 \\ 2I_2 & 0 & 2I_3 & C_R/\Omega \end{bmatrix} \tag{B4}$$

APPENDIX B

$$[C] = K\begin{bmatrix} -a_1H^3A_1 & H^2A_3 & a_1H(A_3 - \epsilon A_2) + B_3 \tan\delta_3 & -(A_5 - \epsilon A_4) + a_1HB_1 \tan\delta_3 \\ -H^2A_3 & -a_2H^3A_1 & (A_5 - \epsilon A_4) - a_2HB_1 \tan\delta_3 & a_2H(A_3 - \epsilon A_2) + B_3 \tan\delta_3 \\ 0 & H^2(A_3 - \epsilon A_2) & (B_3 - \epsilon B_2)\tan\delta_3 & -A_\epsilon \\ -H^2(A_3 - \epsilon A_2) & 0 & A_\epsilon & (B_3 - \epsilon B_2)\tan\delta_3 \end{bmatrix} \quad (B5)^3$$

$$[E] = \begin{bmatrix} 0 & 0 & 0 & 0 \\ 0 & 0 & 0 & 0 \\ 0 & 0 & eS & 0 \\ 0 & 0 & 0 & eS \end{bmatrix} \quad (B6)$$

$$[S] = \Omega^2\begin{bmatrix} \nu_1^2(I_1 + a_1^2R^2M + I_P) & 0 & 0 & 0 \\ 0 & \nu_2^2(I_1 + a_2^2R^2M + I_Y) & 0 & 0 \\ 0 & 0 & \nu_3^2I_3 & -C_R/\Omega \\ 0 & 0 & C_R/\Omega & \nu_3^2I_3 \end{bmatrix} \quad (B7)$$

The notation of reference 1 is maintained here for ease of comparison with the original work. However, several additional terms, not given in reference 1, have been included here to represent the pylon inertia (I_P and I_Y) and viscous-type structural damping for the pylon and rotor (C_{q_1}, C_{q_2}, and C_R). Also, to provide for a more realistic account of the lifting portion of the blade, the limits of integration in the aerodynamic integrals A_n and B_n were taken as η_1 and η_2 (as in the gimbaled proprotor equations) rather than ϵ and 1 (as in ref. 1).

---

[3] If flapping is defined about a line normal to the spanwise axis of the blade and lying in the plane of the hub as is customary, kinematic pitch-flap coupling appears as $\tan\delta_3$. Reference 1 obtained $\sin\delta_3$ because flapping was incorrectly defined there as being about the skewed flapping hinge.

APPENDIX B

The viscous damping coefficients C_R, C_{q_1}, and C_{q_2} appearing in [D] and [S] are evaluated from the expressions:

$$\left.\begin{aligned} C_R &= 2I_3\zeta_\beta\Omega\sqrt{1+\frac{eS}{I_3}} \\ C_{q_1} &= 2\zeta_p\omega_{p,o}I_{p,o} \\ C_{q_2} &= 2\zeta_\gamma\omega_{\gamma,o}I_{\gamma,o} \end{aligned}\right\} \tag{B8}$$

where ζ_β, ζ_p, and ζ_γ are the damping ratios in flap, pitch, and yaw, respectively, $\omega_{p,o} = 2\pi f_{p,o}$, $\omega_{\gamma,o} = 2\pi f_{\gamma,o}$, and $I_{p,o}$ and $I_{\gamma,o}$ are the mass moments of inertia of the model in pitch and yaw with the blades locked to the forward flapping stops.

Following reference 1, introducing the nondimensional time $\tau = \Omega t$ in equation (B1), and dividing by Ω^2 leads to

$$[A]\langle q\rangle'' + \left[[B]+[D]\right]\langle q\rangle' + \left[[C]+[E]+\frac{1}{\Omega^2}[S]\right]\langle q\rangle = \langle 0\rangle \tag{B9}$$

where

$$\left.\begin{aligned} q' &= \Omega\dot{q} \\ q'' &= \Omega^2\ddot{q} \end{aligned}\right\} \tag{B10}$$

By combining matrices in equation (B9), the equations of motion can be cast into the general form

$$[M]\langle q\rangle'' + [C]\langle q\rangle' + [K]\langle q\rangle = \langle 0\rangle \tag{B11}$$

where

$$\left.\begin{aligned} [M] &= [A] \\ [C] &= [B]+[D] \\ [K] &= [C]+[E]+\frac{1}{\Omega^2}[S] \end{aligned}\right\} \tag{B12}$$

By premultiplying equation (B11) through by $[K]^{-1}$

$$[K]^{-1}[M]\langle q\rangle'' + [K]^{-1}[C]\langle q\rangle' + [I]\langle q\rangle = \langle 0\rangle \tag{B13}$$[4]

---

[4]The equations of reference 1 employed here are cast into standard eigenvalue form by first premultiplying the matrix equation by the inverse of [K] rather than by the inverse of [M] as in appendix A. The choice is arbitrary.

and introducing the four generalized velocities as auxiliary variables by means of the matrix identity

$$\{q\}' - \{q\}' = \{0\} \tag{B14}$$

equations (B13) and (B14) can be combined to yield

$$\left\{\begin{array}{c}\{q\}' \\ \hline \{q\}\end{array}\right\} = \left[\begin{array}{c|c} 0 & [I] \\ \hline -[K]^{-1}[M] & -[K]^{-1}[C]\end{array}\right]\left\{\begin{array}{c}\{q\}'' \\ \hline \{q\}'\end{array}\right\} \tag{B15}$$

By defining

$$\{X\} = \left\{\begin{array}{c}\{q\}' \\ \hline \{q\}\end{array}\right\} \tag{B16}$$

equation (B15) can be written in the compact form

$$\{X\} = [A]\{X\}' \tag{B17}$$

where the definition of $[A]$ follows from equation (B15). Substituting the assumed solution

$$\{X\} = \{X_o\}e^{\lambda\tau} \tag{B18}$$

into equation (B17) reduces equation (B17) to

$$\{X_o\} = \lambda[A]\{X_o\} \tag{B19}$$

or, by rearranging, to the familiar standard eigenvalue form

$$[A]\{X_o\} = \bar{\lambda}\{X_o\} \tag{B20}$$

where

$$\lambda = 1/\bar{\lambda} \tag{B21}$$

Solution of equation (B20) leads to eight complex eigenvalues λ_p and eigenvectors $\{X_o^{(p)}\}$ which occur in four complex conjugate pairs. The pth complex eigenvalue having a positive imaginary part has the form

$$\lambda_p = \mu_p + i\nu_p \tag{B22}$$

and can be interpreted as

$$\lambda_p = -\frac{\omega_p\zeta_p}{\Omega} + i\,\frac{\omega_p\sqrt{1-\zeta_p^2}}{\Omega} \tag{B23}$$

where ω_p is the undamped coupled frequency and ζ_p is the damping as a fraction of critical damping.

APPENDIX B

The complex vector associated with the eigenvalue λ_p has the form

$$\left\{X_o^{(p)}\right\} = \left\{\begin{array}{c}\lambda_p\left\{x^{(p)}\right\} \\ \hline \left\{x^{(p)}\right\}\end{array}\right\} \tag{B24}$$

where the lower four elements $\left\{x^{(p)}\right\}$ in each modal vector of eight elements define the mode shape. As before, the relative amplitude and phasing between the pylon pitching and yawing motions in a given mode can be ascertained by converting the complex elements of the mode to polar form and then normalizing on one of them.

APPENDIX B

Degrees of freedom

q_1 Pylon pitch rotation

q_2 Pylon yaw rotation

q_3 Longitudinal flapping of proprotor disc

q_4 Lateral flapping of proprotor disc

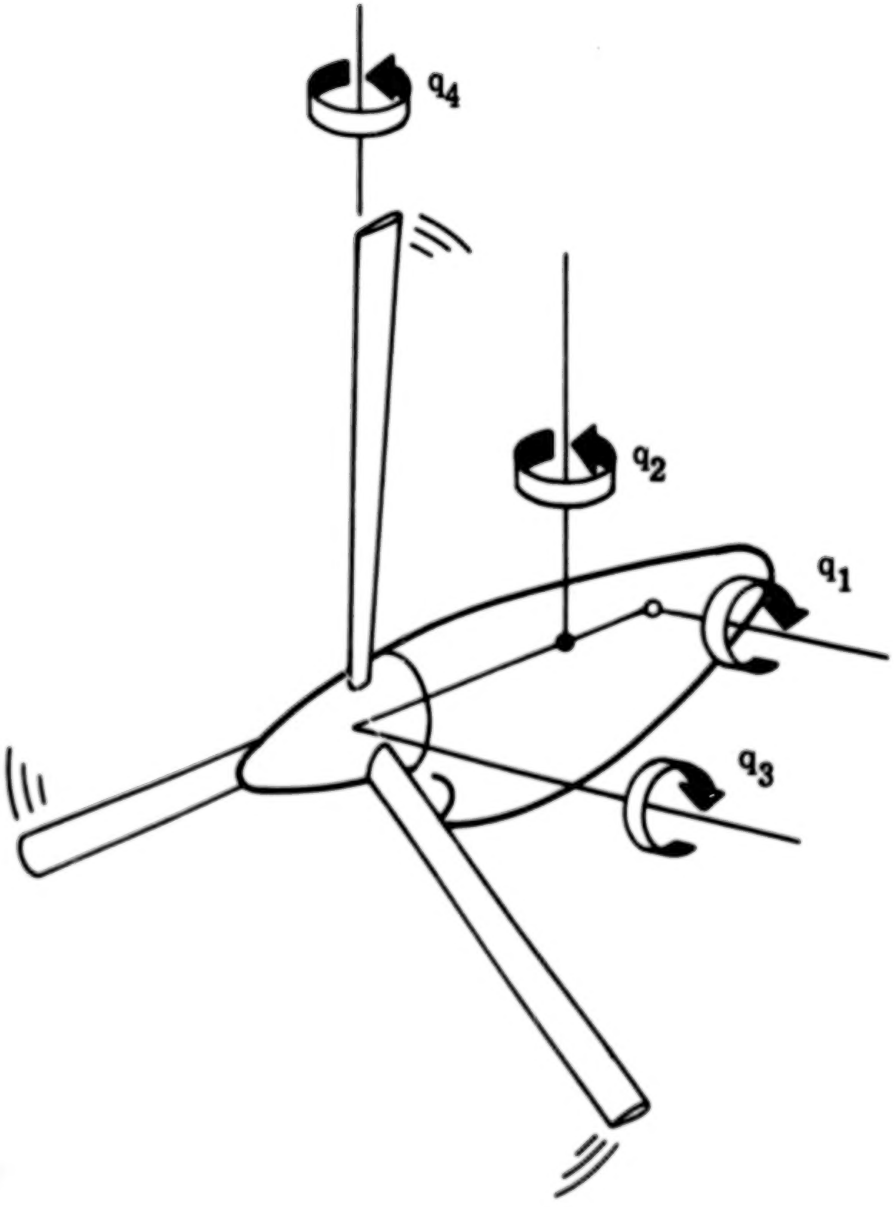

Figure B1.- Four-degree-of-freedom mathematical model for proprotor with offset flapping hinges (positive directions shown).

APPENDIX C

DETERMINATION OF EQUIVALENT HUB SPRING

Blade Flapping Natural Frequency

Gimbaled proprotor.- An expression for the blade flapping natural frequency can be derived from the equations of motion developed in appendix A by considering the degenerate case obtained by retaining only the two cyclic flapping degrees of freedom of the proprotor disc. If precone and structural damping are neglected, the resulting equations for the case of a symmetric hub restraint reduce to

$$I_R\ddot{a}_1 + 2I_R\Omega\dot{b}_1 + K_H a_1 = \frac{1}{2}\gamma\Omega^2 I_R\left[-B_3 a_1 \tan\delta_3 - \frac{A_5}{\Omega}\dot{a}_1 - A_5 b_1\right] \tag{C1a}$$

$$I_R\ddot{b}_1 - 2I_R\Omega\dot{a}_1 + K_H b_1 = -\frac{1}{2}\gamma\Omega^2 I_R\left[B_3 b_1 \tan\delta_3 + \frac{A_5}{\Omega}\dot{b}_1 - A_5 a_1\right] \tag{C1b}$$

Now, from reference 15, the flapping angle β of the reference blade is related to the cyclic flapping degrees of freedom of the proprotor disc by

$$\beta = a_1 \sin\psi - b_1 \cos\psi \tag{C2}$$

where $\psi = \Omega t$ is the azimuth angle of the reference blade. Multiplying equation (C1a) by $\sin\psi$ and equation (C1b) by $\cos\psi$, subtracting the second equation from the first, and making use of equation (C2) and the additional relations

$$\left.\begin{aligned}\dot{\beta} &= \dot{a}_1 \sin\psi - \dot{b}_1 \cos\psi + a_1\Omega\cos\psi + b_1\Omega\sin\psi \\ \ddot{\beta} &= \ddot{a}_1 \sin\psi - \ddot{b}_1 \cos\psi + 2\dot{a}_1\Omega\cos\psi + 2\dot{b}_1\Omega\sin\psi \\ &\quad - a_1\Omega^2\sin\psi + b_1\Omega^2\cos\psi\end{aligned}\right\} \tag{C3}$$

which follow from equation (C2), the resulting equation can be put into the form

$$\ddot{\beta} + \frac{1}{2}\gamma\Omega A_5\dot{\beta} + \left(\Omega^2 + \frac{K_H}{I_R} + \frac{1}{2}\gamma\Omega^2 B_3 \tan\delta_3\right)\beta = 0 \tag{C4}$$

From equation (C4) the undamped flapping natural frequency ω_β, nondimensionalized by the rotor rotational speed, is given by

$$\bar{\omega}_\beta \equiv \frac{\omega_\beta}{\Omega} = \left(1 + \frac{K_H}{I_R\Omega^2} + \frac{1}{2}\gamma B_3 \tan\delta_3\right)^{1/2} \tag{C5}$$

and the aerodynamic flap damping by

$$\zeta_\beta = \frac{\gamma A_5}{4\bar{\omega}_\beta} \tag{C6}$$

In the absence of hub restraint and pitch-flap coupling, the blade flapping natural frequency in the rotating system is equal to the rotational speed Ω, that is, one per revolution. The use of hub restraint in combination with positive or negative δ_3 raises or lowers the natural frequency from one per revolution. The effect of δ_3 on the blade flapping frequency is seen to be that of an aerodynamic spring which increases or decreases the frequency depending on whether δ_3 is positive or negative.

Proprotor with offset flapping hinges.- By using the equations of motion given in appendix B for a proprotor having hinged blades, the expressions analogous to equations (C5) and (C6) can be shown to be

$$\bar{\omega}_\beta = \left(1 + \frac{eS}{I_3} + \nu_3^2 + \frac{\gamma\epsilon}{2}(B_3 - \epsilon B_2)\tan\delta_3\right)^{1/2} \tag{C7}$$

$$\zeta_\beta = \frac{\gamma\epsilon}{4\bar{\omega}_\beta}(A_5 - 2\epsilon A_4 + \epsilon^2 A_3) \tag{C8}$$

where

$$\gamma_\epsilon = \frac{\rho a c R^4}{2I_3/N} \tag{C9}$$

is the Lock number defined by using the mass moment of inertia of the blade about the offset flapping hinge rather than about the center line of the shaft. By comparing equations (C5) and (C6) with equations (C7) and (C8), it is seen that several additional terms appear for the proprotor having noncentrally hinged blades. In the absence of flapping restraint, hinge offset, and pitch-flap coupling, the flapping natural frequency is one per revolution. The use of flapping restraint or hinge offset in combination with positive or negative δ_3 raises or lowers the natural frequency from one per revolution.

Basis of Establishing Equivalence

A gimbaled proprotor is essentially a proprotor having centrally hinged blades. On the supposition that an "equivalent" hub spring can be used to represent the inertial and aerodynamic restoring moment effects associated with an offset flapping hinge, analyses developed for the gimbaled proprotor would then also be applicable to proprotors having blades with offset flapping hinges, at least for preliminary design calculations. An equivalent hub spring can be established by requiring that the flapping natural frequency be preserved, that is, that

$$\bar{\omega}_\beta|_{\text{gimbaled}} = \bar{\omega}_\beta|_{\text{hinged}} \tag{C10}$$

This requirement implies that

$$\frac{K_H}{I_R\Omega^2} + \frac{1}{2}\gamma B_3 \tan\delta_3 = \frac{eS}{I_3} + \nu_3^2 + \frac{\gamma\epsilon}{2}(B_3 - \epsilon B_2)\tan\delta_3 \qquad \text{(C11)}$$

By approximating γ_ϵ by γ, equation (C11) leads to

$$\frac{K_H}{I_R\Omega^2} = \frac{eS}{I_3} + \nu_3^2 - \frac{1}{2}\gamma\epsilon B_2 \tan\delta_3 \qquad \text{(C12)}$$

so that the equivalent hub spring is given by

$$K_{H,eq} = I_R\Omega^2\left(\frac{eS}{I_3} + \nu_3^2 - \frac{1}{2}\gamma\epsilon B_2 \tan\delta_3\right) \qquad \text{(C13)}$$

For a given flapping hinge proprotor configuration, and a selected rotational speed and airspeed, the equivalent hub restraint is easily determined from equation (C13). It should be noted that a new equivalent hub restraint must be determined for each Ω,V combination.

The equivalent hub restraint given by equation (C13) was established by requiring that the flapping natural frequency be preserved while retaining both the dynamic and aerodynamic terms in the expressions for $\bar{\omega}_\beta$. An equivalent hub spring established on the basis of preserving the in-vacuum flapping natural frequency by discarding the aerodynamic terms in equation (C11) would not be satisfactory.

REFERENCES

1. Richardson, J. R.; and Naylor, H. F. W.: Whirl Flutter of Propellers With Hinged Blades. Rep. No. 24, Directorate Eng. Res., Defence Board (Canada), Mar. 1962.

2. Gallardo, Vincente, Jr.: Propeller-Nacelle Whirl Flutter Analysis of K-16B Amphibious VTOL/STOL Aircraft. Rep. No. G-113-41, Kaman Aircraft Corp., Aug. 1962.

3. Reed, Wilmer H., III; and Bennett, Robert M.: Propeller Whirl Considerations for V/STOL Aircraft. CAL/TRECOM Symposium Proceedings Vol II - Dynamic Load Problems Associated With Helicopters and V/STOL Aircraft, June 1963.

4. Reed, Wilmer H., III: Propeller-Rotor Whirl Flutter: A State-of-the-Art Review. J. Sound Vib., vol. 4, no. 3, Nov. 1966, pp. 526-544.

5. Reed, Wilmer H., III: Review of Propeller-Rotor Whirl Flutter. NASA TR R-264, 1967.

6. Hall, W. Earl: Prop-Rotor Stability at High Advance Ratios. J. American Helicopter Soc., vol. 11, no. 2, Apr. 1966, pp. 11-26.

7. Edenborough, H. Kipling: Investigation of Tilt-Rotor VTOL Aircraft Rotor-Pylon Stability. J. Aircr., vol. 5, no. 6, Mar.-Apr. 1968, pp. 97-105.

8. Young, Maurice I.; and Lytwyn, Roman T.: The Influence of Blade Flapping Restraint on the Dynamic Stability of Low Disk Loading Propeller-Rotors. J. American Helicopter Soc., vol. 12, no. 4, Oct. 1967, pp. 38-54.

9. Gaffey, T. M.; Yen, J. G.; and Kvaternik, R. G.: Analysis and Model Tests of the Proprotor Dynamics of a Tilt-Proprotor VTOL Aircraft. Proceedings of the V/STOL Technology and Planning Conference (Las Vegas, Nevada), Sept. 1969. (Available from DDC as AD 864 917.)

10. DeLarm, L. N.: Whirl Flutter and Divergence Aspects of Tilt-Wing and Tilt-Rotor Aircraft. Proceedings of the V/STOL Technology and Planning Conference (Las Vegas, Nevada), Sept. 1969. (Available from DDC as AD 864 917.)

11. Krishna Rao, K. V.; and Sundararajan, D.: Whirl Flutter of Flapped Blade Rotor Systems. NAL TN 18, National Aeronautical Lab. (Bangalore, India), Oct. 1969.

12. Scheiman, James: Analytical Investigation of the Tilt Rotor Whirl Instability. Ph.D. Thesis, Virginia Polytech. Inst. & State Univ., 1972.

13. Johnston, Robert A.: Parametric Studies of Instabilities Associated With Large, Flexible Rotor Propellers. Preprint No. 615, 28th Annual National Forum, American Helicopter Soc., May 1972.

14. Alexander, H. R.; and Leone, P. F.: V/STOL Dynamics and Aeroelastic Rotor-Airframe Technology. Volume I. State-of-the-Art Review of V/STOL Rotor Technology. AFFDL-TR-72-40, Volume I, U.S. Air Force, Jan. 1973.

15. Kvaternik, Raymond George: Studies in Tilt-Rotor VTOL Aircraft Aeroelasticity. Ph.D. Thesis, Case Western Reserve Univ., 1973.

16. Kaza, Krishna Rao Venkata: Effect of Steady State Coning Angle and Damping on Whirl Flutter Stability. J. Aircr., vol. 10, no. 11, Nov. 1973, pp. 664-669.

17. Kiessling, F.: Some Problems in Research on Whirl Flutter in V/STOL Aircraft. ESRO TT-160, May 1975. (Zur Problematik der Whirl-Flatteruntersuchungen von V/STOL-Flugzeugen. DFVLR DLR-FB 74-11, Feb. 1974.)

18. Baird, Eugene F.; Bauer, Elmer M.; and Kohn, Jerome S.: Model Tests and Analysis of Prop-Rotor Dynamics for Tilt-Rotor Aircraft. Status of Testing and Modeling Techniques for V/STOL Aircraft, American Helicopter Soc., Oct. 1972.

19. Kvaternik, Raymond G.: A Review of Some Tilt-Rotor Aeroelastic Research at NASA-Langley. J. Aircr., vol. 13, no. 5, May 1976, pp. 357-363.

TABLE I.- PHYSICAL PROPERTIES OF MODEL

	SI Units		U.S. Customary Units	
	e/R = 0.05	e/R = 0.13	e/R = 0.05	e/R = 0.13
Rotor:[a]				
Blade radius	0.744 m	0.805 m	2.44 ft	2.64 ft
Blade chord	0.0902 m	0.0902 m	0.296 ft	0.296 ft
Blade mass	0.533 kg	0.508 kg	0.0365 slug	0.0348 slug
Blade static moment about flapping hinge	0.111 kg-m	0.106 kg-m	0.025 slug-ft	0.0238 slug-ft
Blade moment of inertia about flapping hinge	0.0439 kg-m^2	0.0436 kg-m^2	0.0324 slug-ft^2	0.0322 slug-ft^2
Distance from pylon pitch axis to rotor hub	0.320 m	0.320 m	1.05 ft	1.05 ft
Distance from pylon yaw axis to rotor hub	0.277 m	0.277 m	0.91 ft	0.91 ft
Pylon:[b,c]				
Mass effective in pitch	3.37 (3.46) kg	3.87 kg	0.231 (0.237) slug	0.265 slug
Mass effective in yaw	3.01 kg	3.08 kg	0.206 slug	0.211 slug
Pitch inertia about center of gravity	0.0496 (0.0526) kg-m^2	0.0565 kg-m^2	0.0366 (0.0388) slug-ft^2	0.0417 slug-ft^2
Yaw inertia about center of gravity	0.0343 kg-m^2	0.0502 kg-m^2	0.0253 slug-ft^2	0.0370 slug-ft^2
Distance from pylon pitch axis to pylon center of gravity	0.212 (0.207) m	0.187 m	0.694 (0.679) ft	0.614 ft
Distance from pylon yaw axis to pylon center of gravity	0.193 m	0.168 m	0.632 ft	0.552 ft

[a]Blade inertial properties varied slightly from blade to blade. Values shown are average for the three blades.

[b]Pylon inertial properties include rotor hub but exclude blades.

[c]Values in parentheses reflect changes to pitch spring mechanism for runs 62 to 68.

TABLE II.- EXPERIMENTAL WHIRL FLUTTER RESULTS

Run	Point	e/R	δ_3, deg	$f_{p,o}$, Hz	$f_{\gamma,o}$, Hz	$2\zeta_p$	$2\zeta_\gamma$	n, Hz	ω_p/Ω	ω_γ/Ω	$V_F/\Omega R$	ω_F/Ω	Whirl		
													+ or -	A_F	ϕ_F, deg
40	26	0.05	20	5.60	5.80	0.024	0.051	13.3	0.444	0.462	0.78	0.42	+	1.66	72
	27	.05	20	5.60	5.80	.024	.051	14.0	.422	.439	.75	.39	+	1.47	82
41	6	.05	20	5.40	5.50	.024	.051	8.0	.712	.729	1.22	.66	+	1.48	61
	9	.05	20	5.40	5.50	.024	.051	11.1	.513	.525	.88	.50	+	1.64	65
	13	.05	20	5.40	5.50	.024	.051	17.0	.335	.343	.60	.34	+	1.54	72
42	6	.05	20	3.76	3.82	.012	.048	13.9	.285	.292	.56	.29	+	2.11	73
	8	.05	20	3.76	3.82	.012	.048	8.0	.496	.507	.76	.50	+	1.24	90
	12	.05	20	3.76	3.82	.012	.048	11.0	.361	.368	.60	.36	+	1.27	76
	15	.05	20	3.76	3.82	.012	.048	17.0	.233	.238	.44	.24	+	1.78	65
43	5	.05	20	3.74	5.70	.012	.046	8.0	.496	.760	1.12	.24	-	.58	-54
	7	.05	20	3.74	5.70	.012	.046	11.0	.360	.551	.81	.24	-	.35	-99
	8	.05	20	3.74	5.70	.012	.046	14.0	.281	.430	.56	.23	-	.19	-72
	12	.05	20	3.74	5.70	.012	.046	16.8	.235	.359	.47	.20	-	.24	-60
44	3	.05	30	3.74	3.90	.012	.048	8.0	.490	.513	.56	.56	+	1.36	65
	4	.05	30	3.74	3.90	.012	.048	10.8	.365	.383	.40	.41	+	1.76	61
45	4	.05	30	5.64	5.54	.019	.041	8.0	.748	.739	.78	.77	+	1.36	87
	8	.05	30	5.64	5.54	.019	.041	10.9	.545	.538	.55	.56	+	1.34	86
	10	.05	30	5.64	5.54	.019	.041	13.8	.431	.425	.41	.46	+	1.43	81
	11	.05	30	5.64	5.54	.019	.041	15.8	.377	.372	.38	.40	+	1.32	94
46	7	.05	30	6.76	6.78	.018	.021	10.9	.654	.659	.64	.70	+	2.05	68
	14	.05	30	6.76	6.78	.018	.021	14.0	.511	.515	.50	.54	+	1.96	68
	15	.05	30	6.76	6.78	.018	.021	17.0	.421	.424	.40	.46	+	1.97	97
	18	.05	30	6.76	6.78	.018	.021	10.8	.660	.666	.66	.70	+	1.95	75
48	9	.05	6.75	6.76	6.78	.013	.037	10.9	.363	.361	.82	.28	+	1.02	83
	11	.05	6.75	6.76	6.78	.013	.037	13.8	.286	.286	.59	.23	-	1.24	-61
	15	.05	6.75	6.76	6.78	.013	.037	16.9	.235	.234	.51	.18	-	2.06	-69

TABLE II.- Continued

Run	Point	e/R	δ_3, deg	$f_{P,o}$, Hz	$f_{Y,o}$, Hz	$2\zeta_P$	$2\zeta_Y$	n, Hz	ω_P/Ω	ω_Y/Ω	$V_P/\Omega R$	ω_F/Ω	Whirl		
													+ or -	A_P	ϕ_F, deg
50	11	0.05	6.75	5.54	5.34	0.005	0.049	16.9	0.347	0.336	0.74	0.28	+	1.07	80
51	14	.13	20	5.30	4.65	.011	.055	10.8	.518	.456	.92	.21	-	NA	NA
	22	.13	20	5.30	4.65	.011	.055	14.1	.397	.350	.72	.16	-	NA	NA
52	9	.13	20	5.30	4.65	.027	.088	16.6	.335	.296	.65	.13	-	2.01	-76
53	9	.13	20	3.72	3.56	.009	.034	10.9	.360	.347	.73	.16	-	NA	NA
	12	.13	20	3.72	3.56	.009	.034	13.9	.283	.271	.60	.12	-	NA	NA
	17	.13	20	3.72	3.56	.009	.034	16.8	.234	.225	.50	.10	-	NA	NA
	19	.13	20	3.72	3.56	.009	.034	7.8	.506	.486	.92	.22	-	NA	NA
54	7	.13	10.5	3.72	3.52	.013	.040	8.0	.410	.466	1.01	.19	-	NA	NA
55	13	.05	20	3.70	3.58	.013	.040	11.1	.351	.341	.42	.38	+	.68	98
	15	.05	20	3.70	3.58	.013	.040	13.8	.283	.274	.34	.30	+	.50	81
56	2	.05	20	3.75	3.56	.013	.037	10.9	.363	.347	.38	.38	+	.66	87
	3	.05	20	3.75	3.56	.013	.037	13.2	.300	.286	.34	.31	+	.96	75
	7	.05	20	3.75	3.56	.013	.037	8.0	.495	.472	.53	.51	+	.65	101
57	14	.05	20	3.72	3.82	.008	.031	8.0	.490	.507	.68	.50	+	.75	64
	15	.05	20	3.72	3.82	.008	.031	10.1	.353	.365	.44	.37	+	.82	63
	17	.05	20	3.72	3.82	.008	.031	14.2	.276	.285	.34+	.30	+	.73	63
	18	.05	20	3.72	3.82	.008	.031	15.2	.257	.265	.34-	.27	+	.67	95
58	8	.05	20	3.72	5.60	.008	.061	8.0	.487	.727	1.08	.23	-	.28	-87
	12	.05	20	3.72	5.60	.008	.061	11.1	.353	.527	.79	.23	-	.19	-88
	15	.05	20	3.72	5.60	.008	.061	14.2	.276	.412	.55	.22	-	.15	-60
60	4	.05	20	5.48	5.44	.010	.049	11.0	.525	.524	.61	.54	+	.46	86
	6	.05	20	5.48	5.44	.010	.049	14.0	.412	.411	.46	.42	+	.45	97
	8	.05	20	5.48	5.44	.010	.049	16.9	.342	.341	.36	.37	+	.53	75

TABLE II.- Concluded

Run	Point	e/R	δ_3, deg	$f_{P,o}$, Hz	$f_{Y,o}$, Hz	$2\zeta_P$	$2\zeta_Y$	n, Hz	ω_P/Ω	ω_Y/Ω	$V_P/\Omega R$	ω_P/Ω	Whirl		
													+ or -	A_P	ϕ_P, deg
62	5	0.05	20	5.40	5.68	0.017	0.034	8.1	0.704	0.743	1.13	0.68	+	NA	NA
	9	.05	20	5.40	5.68	.017	.034	11.2	.508	.537	.76	.51	+	NA	NA
	10	.05	20	5.40	5.68	.017	.034	14.1	.404	.427	.56	.42	+	NA	NA
	11	.05	20	5.40	5.68	.017	.034	17.3	.329	.348	.46	.35	+	NA	NA
63	12	.05	20	7.06	7.40	.022	.034	11.2	.664	.700	1.07	.64	+	.52	83
	13	.05	20	7.06	7.40	.022	.034	14.2	.526	.554	.81	.50	+	.67	65
	20	.05	20	7.06	7.40	.022	.034	17.4	.429	.452	.66	.44	+	.63	90
	27	.05	20	7.06	7.40	.022	.034	9.0	.827	.871	1.36	.78	+	.58	65
64	6	.05	20	4.00	3.96	.024	.044	8.2	.517	.514	.67	.53	+	.61	104
	8	.05	20	4.00	3.96	.024	.044	11.2	.377	.375	.46	.40	+	.62	65
	9	.05	20	4.00	3.96	.024	.044	14.2	.298	.297	.36	.32	+	.60	72
	11	.05	20	4.00	3.96	.024	.044	15.2	.278	.277	.35	.31	+	.60	79
65	15	.05	20	4.60	3.96	.024	.044	8.2	.592	.512	1.06	.50	+	NA	NA
	22	.05	20	4.60	3.96	.024	.044	11.1	.437	.378	.75	.36	+	NA	NA
	31	.05	20	4.60	3.96	.024	.044	14.3	.341	.294	.61	.29	+	NA	NA
	36	.05	20	4.60	3.96	.024	.044	17.2	.282	.244	.50	.26	+	NA	NA
	39	.05	20	4.60	3.96	.024	.044	17.1	.284	.246	.54	.24	+	NA	NA
66	14	.05	20	4.04	15.8	.032	.044	8.2	.520	2.04	1.23	.27	-	NA	NA
	18	.05	20	4.04	15.8	.032	.044	11.2	.381	1.50	.87	.25	-	NA	NA
	21	.05	20	4.04	15.8	.032	.044	14.2	.300	1.18	.62	.24	-	NA	NA
67	11	.05	20	4.04	7.55	.024	.039	11.2	.382	.718	.87	.24	-	.07	-43
	13	.05	20	4.04	7.55	.024	.039	14.2	.300	.564	.61	.23	-	.06	-61
	16	.05	20	4.04	7.55	.024	.039	17.2	.247	.464	.50	.20	-	.08	-39
68	6	.05	20	6.75	3.66	.021	.065	11.1	.641	.350	.78	.21	-	4.75	-97
	12	.05	20	6.75	3.66	.021	.065	14.2	.503	.273	.60	.20	-	7.28	-112
	18	.05	20	6.75	3.66	.021	.065	16.6	.429	.233	.52	.17	-	5.35	-93

TABLE III.- ANALYTICAL WHIRL FLUTTER RESULTS

Run	Point	Theory (ref. 15)							Theory (ref. 1)						
		ω_p/Ω	ω_γ/Ω	$V_F/\Omega R$	ω_F/Ω	Whirl			ω_p/Ω	ω_γ/Ω	$V_F/\Omega R$	ω_F/Ω	Whirl		
						+ or -	A_F	ϕ_F, deg					+ or -	A_F	ϕ_F, deg
40	26	0.444	0.463	0.76	0.44	+	1.32	110	0.446	.465	0.75	0.45	+	1.29	109
	27	.422	.440	.72	.42	+	1.33	109	.424	.441	.70	.43	+	1.30	108
41	6	.712	.730	1.26	.68	+	1.10	102	.715	.733	1.24	.70	+	1.11	103
	9	.513	.526	.86	.50	+	1.16	105	.515	.528	.85	.52	+	1.17	105
	13	.335	.343	.52	.34	+	1.32	109	.336	.345	.52	.35	+	1.29	108
42	6	.285	.292	.42	.30	+	1.36	114	.288	.293	.41	.31	+	1.29	110
	8	.496	.507	.78	.49	+	1.15	109	.498	.509	.77	.50	+	1.15	108
	12	.361	.368	.54	.37	+	1.28	112	.362	.370	.52	.38	+	1.25	111
	15	.233	.238	.35	.25	+	1.39	112	.234	.239	.35	.26	+	1.29	109
43	5	.496	.761	1.11	.29	-	.23	-106	.498	.764	1.09	.28	-	.26	-102
	7	.360	.551	.70	.28	-	.15	-103	.361	.554	.72	.27	-	.18	-110
	8	.281	.430	.45	.26	-	.10	-118	.282	.432	.48	.25	-	.14	-114
	12	.235	.360	.36	.22	-	.09	-119	.236	.362	.40	.21	-	.14	-114
44	3	.490	.514	.62	.53	+	1.33	122	.492	.516	.61	.54	+	1.29	119
	4	.365	.383	.42	.40	+	1.46	122	.367	.385	.42	.41	+	1.37	118
45	4	.749	.739	.86	.79	+	.99	99	.751	.743	.84	.79	+	1.01	98
	8	.546	.539	.54	.58	+	1.02	103	.548	.542	.53	.59	+	1.04	102
	10	.431	.426	.37	.47	+	1.04	106	.433	.428	.37	.48	+	1.05	104
	11	.377	.372	.31	.41	+	1.05	105	.378	.374	.31	.42	+	1.06	105
46	7	.656	.658	.64	.71	+	1.25	111	.659	.661	.63	.72	+	1.23	109
	14	.513	.514	.44	.56	+	1.30	118	.515	.516	.43	.57	+	1.28	113
	15	.422	.423	.32	.47	+	1.34	116	.424	.425	.29	.47	+	1.27	113
	18	.662	.664	.65	.71	+	1.23	110	.665	.667	.64	.72	+	1.23	109

TABLE III.- Continued

Run	Point	Theory (ref. 15)							Theory (ref. 1)						
		ω_p/Ω	ω_Y/Ω	$V_p/\Omega R$	ω_p/Ω	Whirl			ω_p/Ω	ω_Y/Ω	$V_p/\Omega R$	ω_p/Ω	Whirl		
						+ or -	A_p	ϕ_p, deg					+ or -	A_p	ϕ_p, deg
48	9	0.363	0.362	0.73	0.29	-	1.02	-111	0.364	0.364	0.75	0.27	-	1.11	-107
				.85	.27	+	.92	103			.84	.28	+	.94	99
	11	.287	.286	.50	.26	-	.52	-108	.288	.287	.55	.24	-	.88	-113
				.66	.22	+	1.09	106			.65	.23	+	1.07	102
	15	.236	.235	.41	.22	-	.36	-100	.236	.236	.45	.21	-	.76	-119
				.56	.18	+	1.26	106			.55	.19	+	1.20	104
50	11	.347	.330	.70	.25	-	2.36	-125	.348	.331	.71	.24	-	2.10	-115
				.73	.28	+	.47	116			.73	.29	+	.55	105
51	14	.516	.455	.93	.23	-	1.79	-103	.518	.457	.86	.24	-	1.69	-112
	22	.395	.348	.75	.18	-	1.84	-108	.396	.350	.69	.19	-	1.71	-104
52	9	.335	.295	.67	.15	-	1.81	-112	.336	.296	.62	.16	-	1.68	-105
53	9	.359	.345	.72	.18	-	1.37	-104	.360	.346	.66	.19	-	1.32	-100
	12	.281	.271	.60	.14	-	1.38	-105	.282	.272	.55	.14	-	1.32	-100
	17	.233	.224	.52	.11	-	1.36	-105	.234	.225	.48	.11	-	1.31	-100
	19	.505	.485	.95	.24	-	1.31	-100	.506	.487	.87	.25	-	1.30	-99
54	7	.489	.465	1.07	.19	-	1.52	-110	.490	.467	1.01	.21	-	1.45	-105
55	13	.352	.342	.41	.37	+	.91	99	.353	.344	.40	.38	+	.96	99
	15	.283	.275	.33	.30	+	.94	102	.284	.276	.33	.31	+	.99	100
56	2	.363	.347	.41	.38	+	.77	87	.364	.348	.39	.39	+	.83	89
	3	.300	.286	.33	.32	+	.79	91	.301	.287	.33	.32	+	.87	92
	7	.495	.472	.65	.50	+	.77	82	.496	.474	.61	.51	+	.81	84

TABLE III.- Continued

Run	Point	Theory (ref. 15)							Theory (ref. 1)						
		ω_p/Ω	ω_Y/Ω	$V_F/\Omega R$	ω_F/Ω	Whirl			ω_p/Ω	ω_Y/Ω	$V_F/\Omega R$	ω_F/Ω	Whirl		
						+ or -	A_F	ϕ_F, deg					+ or -	A_F	ϕ_F, deg
57	14	0.491	0.507	0.74	0.50	+	1.38	116	0.492	0.509	0.72	0.51	+	1.33	114
	15	.354	.365	.50	.37	+	1.52	116	.355	.367	.48	.38	+	1.46	116
	17	.276	.285	.38	.30	+	1.62	116	.277	.286	.38	.30	+	1.46	113
	18	.257	.266	.36	.28	+	1.60	114	.258	.267	.36	.28	+	1.45	113
58	8	.488	.738	1.09	.28	-	.24	-108	.489	.741	1.07	.27	-	.25	-99
	12	.354	.535	.67	.29	-	.14	-116	.355	.538	.70	.28	-	.18	-112
	15	.276	.419	.44	.26	-	.10	-120	.277	.420	.48	.24	-	.14	-116
60	4	.526	.525	.78	.52	+	.99	102	.527	.527	.76	.54	+	1.01	103
	6	.413	.412	.57	.42	+	1.04	108	.414	.414	.56	.43	+	1.06	107
	8	.342	.342	.46	.36	+	1.09	110	.343	.343	.45	.36	+	1.09	109
62	5	.703	.744	1.26	.70	+	1.32	114	.706	.747	1.24	.70	+	1.30	112
	9	.509	.538	.87	.51	+	1.45	114	.510	.540	.85	.52	+	1.42	113
	10	.404	.427	.66	.41	+	1.76	114	.405	.429	.66	.42	+	1.53	113
	11	.329	.348	.51	.35	+	1.75	115	.330	.350	.51	.36	+	1.65	115
63	12	.664	.700	1.18	.65	+	1.31	110	.666	.703	1.16	.67	+	1.31	110
	13	.526	.555	.90	.52	+	1.41	112	.528	.557	.88	.54	+	1.38	111
	20	.429	.452	.70	.44	+	1.52	104	.431	.454	.69	.45	+	1.48	111
	27	.828	.872	1.50	.81	+	1.27	109	.830	.876	1.48	.82	+	1.26	109
64	6	.517	.514	.80	.52	+	1.05	98	.518	.517	.78	.52	+	1.06	97
	8	.377	.375	.53	.39	+	1.10	102	.378	.377	.52	.39	+	1.10	98
	9	.298	.297	.41	.31	+	1.16	104	.299	.298	.41	.32	+	1.15	102
	11	.279	.277	.38	.29	+	1.17	104	.279	.279	.38	.30	+	1.16	103

TABLE III.- Concluded

Run	Point	Theory (ref. 15)							Theory (ref. 1)						
		ω_p/Ω	ω_Y/Ω	$V_F/\Omega R$	ω_F/Ω	Whirl			ω_p/Ω	ω_Y/Ω	$V_F/\Omega R$	ω_F/Ω	Whirl		
						+ or -	A_F	ϕ_F, deg					+ or -	A_F	ϕ_F, deg
65	15	0.592	0.512	1.07	0.52	+	0.59	73	0.594	0.515	1.04	0.54	+	0.62	65
				1.09	.27	-	2.00	-89			1.06	.26	-	1.95	-89
	22	.437	.379	.71	.40	+	.50	65	.439	.380	.69	.42	+	.54	65
				.77	.26	-	2.30	-87			.76	.26	-	2.17	-88
	31	.339	.294	.48	.33	+	.47	69	.340	.295	.47	.34	+	.53	68
				.56	.23	-	2.57	-87			.57	.22	-	2.30	-90
	36	.282	.244	.38	.28	+	.44	69	.283	.245	.38	.29	+	.56	71
				.45	.20	-	2.67	-91			.47	.20	-	2.33	-93
	39	.284	.246	.38	.28	+	.44	68	.285	.247	.38	.29	+	.56	71
				.46	.21	-	2.67	-90			.47	.20	-	2.33	-93
66	14	.520	2.044	1.19	.30	-	.02	-108	.522	2.053	1.19	.29	-	.02	-102
	18	.381	1.497	.78	.29	-	.02	-111	.382	1.503	.79	.28	-	.02	-107
	21	.300	1.181	.54	.26	-	.01	-112	.301	1.186	.56	.25	-	.01	-110
67	11	.382	.718	.78	.27	-	.09	-105	.384	.722	.79	.28	-	.10	-107
	13	.300	.564	.53	.26	-	.06	-112	.301	.567	.56	.25	-	.08	-110
	16	.247	.464	.40	.22	-	.06	-105	.248	.466	.44	.22	-	.08	-111
68	6	.642	.350	.72	.25	-	11.8	-84	.644	.351	.73	.25	-	10.2	-86
	12	.503	.274	.54	.22	-	14.0	-86	.504	.275	.56	.22	-	11.5	-88
	18	.429	.234	.45	.20	-	14.9	-89	.430	.235	.48	.19	-	12.9	-90

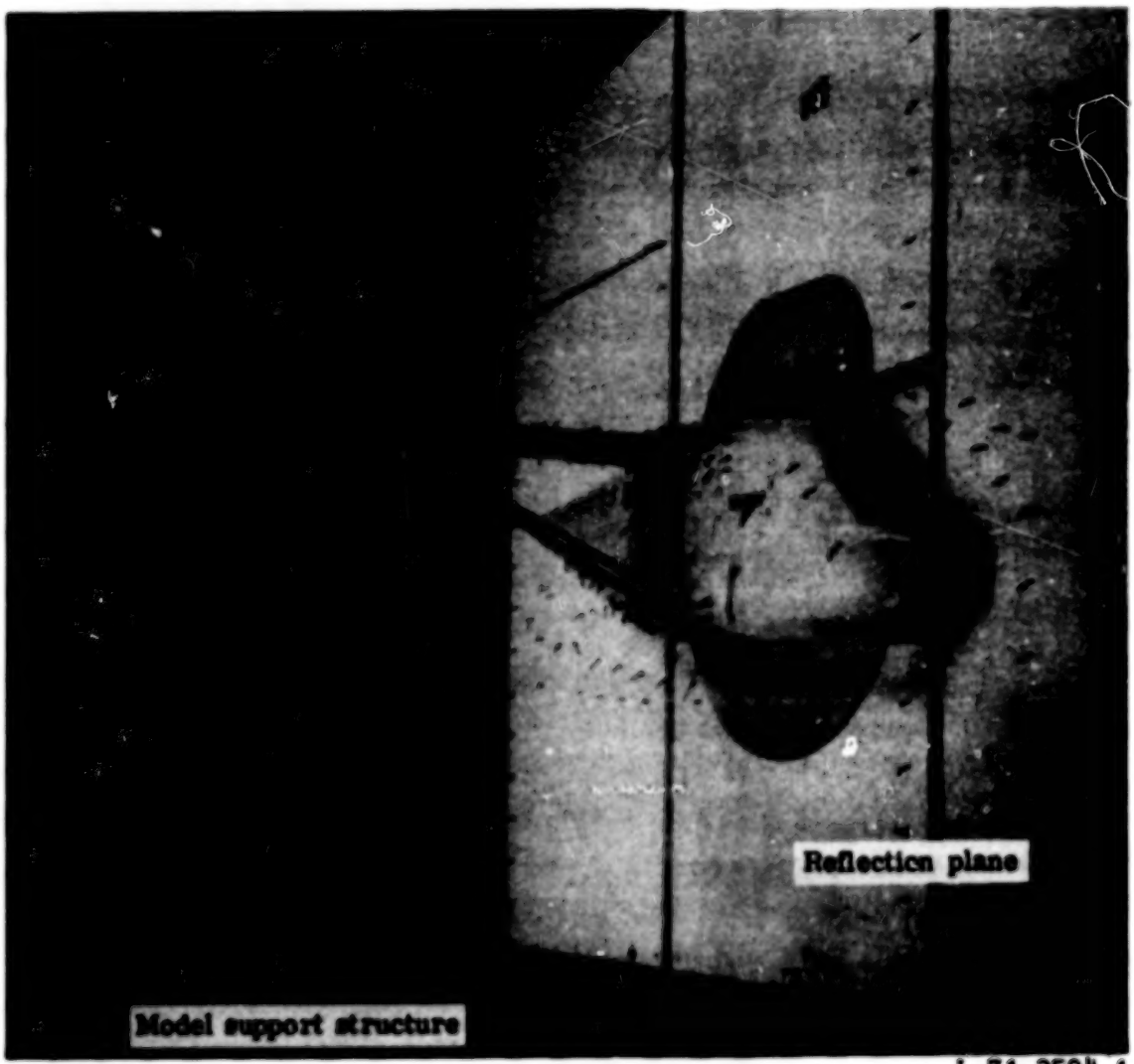

L-71-3504.1

Figure 1.- Overall view of whirl flutter model with 5-percent hinge offset in Langley transonic dynamics tunnel.

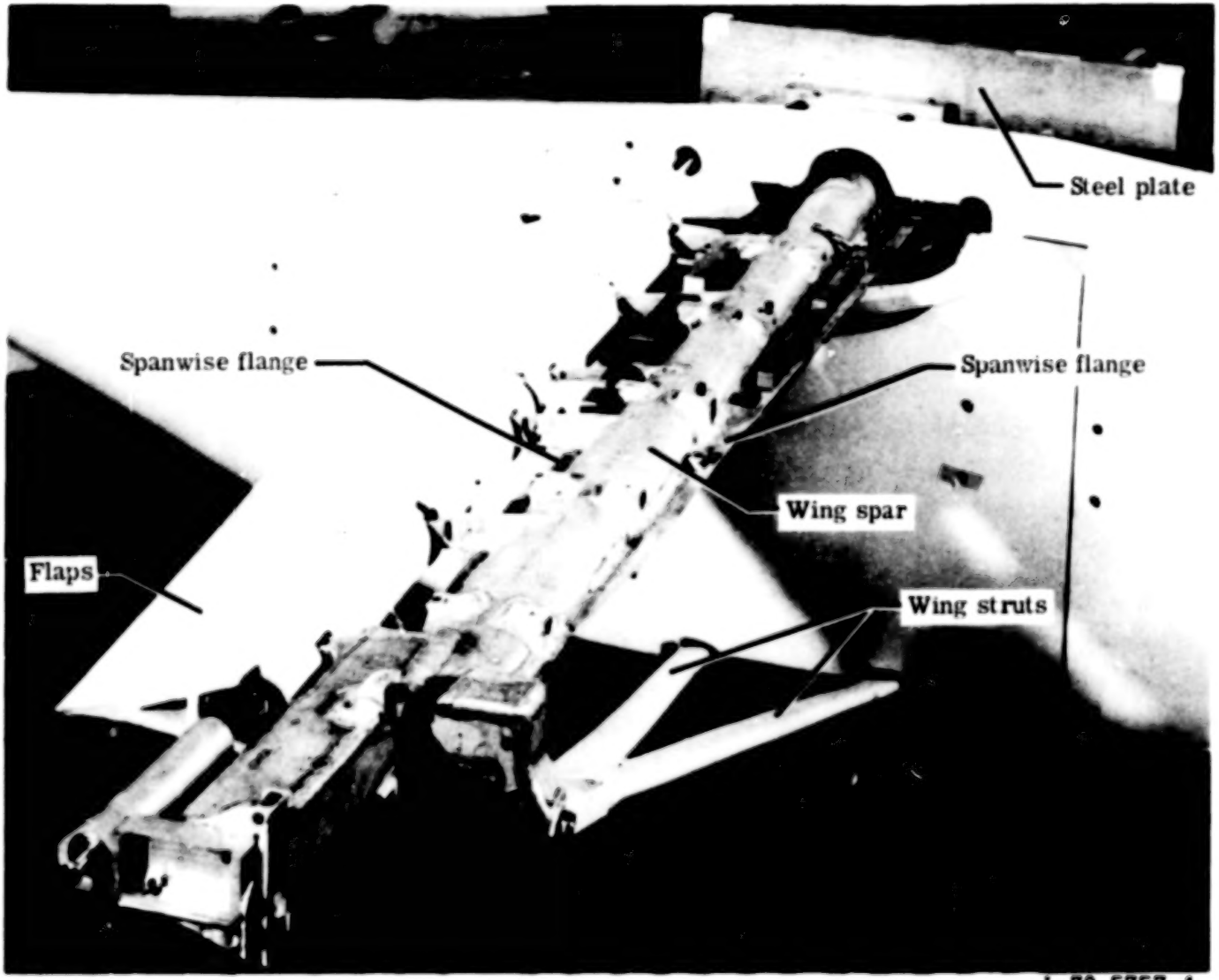

Figure 2.- Details of wing spar construction.

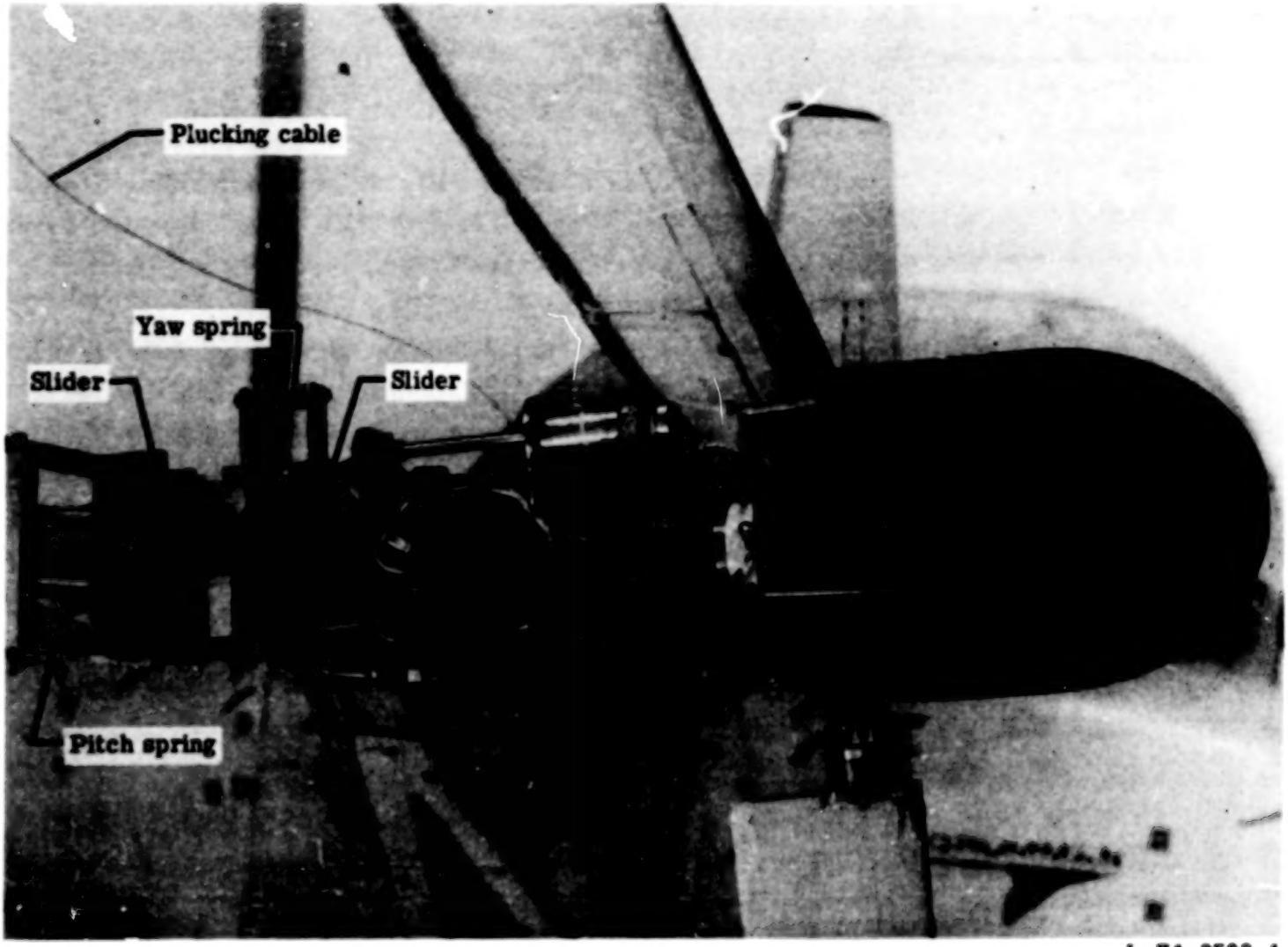

L-71-3503.1

Figure 3.- Close-up view of model pylon with 5-percent hinge offset.

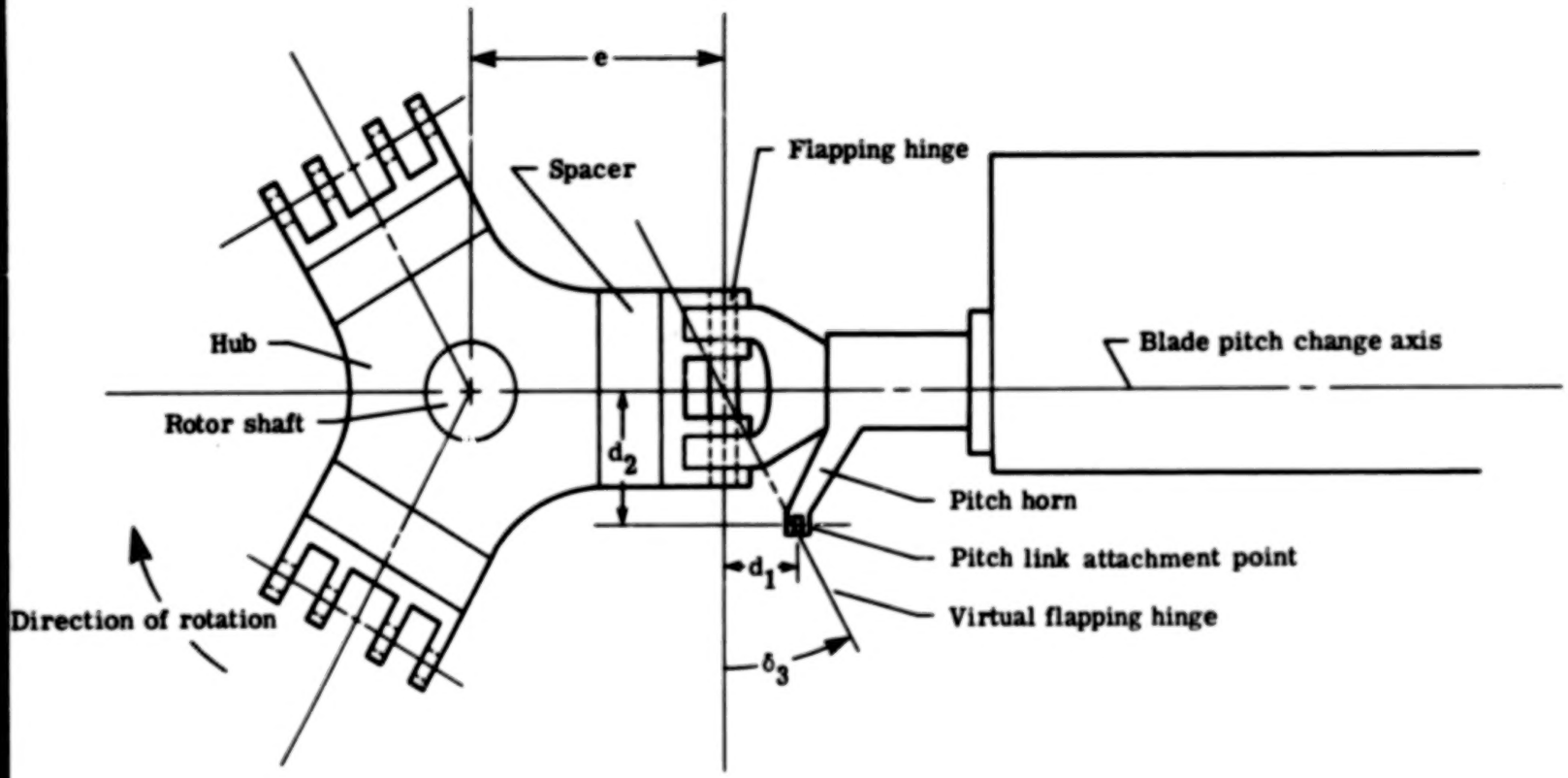

Figure 4.- Hub and control system geometry. Figure is not to scale and pitch horn is in plane of hub. $\delta_3 = \tan^{-1}(d_1/d_2)$.

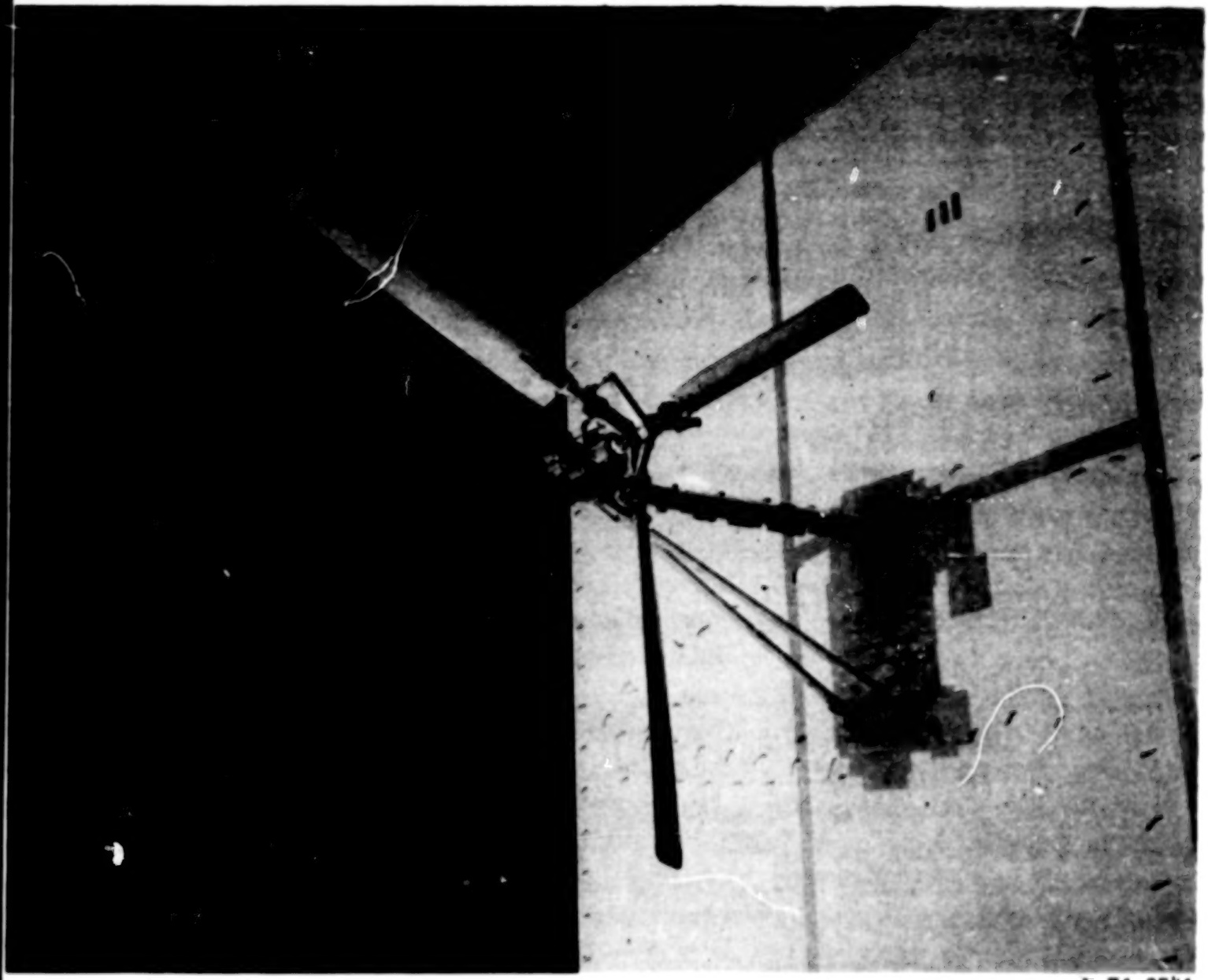

L-71-3541

Figure 5.- Overall view of model with 13-percent hinge offset.

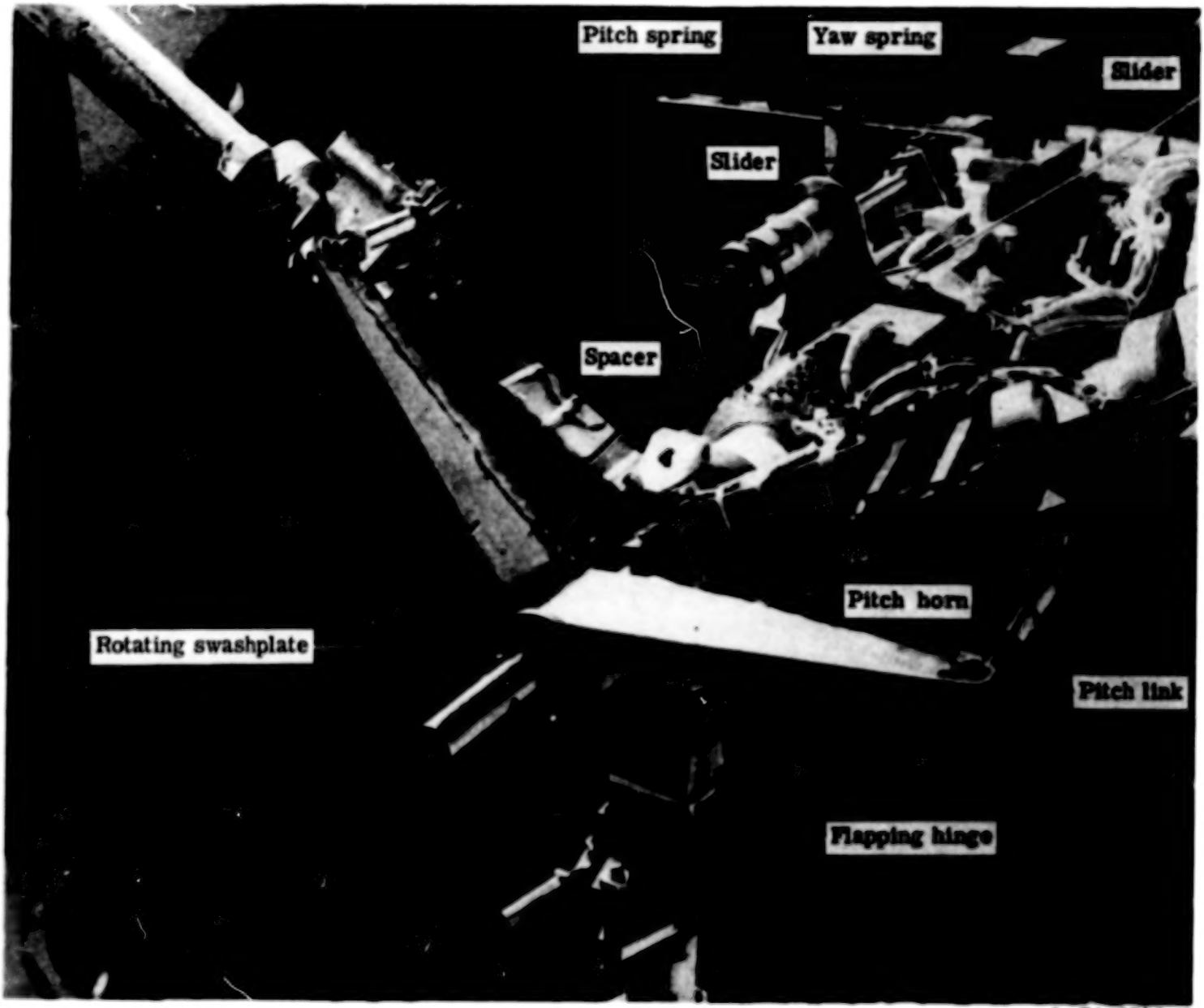

L-71-3540.1

Figure 6.- Close-up view of model pylon with 13-percent hinge offset.

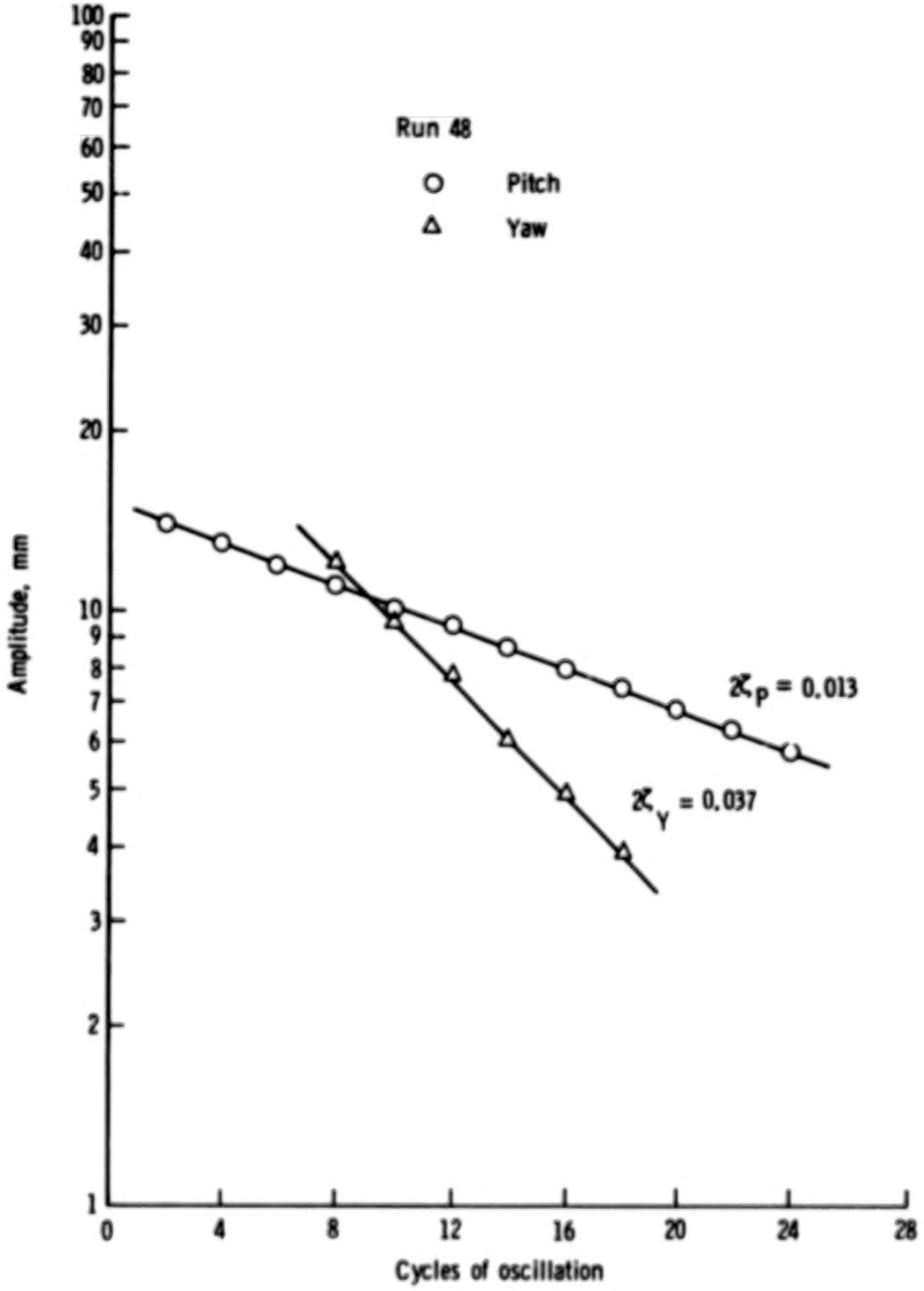

Figure 7.- Typical plots showing decay of free oscillation.

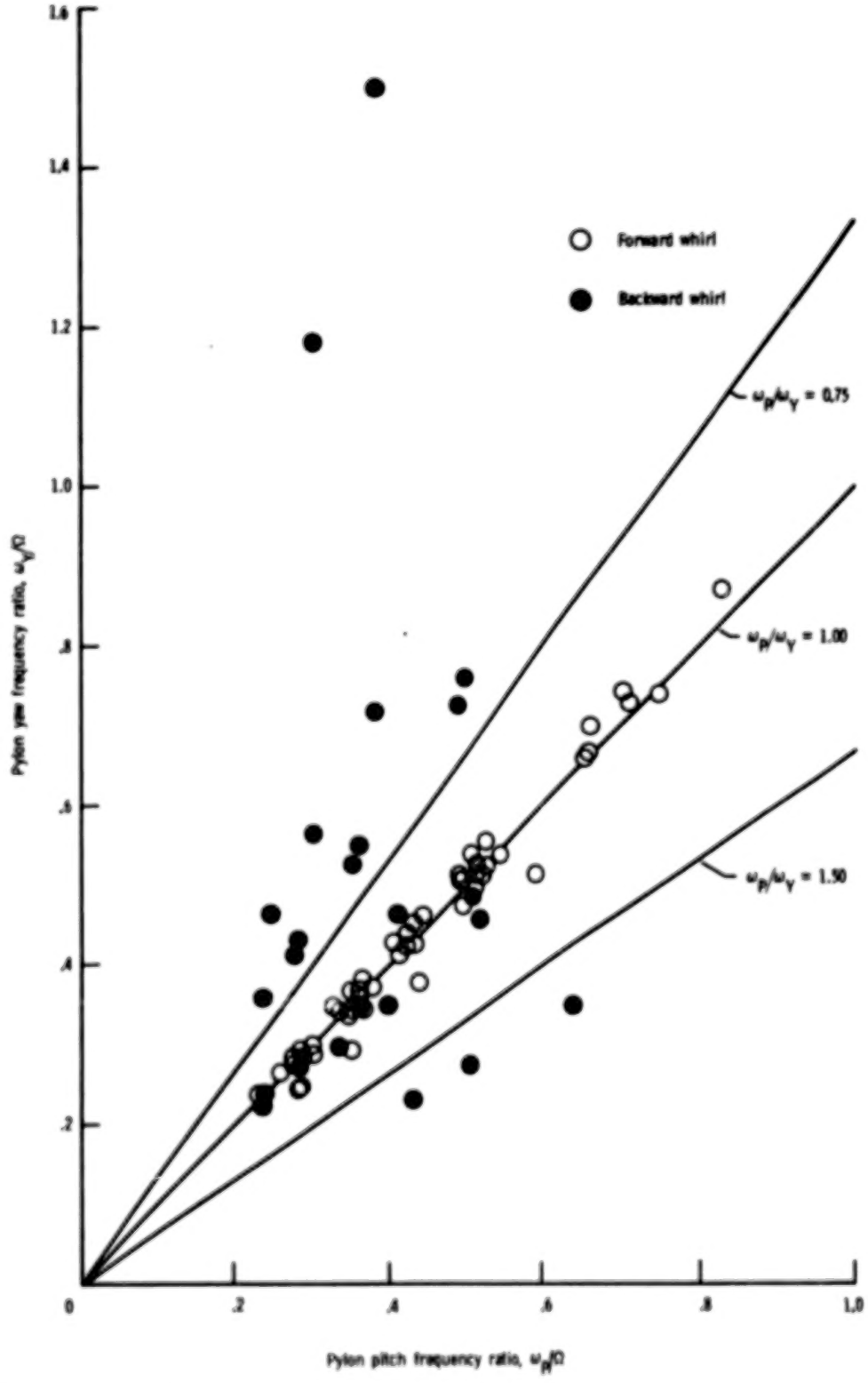

Figure 8.- Summary plot of all experimentally identified whirl flutter points.

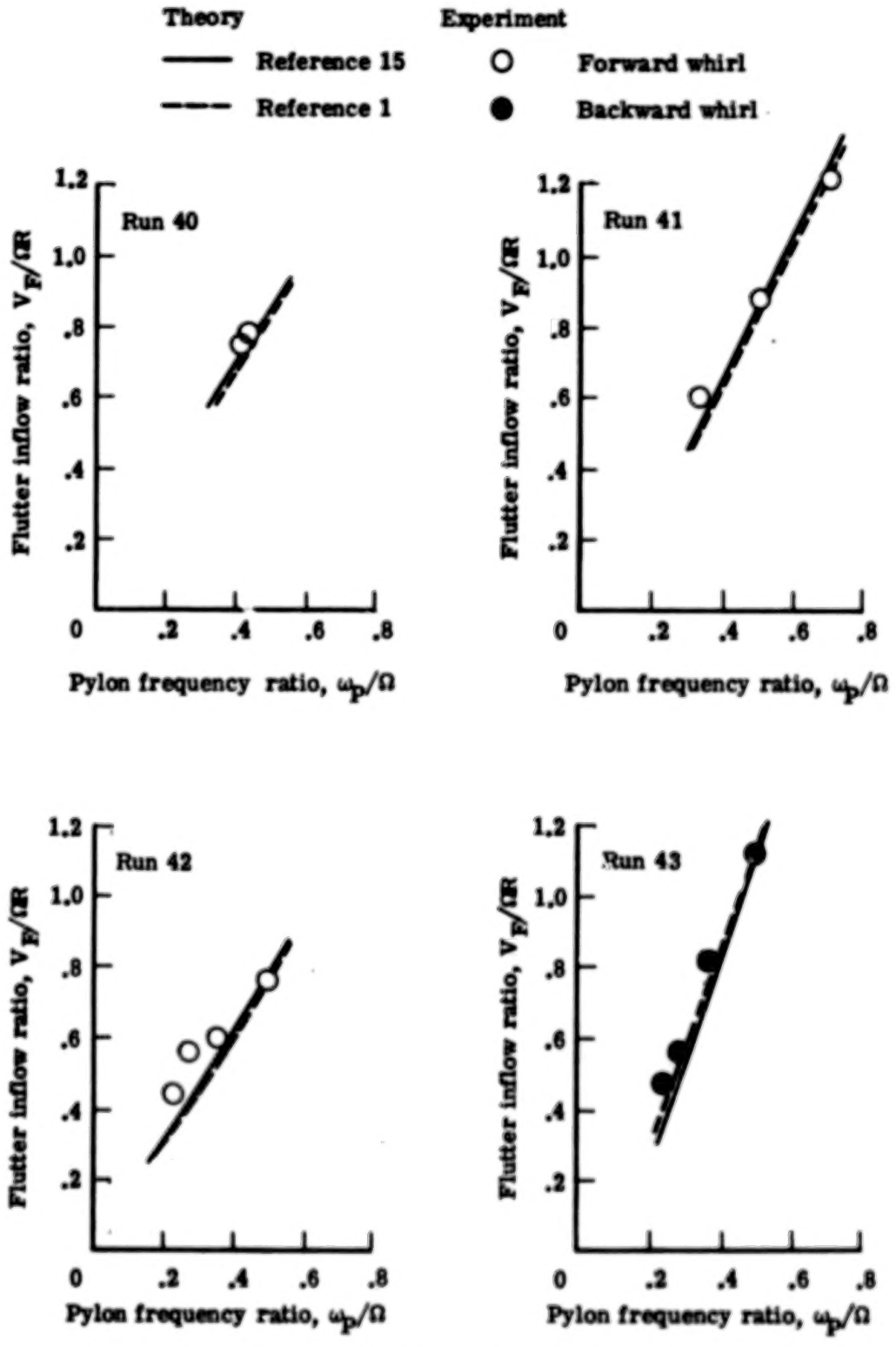

Figure 9.- Run-by-run correlation of experimental and theoretical flutter inflow ratios.

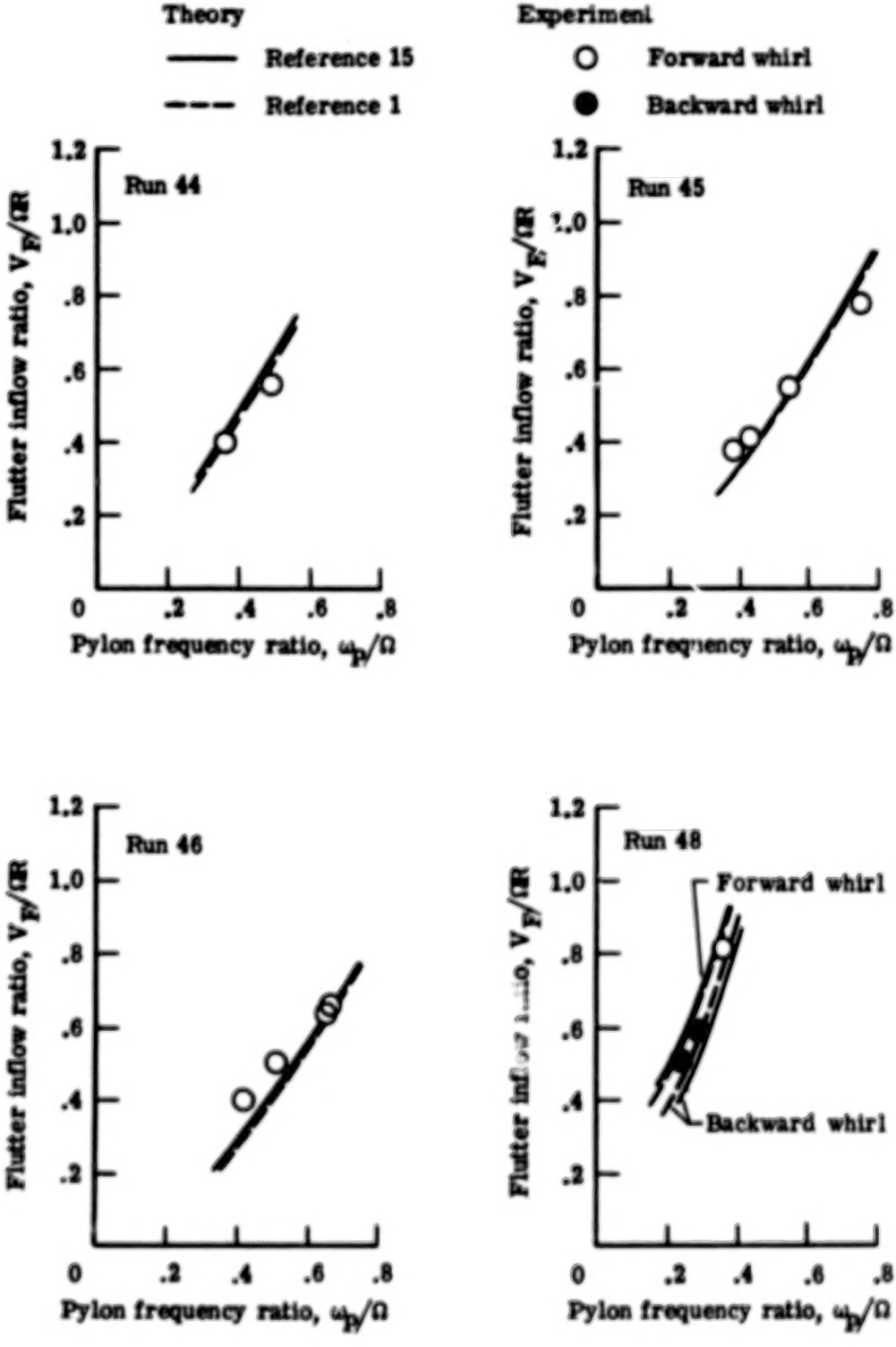

Figure 9.- Continued.

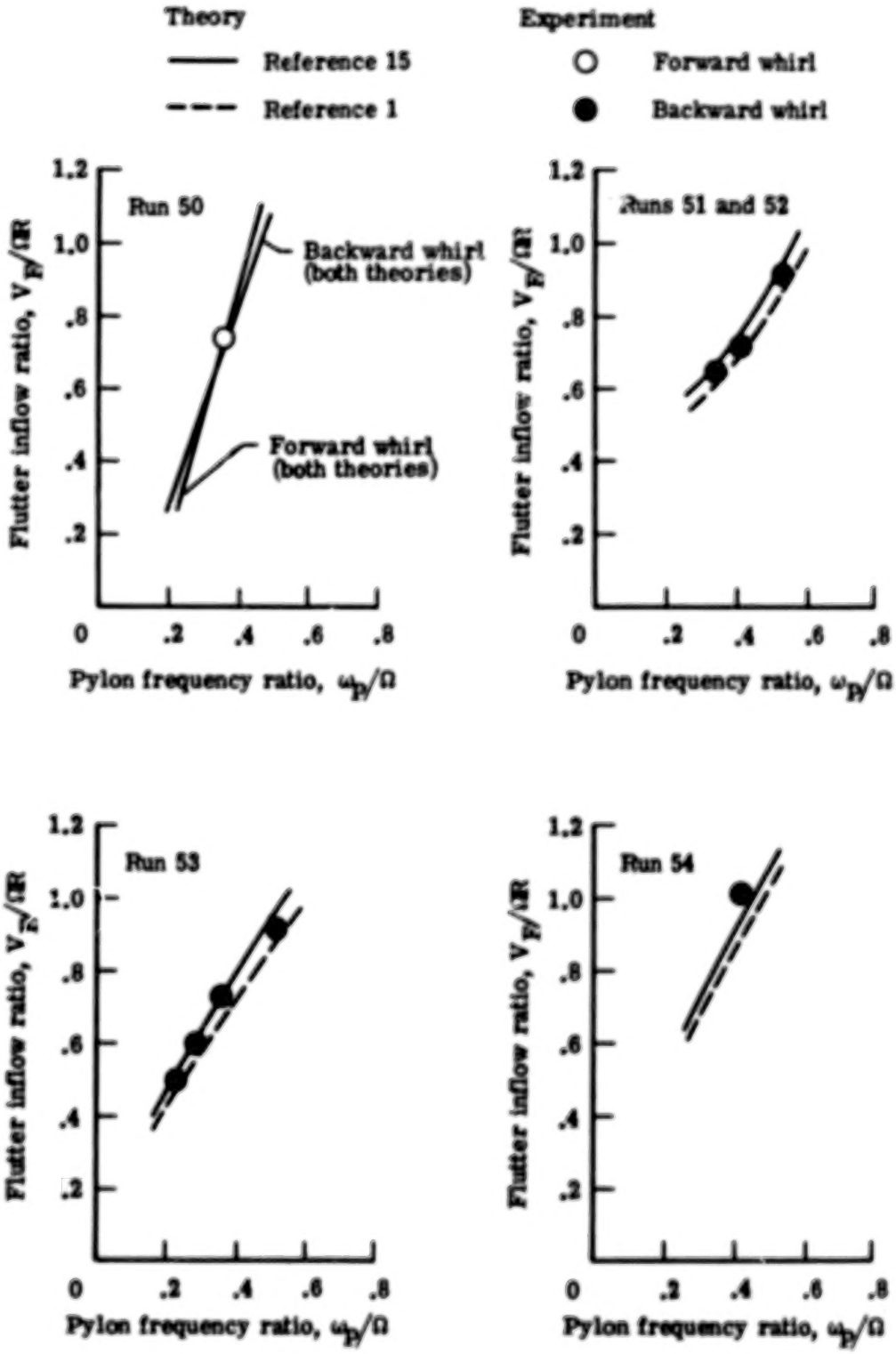

Figure 9.- Continued.

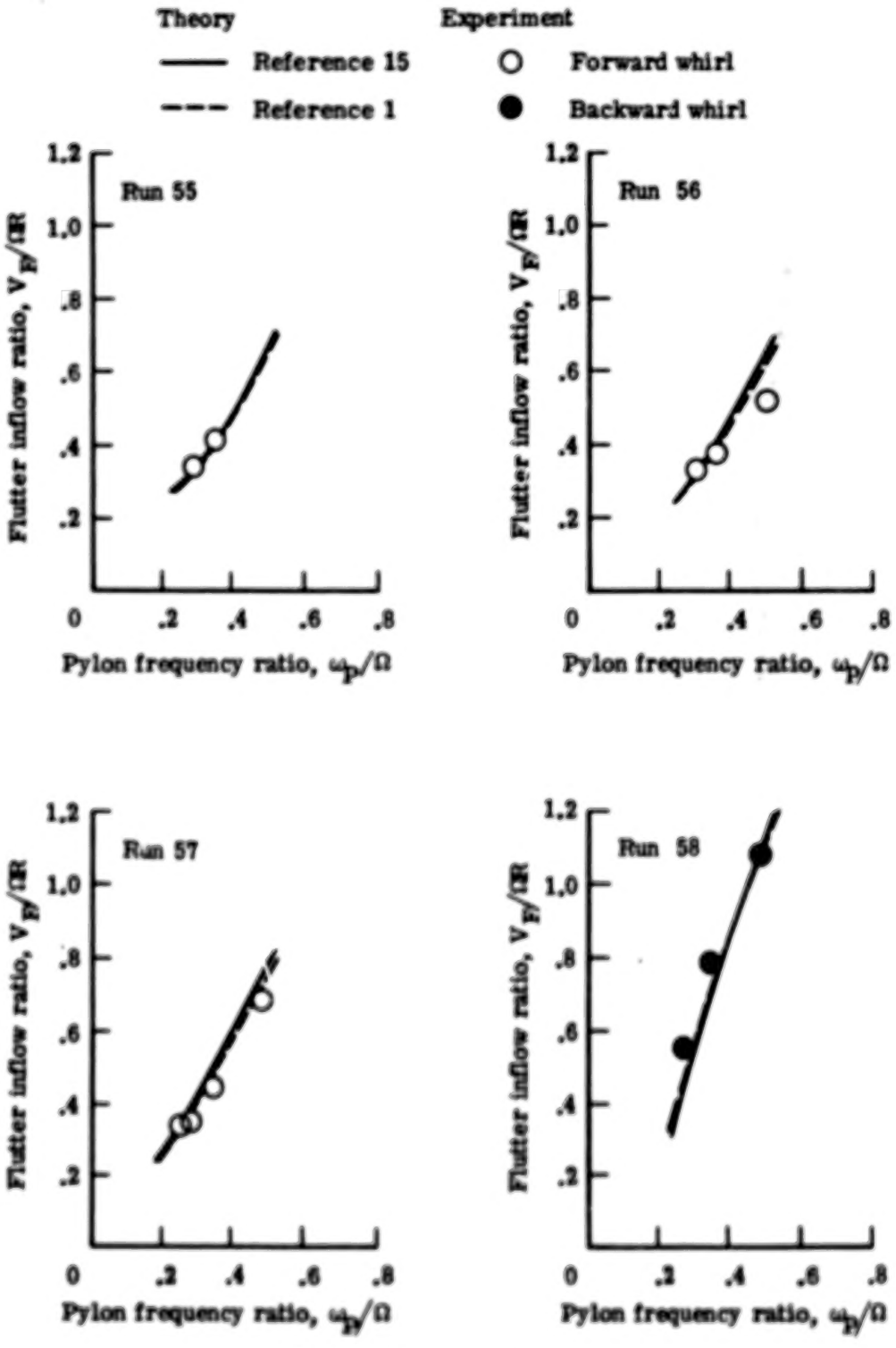

Figure 9.- Continued.

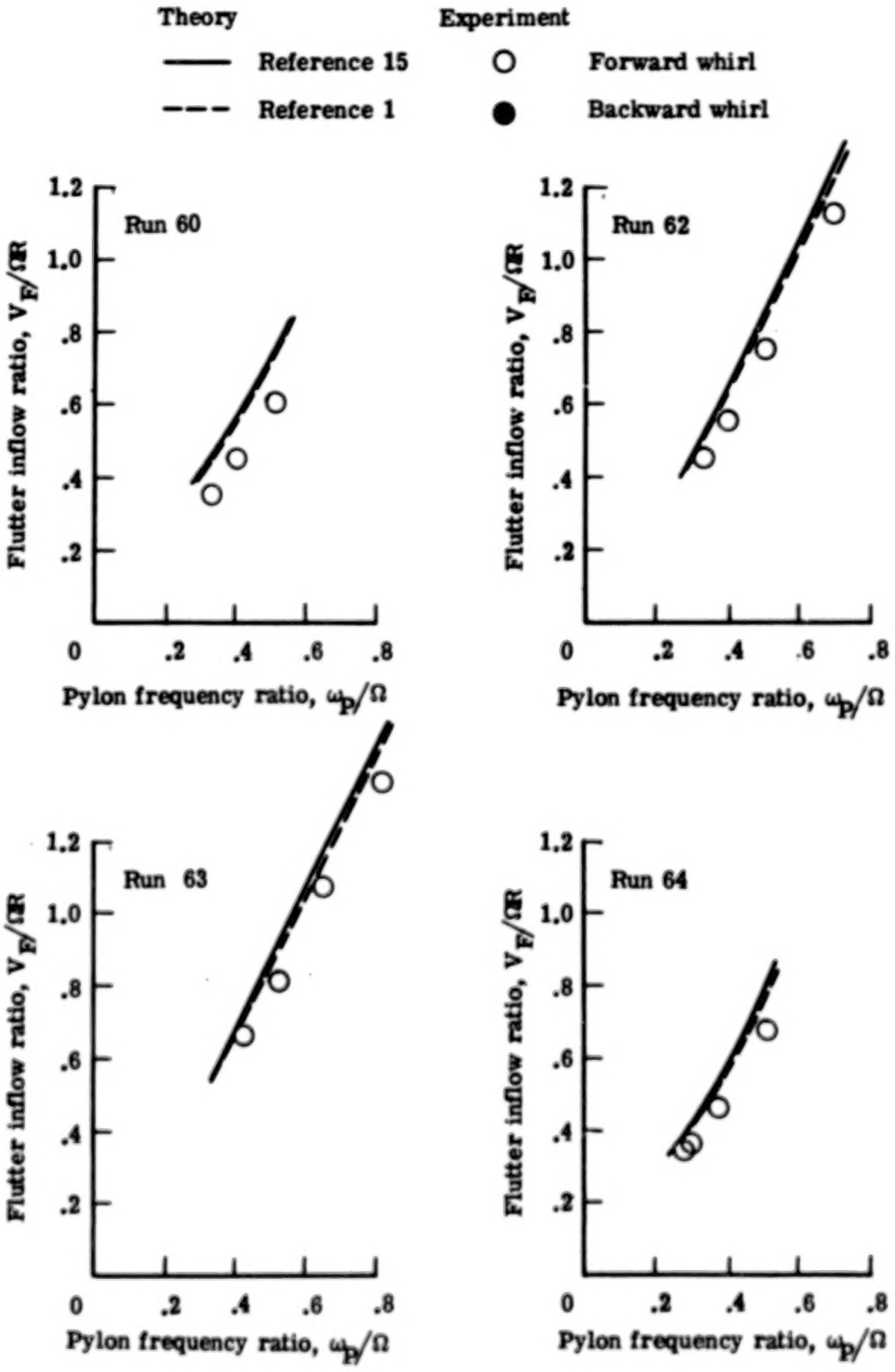

Figure 9.- Continued.

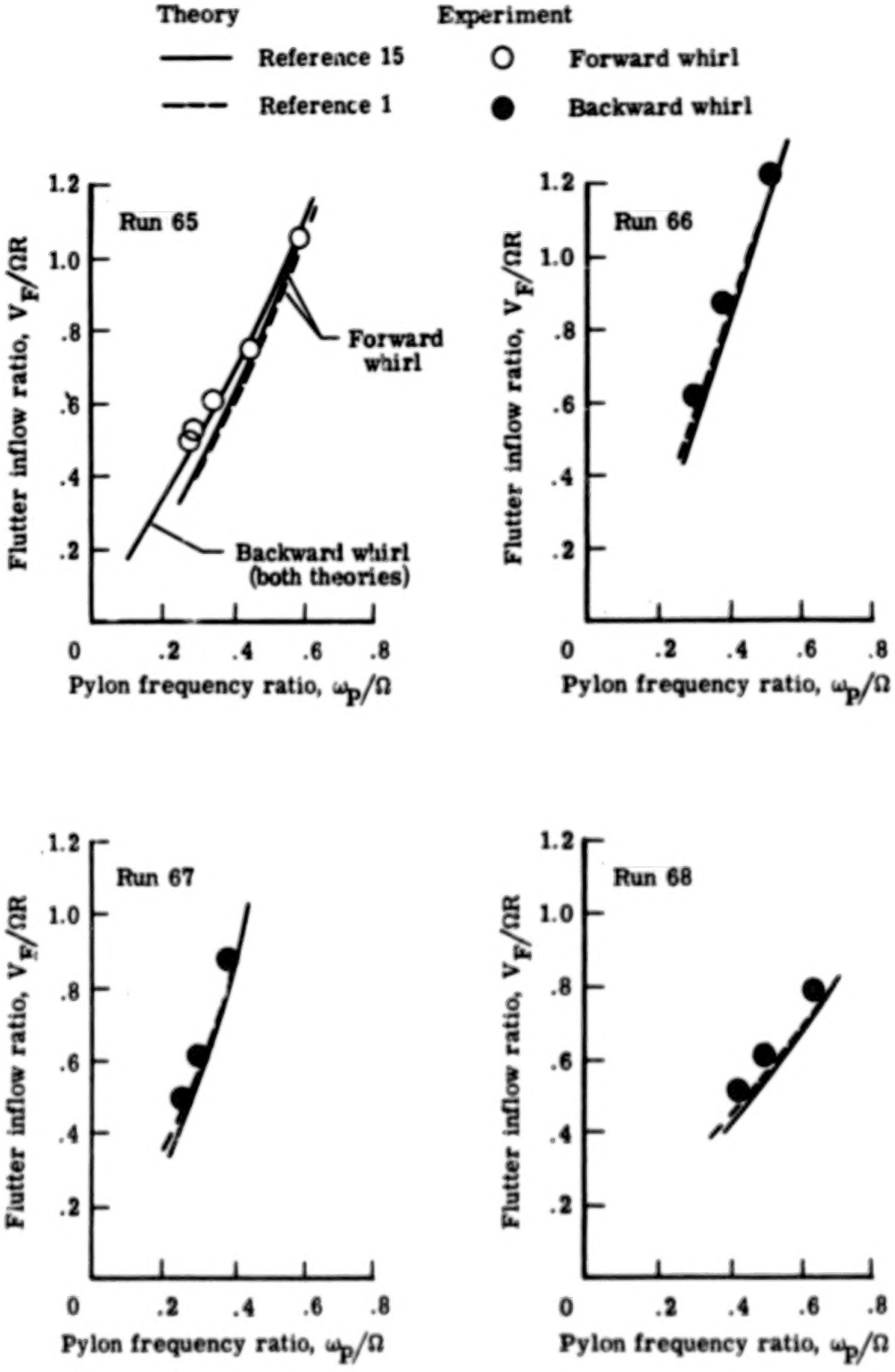

Figure 9.- Concluded.

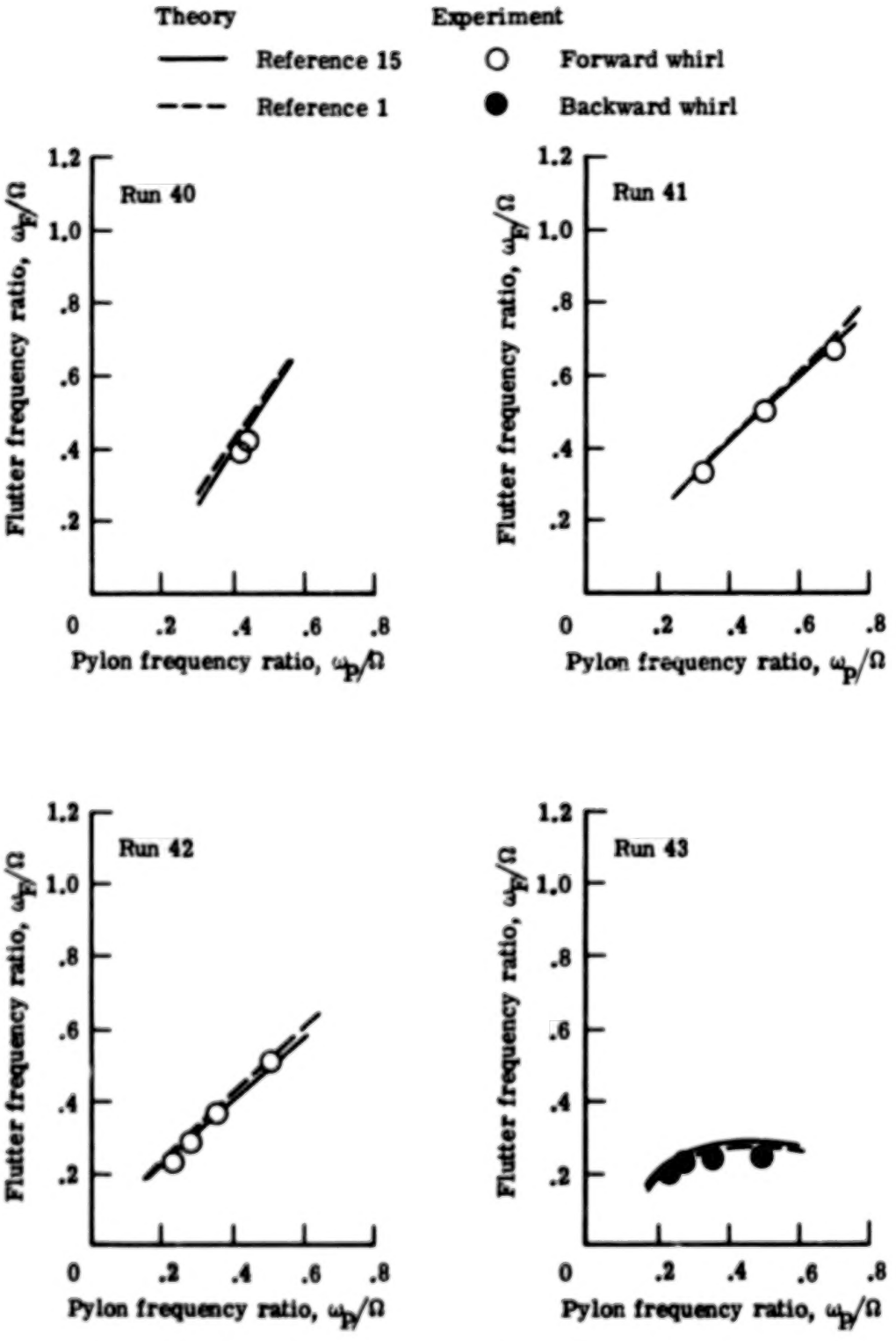

Figure 10.- Run-by-run correlation of experimental and theoretical flutter frequencies.

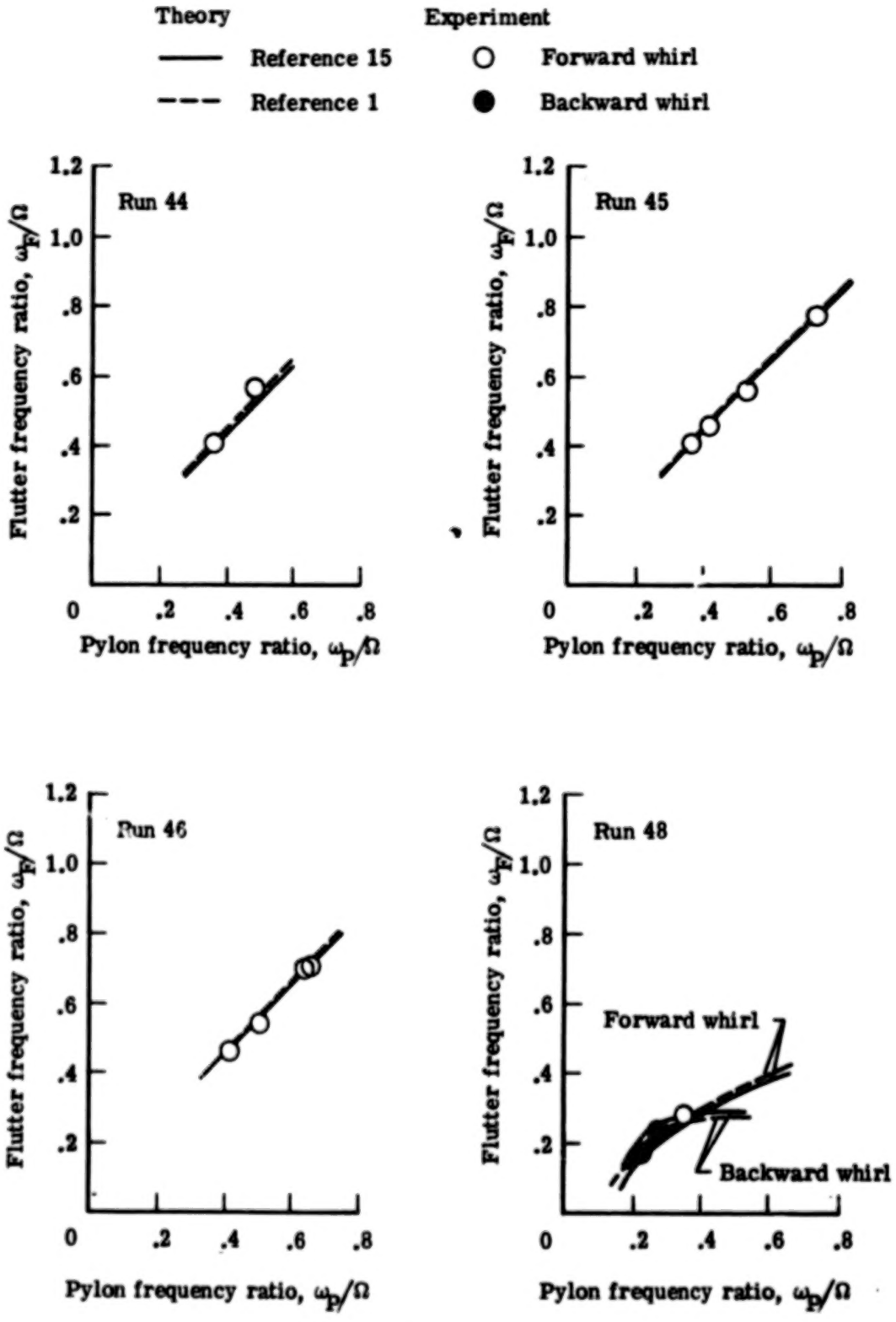

Figure 10.- Continued.

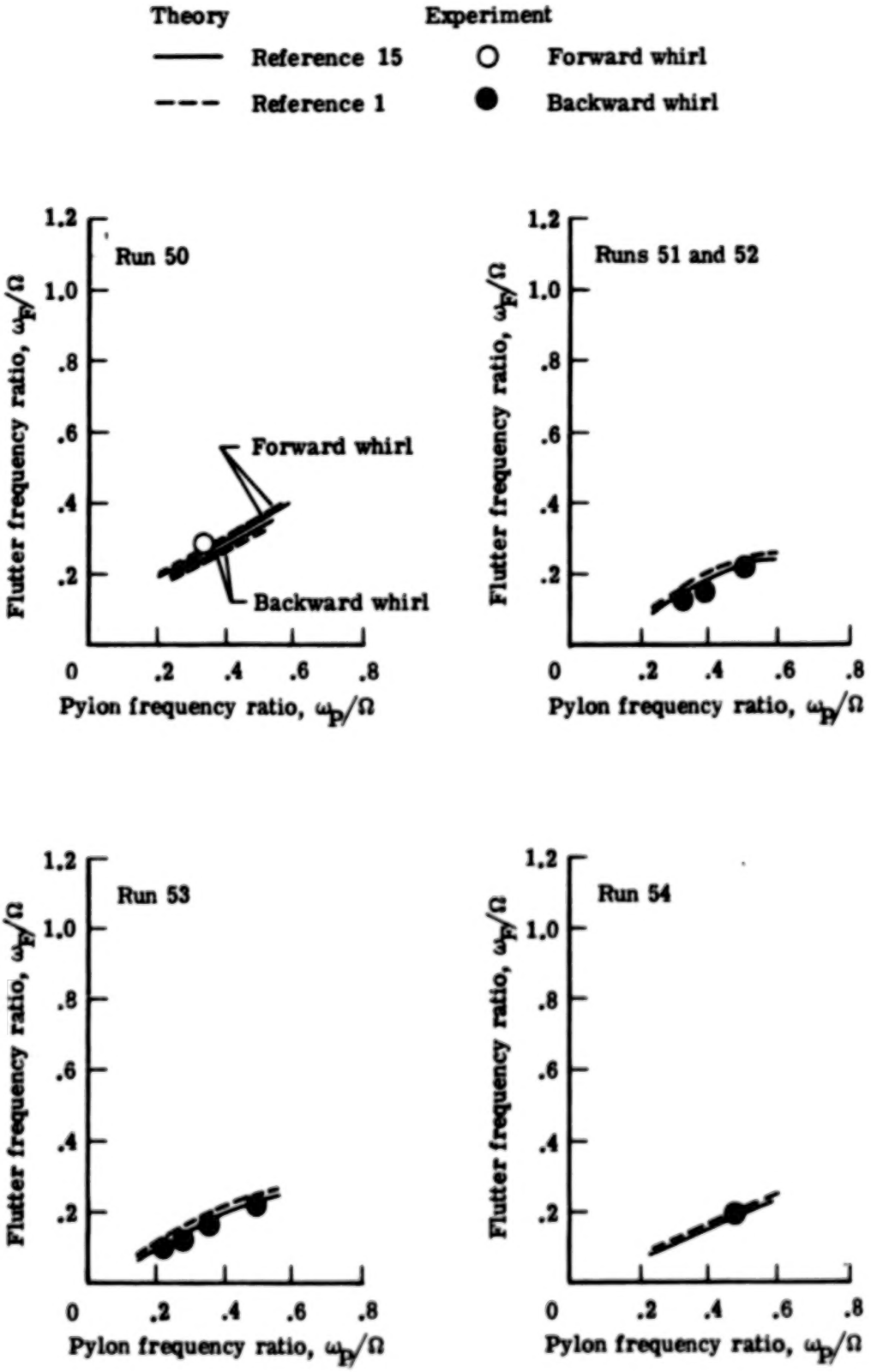

Figure 10.- Continued.

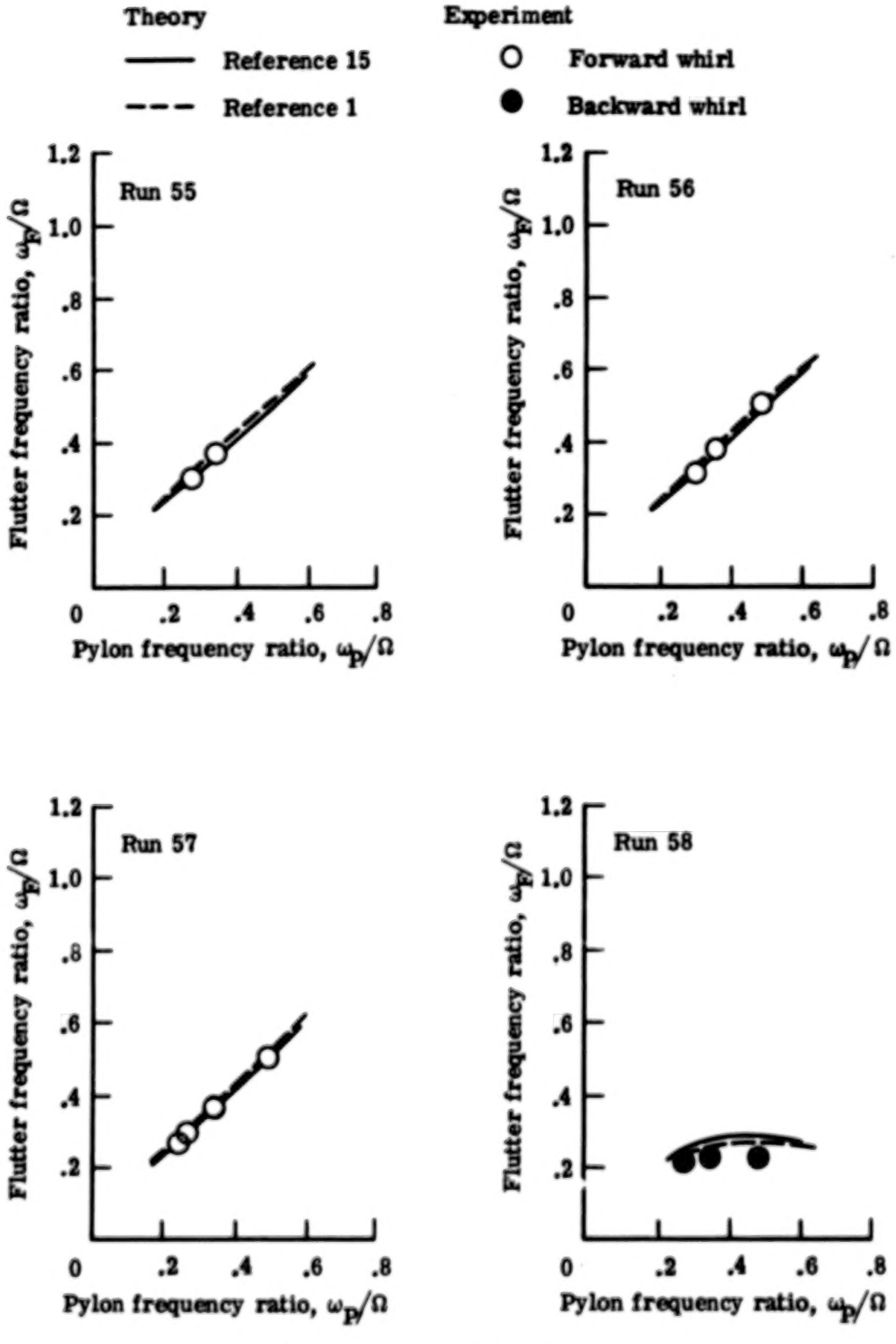

Figure 10.- Continued.

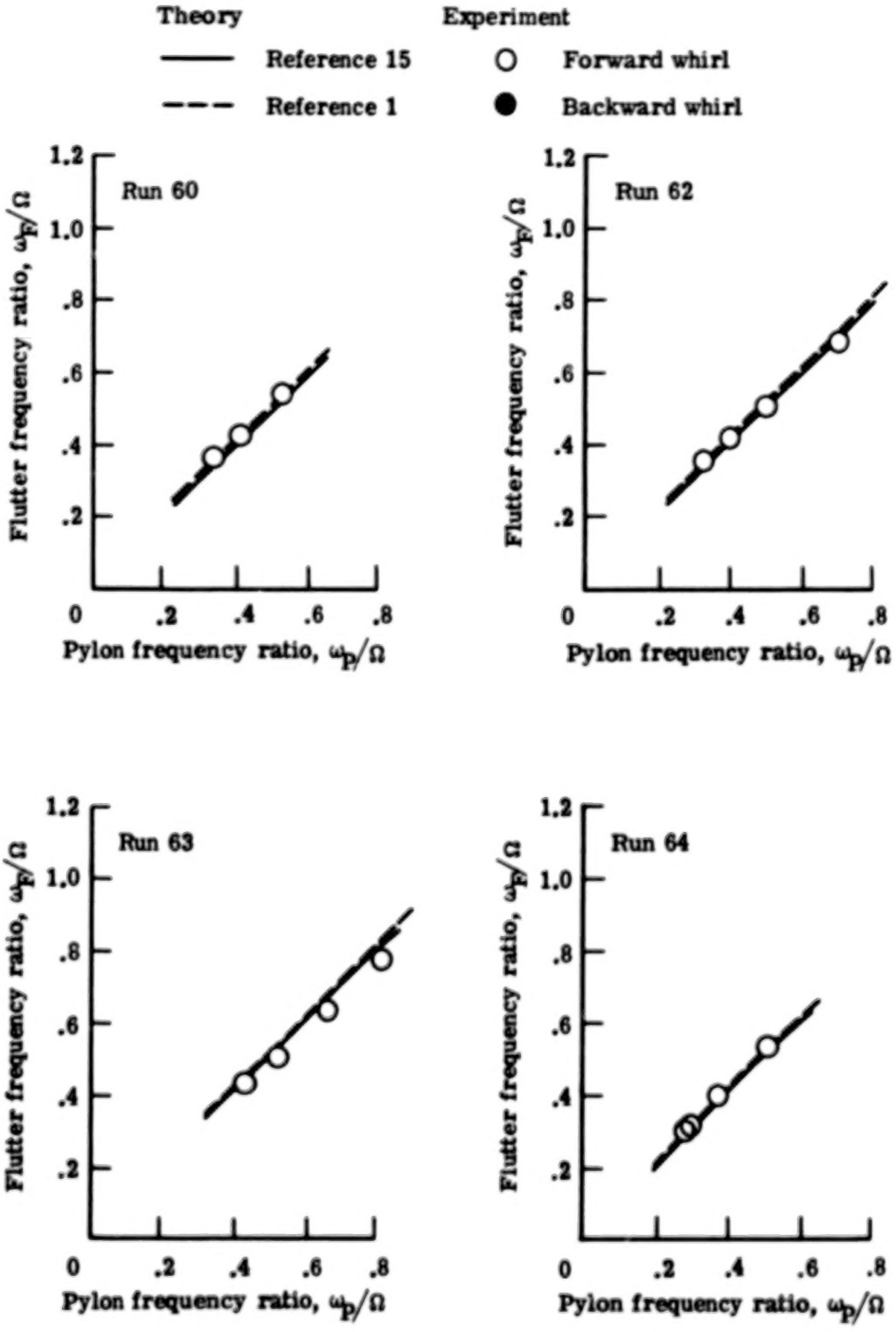

Figure 10.- Continued.

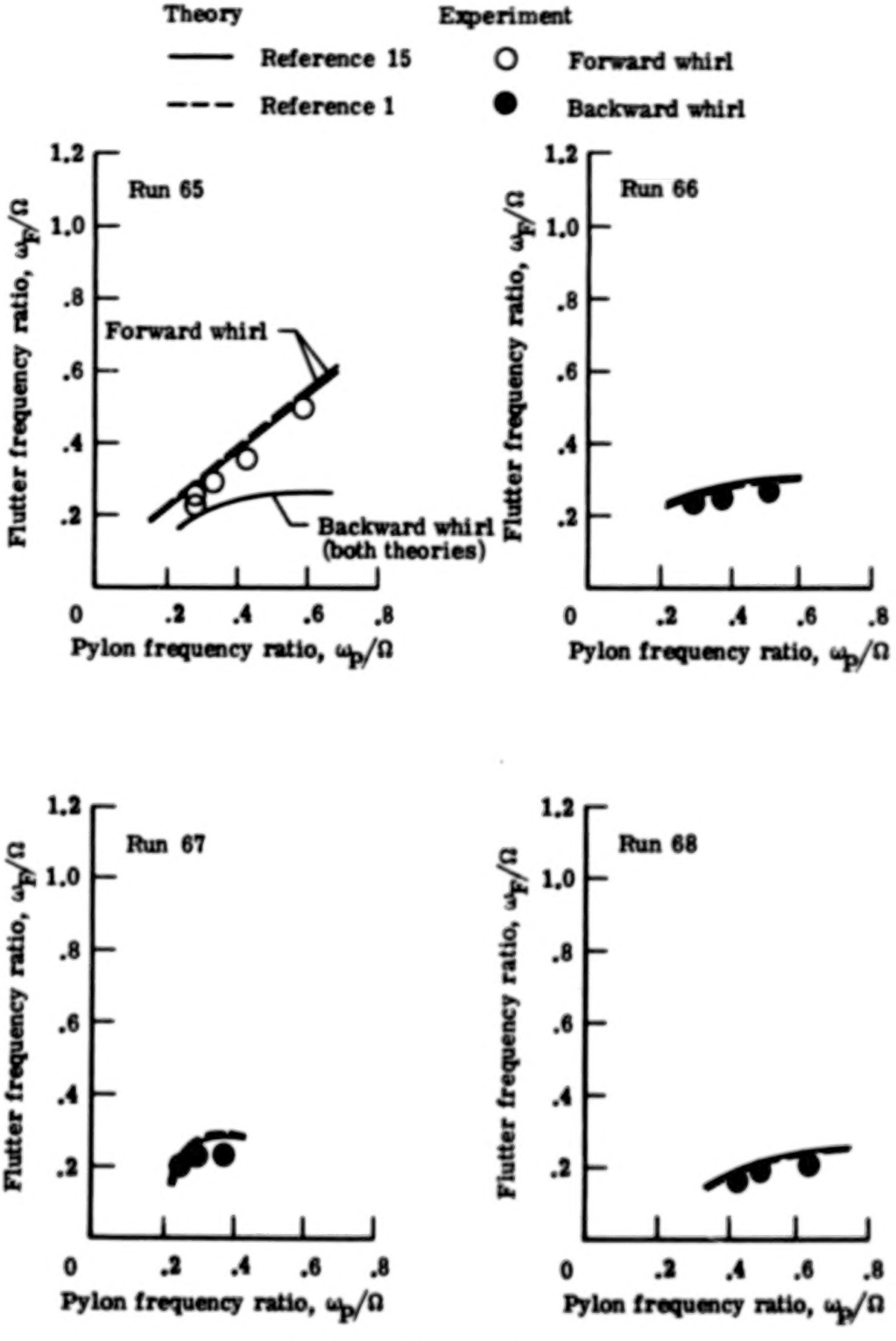

Figure 10.- Concluded.

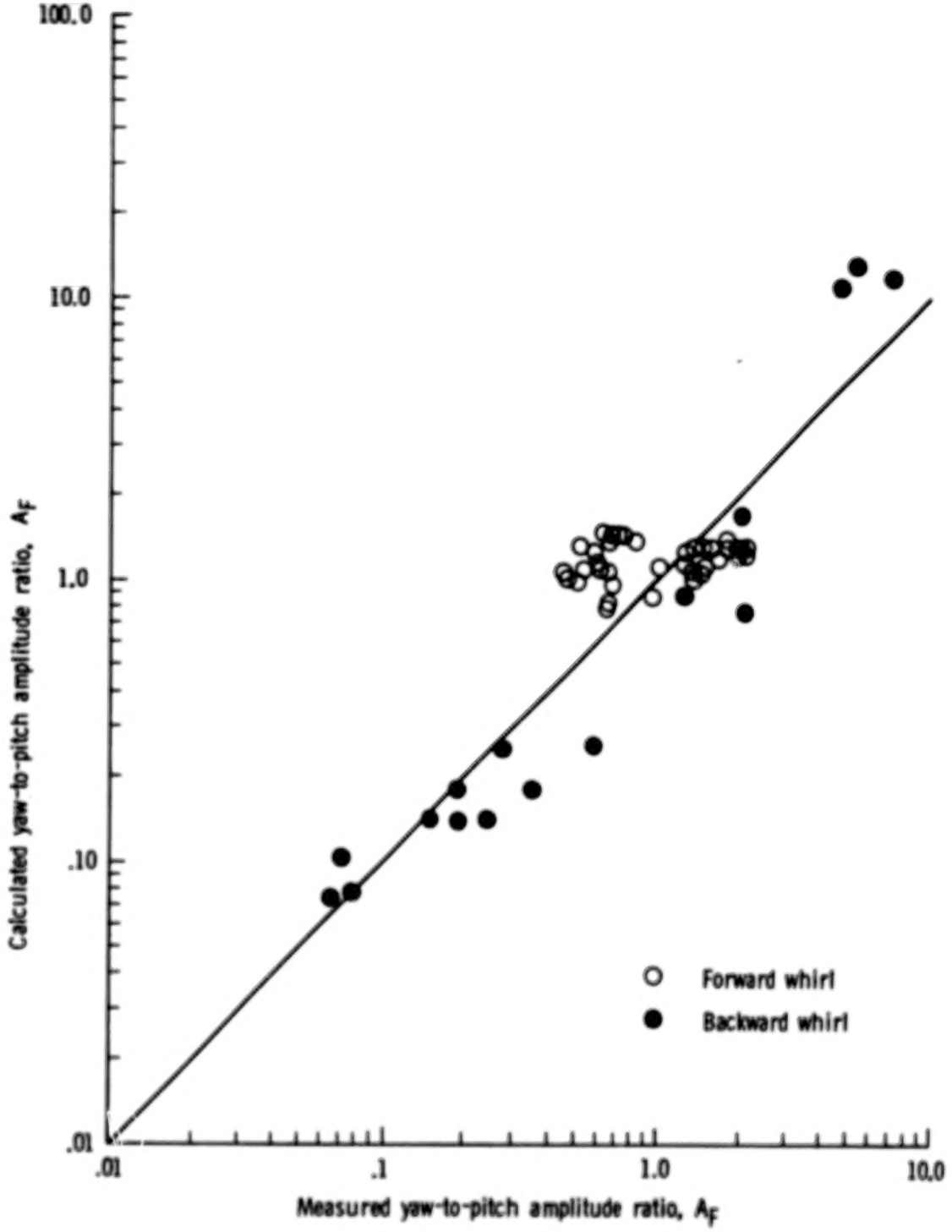

Figure 11.- Comparison of measured pylon yaw-to-pitch amplitude ratio at flutter with theory of reference 1.

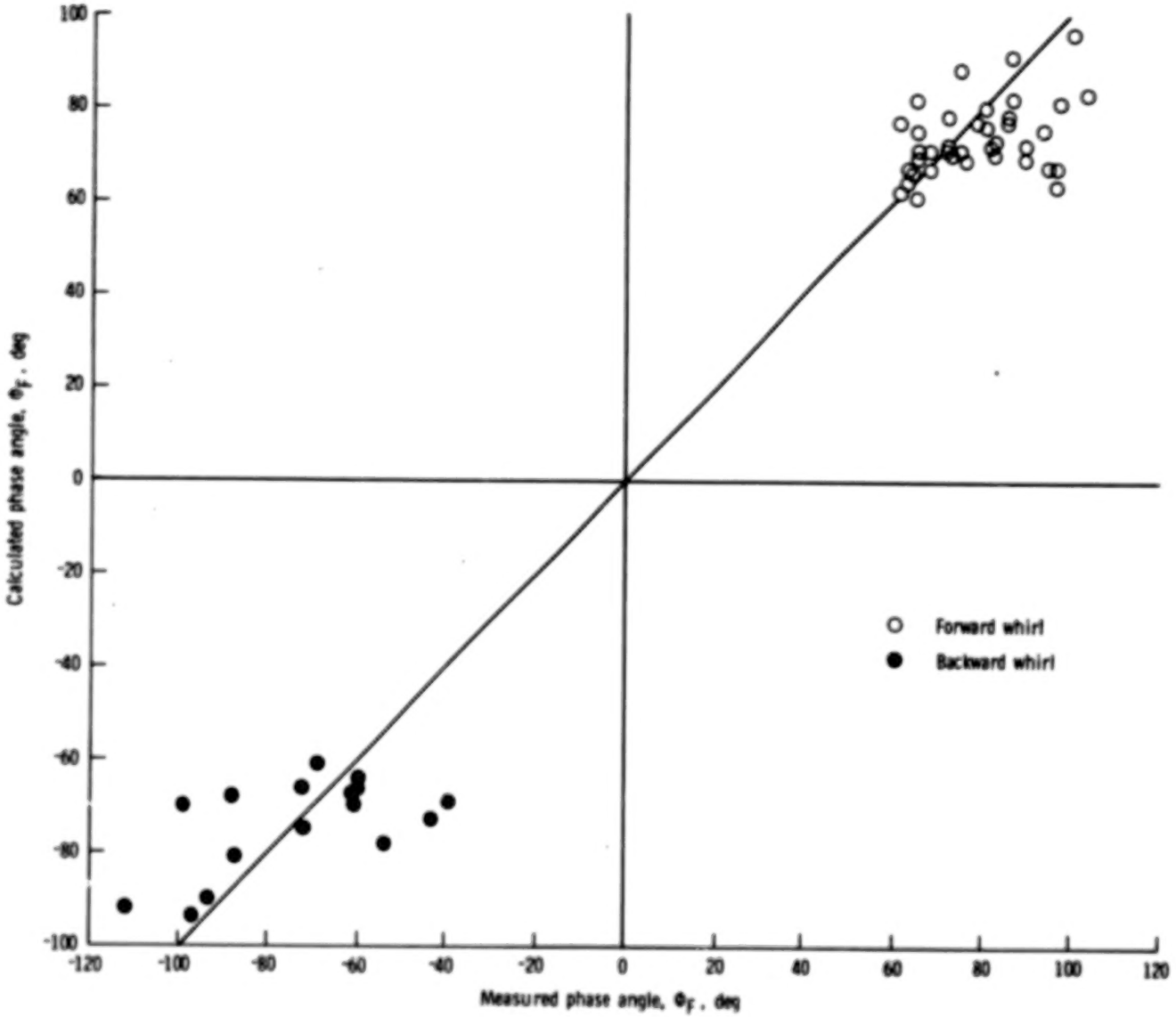

Figure 12.- Comparison of measured pylon yaw-to-pitch phase angle at flutter with theory of reference 1.

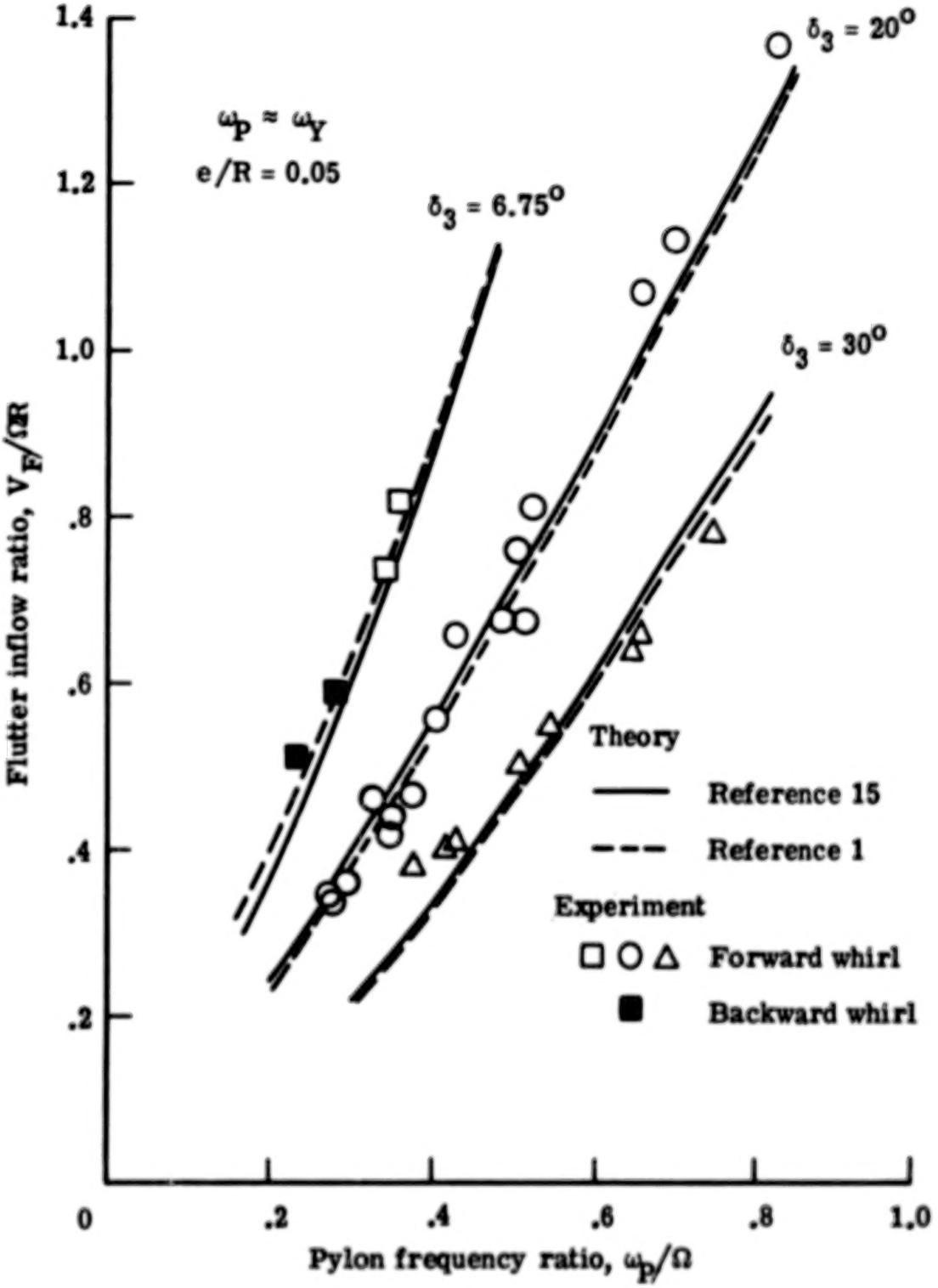

Figure 13.- Effect of pitch-flap coupling on whirl flutter.

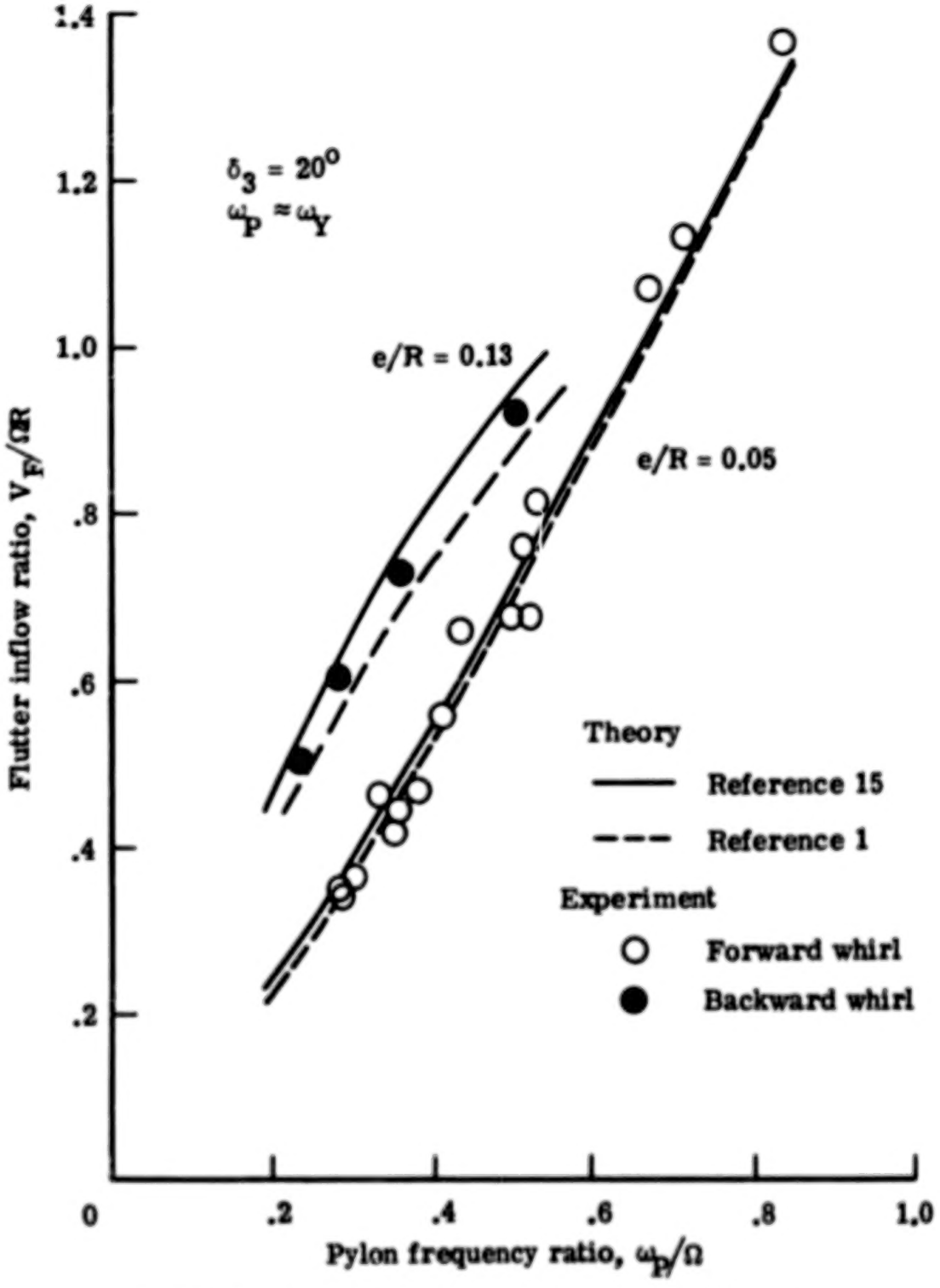

Figure 14.- Effect of hinge offset on whirl flutter.

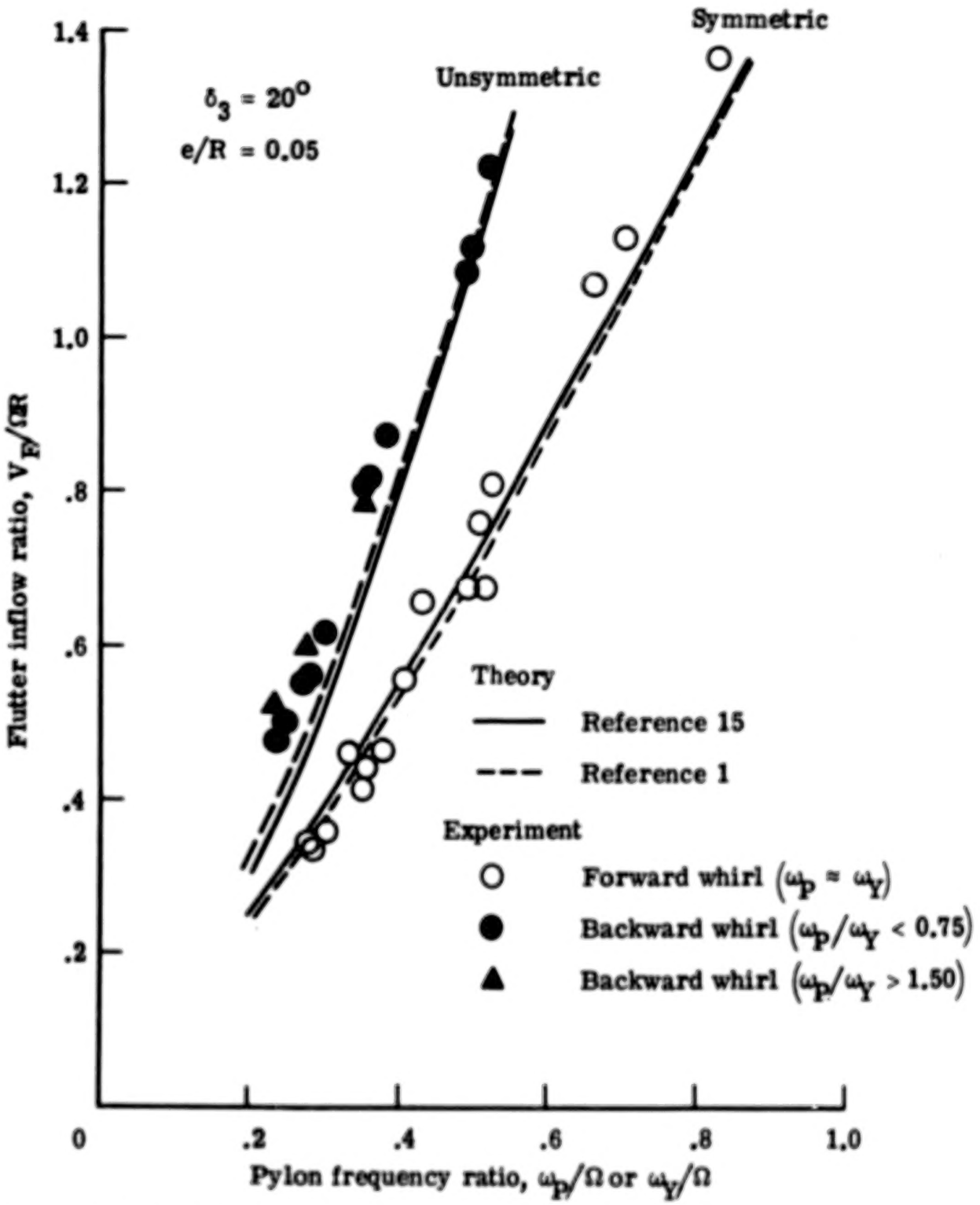

Figure 15.- Effect of pylon support stiffness on whirl flutter. For $\omega_\gamma < \omega_p$, flutter inflow ratio is plotted against ω_γ/Ω.

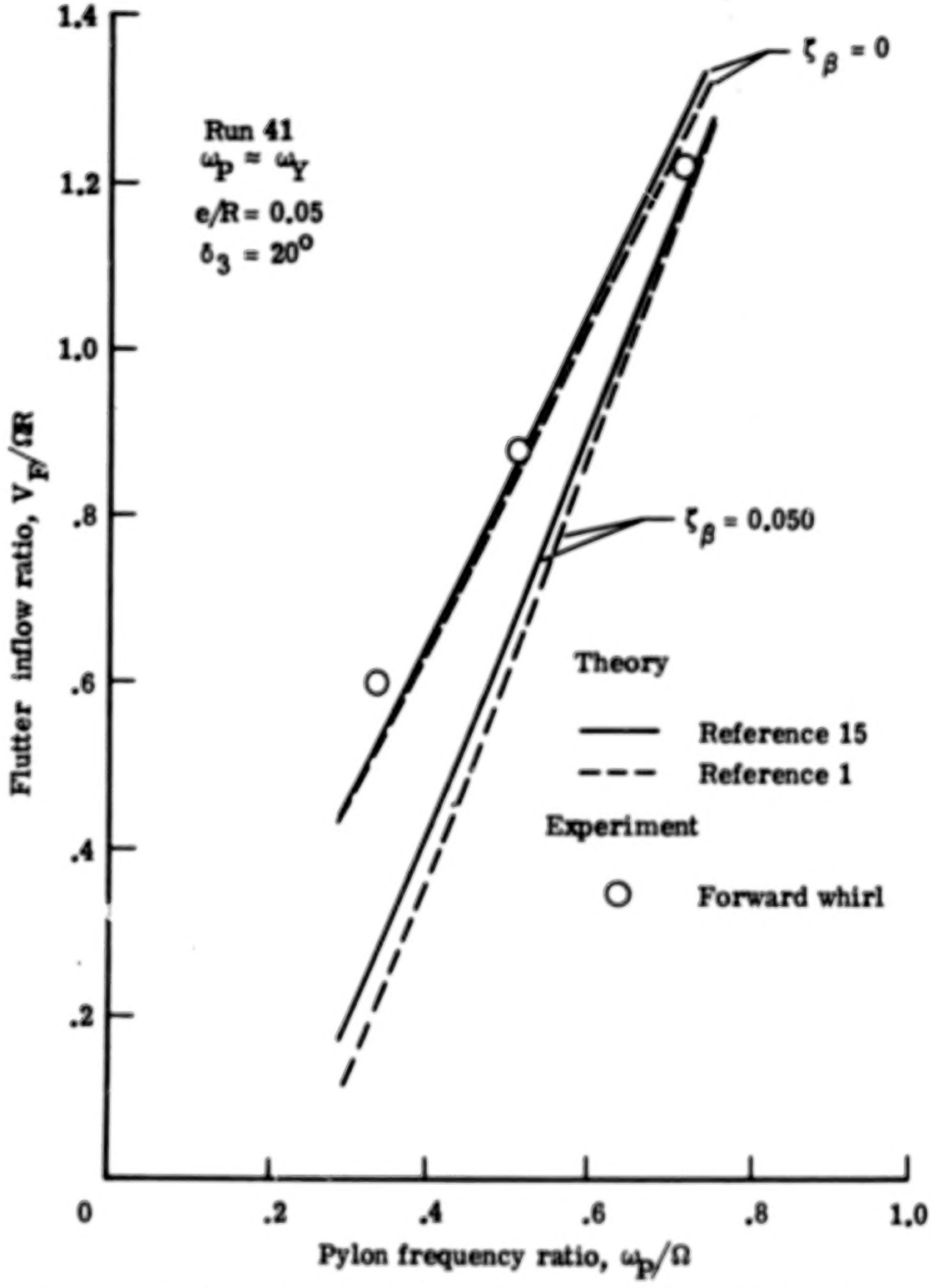

Figure 16.- Effect of flap hinge damping on forward whirl flutter. Symmetric pylon frequency.

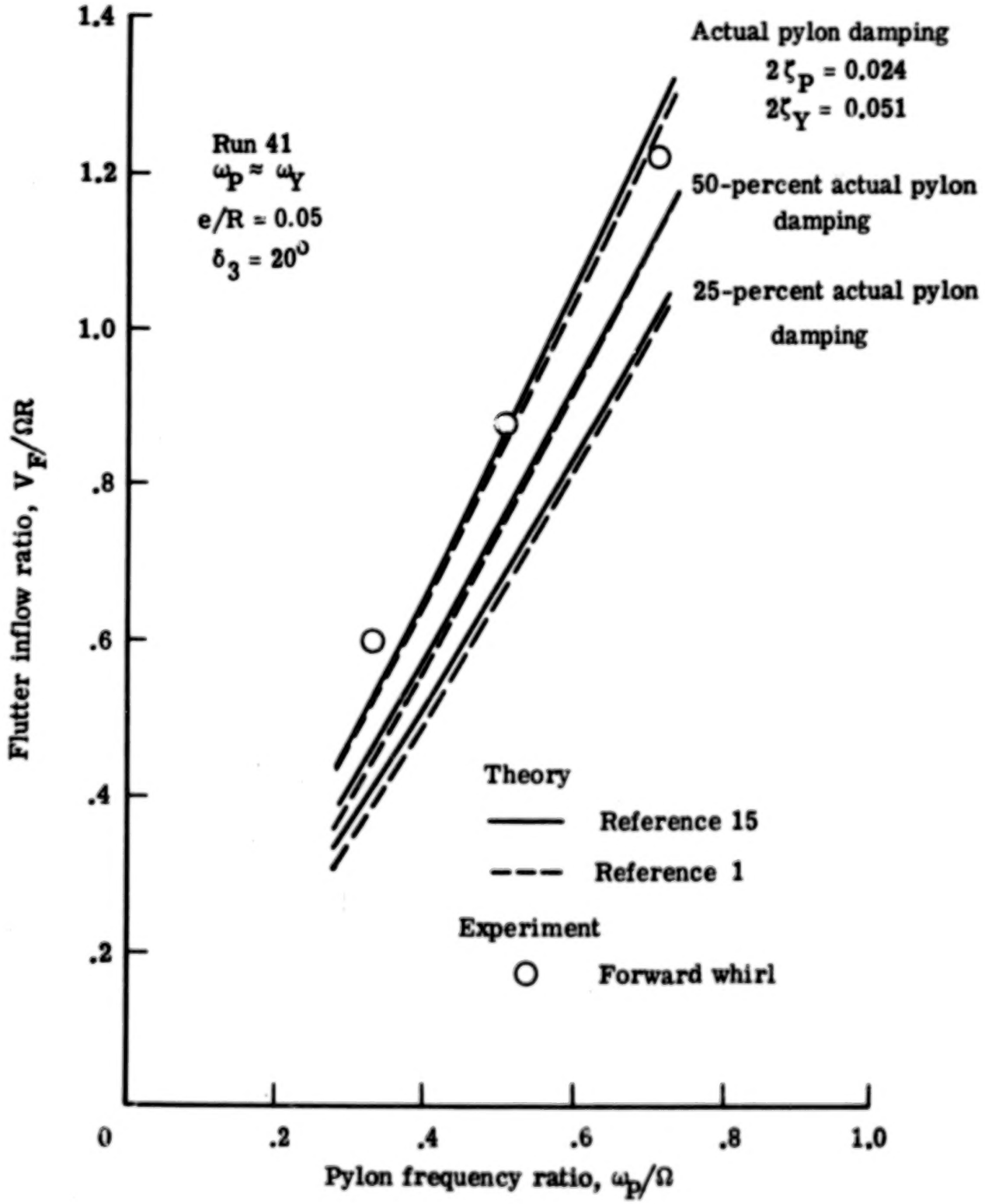

Figure 17.- Effect of pylon damping on forward whirl flutter. Symmetric pylon frequency.

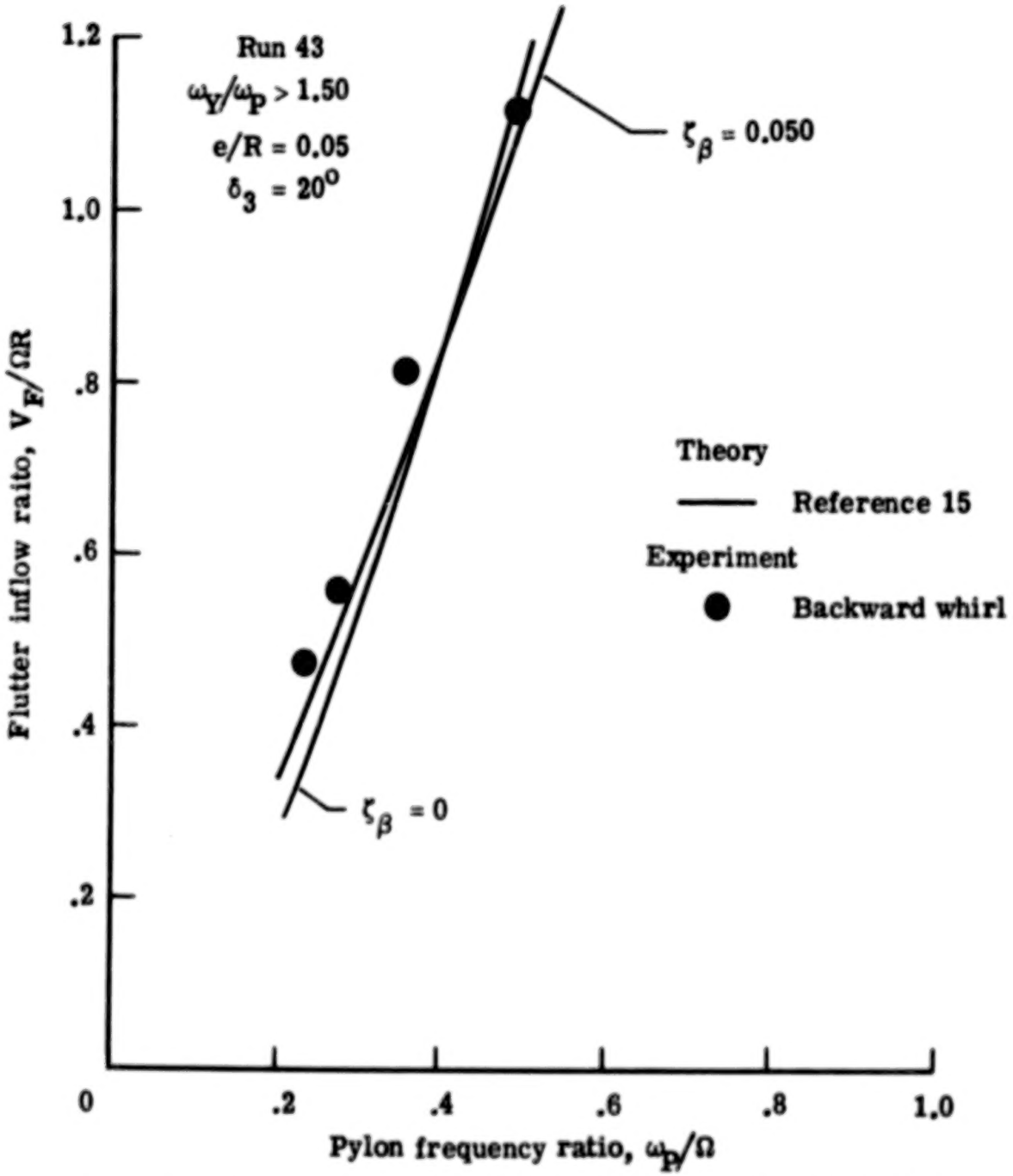

Figure 18.- Effect of flap hinge damping on backward whirl flutter. Nonsymmetric pylon frequency.

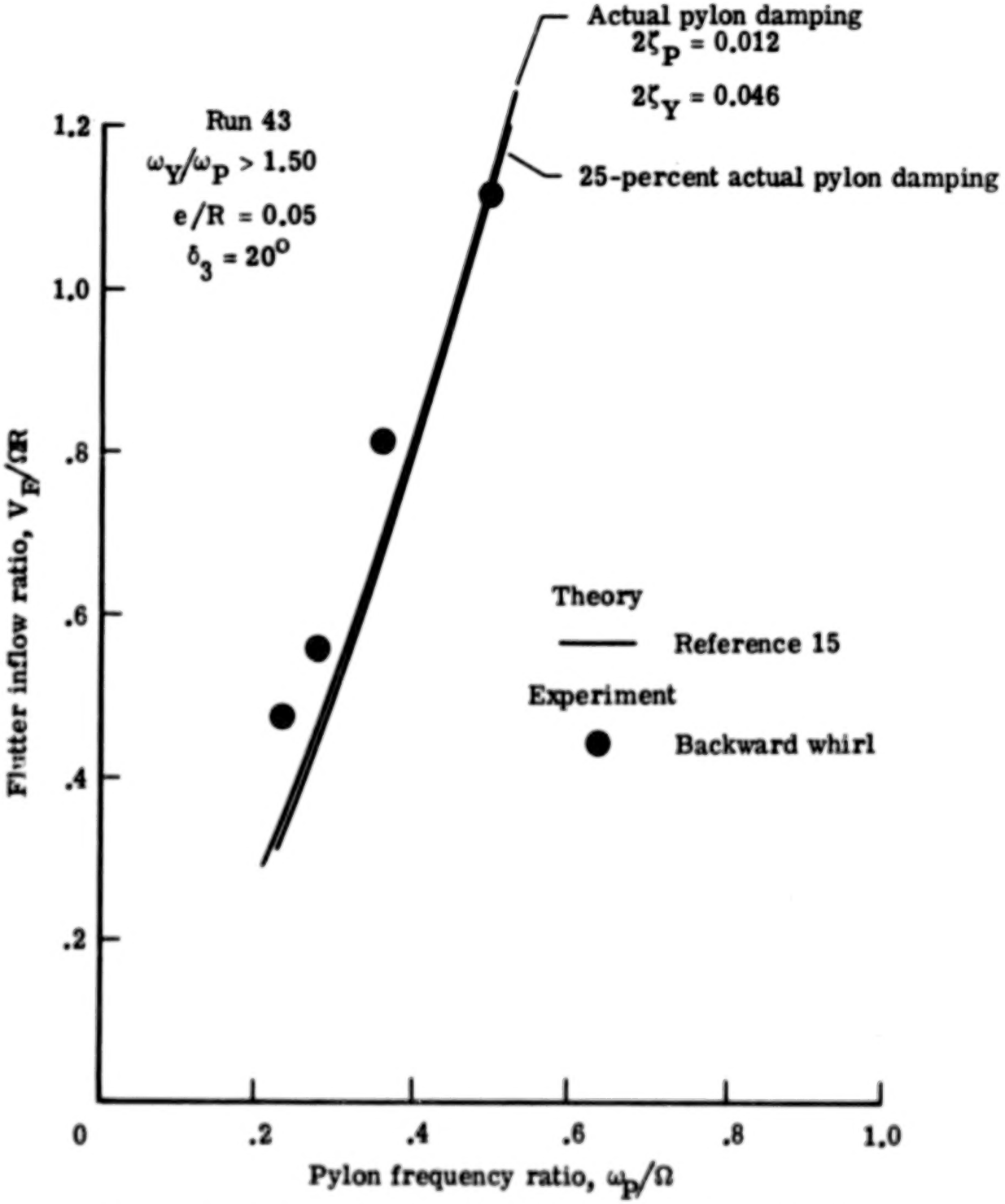

Figure 19.- Effect of pylon damping on backward whirl flutter. Nonsymmetric pylon frequency.

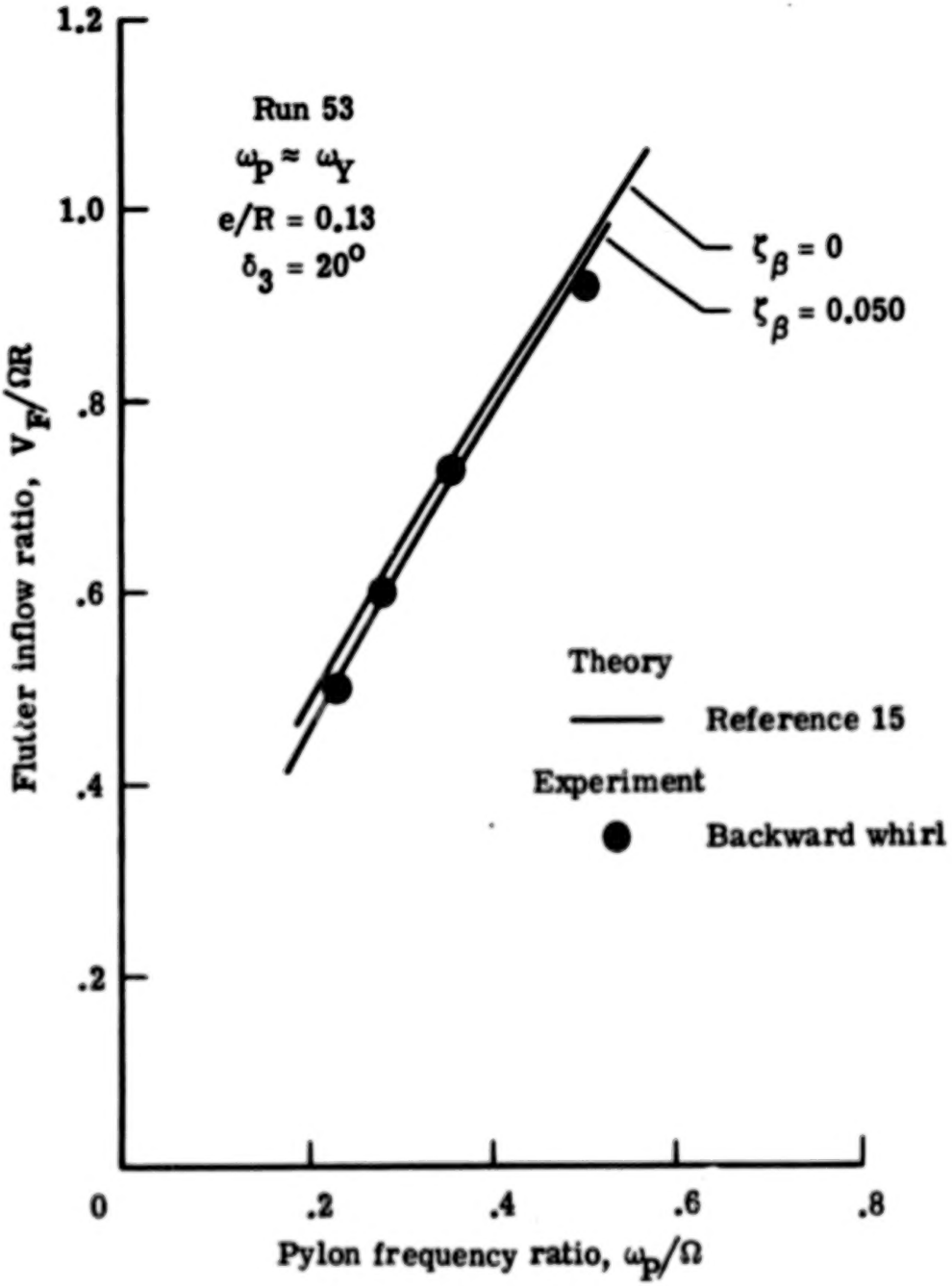

Figure 20.- Effect of flap hinge damping on backward whirl flutter. Symmetric pylon frequency.

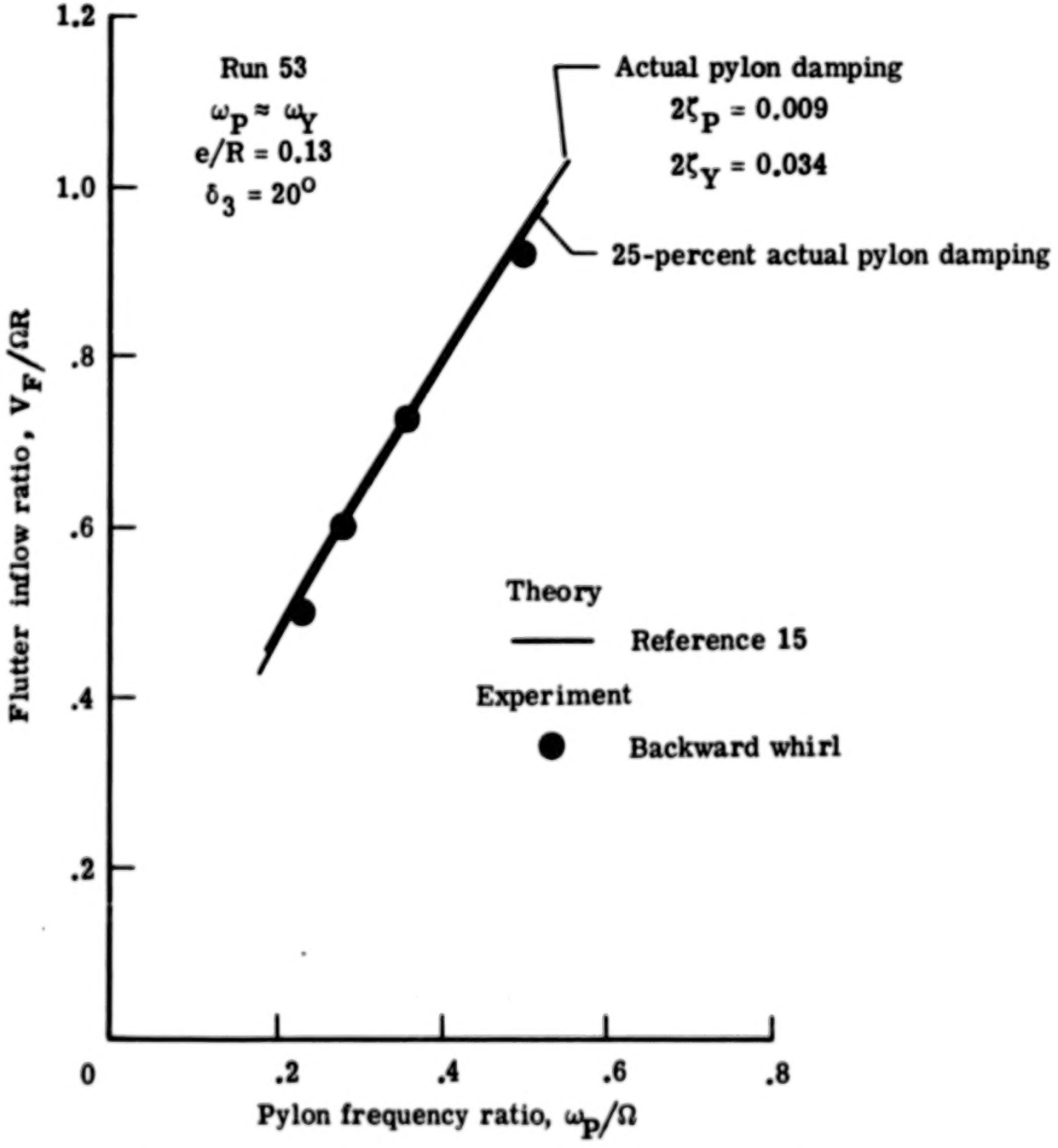

Figure 21.- Effect of pylon damping on backward whirl flutter. Symmetric pylon frequency.

1. Report No.	2. Government Accession No.	3. Recipient's Catalog No.
NASA TP-1047		

4. Title and Subtitle	5. Report Date
AN EXPERIMENTAL AND ANALYTICAL INVESTIGATION OF PROPROTOR WHIRL FLUTTER	December 1977
	6. Performing Organization Code

7. Author(s)	8. Performing Organization Report No.
Raymond G. Kvaternik and Jerome S. Kohn	L-11656
	10. Work Unit No. 505-10-26-01

9. Performing Organization Name and Address	11. Contract or Grant No.
NASA Langley Research Center Hampton, VA 23665	
	13. Type of Report and Period Covered Technical Paper

12. Sponsoring Agency Name and Address	14. Sponsoring Agency Code
National Aeronautics and Space Administration Washington, DC 20546	

15. Supplementary Notes

Jerome S. Kohn: Langley-Industry Research Associate, now at Grumman Aerospace Corporation, Bethpage, New York.

16. Abstract

The results of an experimental parametric investigation of whirl flutter are presented for a model consisting of a windmilling propeller-rotor, or "proprotor," having blades with offset flapping hinges mounted on a rigid pylon with flexibility in pitch and yaw. The investigation was motivated by the need to establish a large data base from which to assess the predictability of whirl flutter for a proprotor since some question has been raised as to whether flutter in the forward whirl mode could be predicted with confidence. In order to provide the necessary data base, the parametric study included variations in the pylon pitch and yaw stiffnesses, flapping hinge offset, and blade kinematic pitch-flap (δ_3) coupling over a large range of advance ratios. Fifty cases of forward whirl flutter and twenty-six cases of backward whirl flutter are documented. The measured whirl flutter characteristics, which include flutter speed, flutter frequency, direction of pylon whirl, and pylon yaw-to-pitch amplitude ratio and phase angle, are shown to be in good to excellent agreement with predictions from two different linear stability analyses which employ simple, two-dimensional, quasi-steady aerodynamics for the blade loading. On the basis of these results, it appears that proprotor whirl flutter, both forward and backward, can be predicted.

17. Key Words (Suggested by Author(s))	18. Distribution Statement
Whirl flutter Proprotor stability	Unclassified - Unlimited Subject Category 02

19. Security Classif. (of this report)	20. Security Classif. (of this page)	21. No. of Pages	22. Price*
Unclassified	Unclassified	73	$5.25

*For sale by the National Technical Information Service, Springfield, Virginia 22161

NASA-Langley, 1977